9. Theory of Synchrotron Radiation

The phenomenon of synchrotron radiation has been introduced in a conceptual way in Chap. 3 and a number of basic relations have been derived. In this chapter we will approach the physics of synchrotron radiation in a more formal way to exhibit detailed characteristics. Specifically, we will derive expressions for the spatial and spectral distribution of photon emission in a way which is applicable later for special insertion devices.

The theory of synchrotron radiation is intimately related to the electromagnetic fields generated by moving charged particles. Wave equations can be derived from Maxwell's equations and we will find that any charged particle under the influence of external forces can emit radiation. We will formulate the characteristics of this radiation and apply the results to highly relativistic particles.

9.1 Radiation Field

The electromagnetic fields for a single moving point charge will be derived first and then applied to a large number of particles. The fields are determined by Maxwell's equations (C.1 to C.4) for moving charges in vacuum, $\epsilon_\mathrm{r} = 1$ and $\mu_\mathrm{r} = 1$. The magnetic field can be derived from a vector potential $\boldsymbol{A}$ defined by

$$\boldsymbol{B} = \boldsymbol{\nabla} \times \boldsymbol{A}\,. \tag{9.1}$$

Inserting the vector potential into Maxwell's curl equation (C.4) we have $\boldsymbol{\nabla} \times \left(\boldsymbol{E} + \frac{[c]}{c}\frac{\partial \boldsymbol{A}}{\partial t}\right) = 0$, or after integration

$$\boldsymbol{E} = -\frac{[c]}{c}\frac{\partial \boldsymbol{A}}{\partial t} - \boldsymbol{\nabla}\varphi\,, \tag{9.2}$$

where φ is the scalar potential. We choose the scalar potential such that $[c]\,\boldsymbol{\nabla}\boldsymbol{A} + \frac{1}{c}\frac{\partial \varphi}{\partial t} = 0$, a condition known as the Lorentz gauge. With (B.24) applied to $\boldsymbol{A}$ the expression for the electric field together with (C.4) results in the wave equation

$$\nabla^2 \boldsymbol{A} - \frac{1}{c^2}\frac{\partial^2 \boldsymbol{A}}{\partial t^2} = \frac{4\pi}{[4\pi\epsilon_0]}\rho\,\boldsymbol{\beta}\,. \tag{9.3}$$

Similarly, we derive the wave equation for the scalar potential

$$\nabla^2\varphi - \frac{1}{c^2}\frac{\partial^2\boldsymbol{\varphi}}{\partial t^2} = -\frac{4\pi}{[4\pi\epsilon_0]}\rho\,. \tag{9.4}$$

These are the well-known wave equations with the solutions

$$\boldsymbol{A}(t) = \frac{1}{[4\pi c\epsilon_0]}\frac{1}{c}\int \left.\frac{\boldsymbol{v}\rho(x,y,z)}{R}\right|_{t_\mathrm{r}} \mathrm{d}x\,\mathrm{d}y\,\mathrm{d}z \tag{9.5}$$

and

$$\boldsymbol{\varphi}(t) = \frac{1}{[4\pi c\epsilon_0]}\frac{1}{c}\int \left.\frac{\rho(x,y,z)}{R}\right|_{t_\mathrm{r}} \mathrm{d}x\,\mathrm{d}y\,\mathrm{d}z\,. \tag{9.6}$$

Because of the finite velocity of light, all quantities under the integrals must be evaluated at the retarded time

$$t_\mathrm{r} = t - \frac{1}{c}R(t_\mathrm{r}) \tag{9.7}$$

when the radiation was emitted by the moving charge, in contrast to the time t when the radiation is observed at a distant point. The quantity R is the distance between the observation point $P(x,y,z)$ and the location of the charge element $\rho(x_\mathrm{r},y_\mathrm{r},z_\mathrm{r})\mathrm{d}x_\mathrm{r}\mathrm{d}y_\mathrm{r}\mathrm{d}z_\mathrm{r}$ at the retarded time t_r. The vector

$$\boldsymbol{R} = (x_\mathrm{r}-x, y_\mathrm{r}-y, z_\mathrm{r}-z) \tag{9.8}$$

points away from the observation point to the charge element at the retarded time as shown in Fig. 9.1.

Special care must be exercised in performing the integrations. Although we consider only a point charge q, the integral in (9.6) cannot be replaced by q/R but must be integrated over a finite volume followed by a transition to a point charge. As we will see this is a consequence of the fact that the velocity of light is finite and therefore the movement of charge elements must be taken into account.

To define the quantities involved in the integration we use Fig. 9.1. The combined field at the observation point P at time t comes from all charges located at a distance R away from P. We consider the contribution from all charges contained within a spherical shell centered at P with a radius R and thickness $\mathrm{d}r$ to the radiation field at P and time t. Radiation emitted at time t_r will reach P at the time t. If $\mathrm{d}\sigma$ is a surface element of the spherical shell, the volume element of charge is $\mathrm{d}x\,\mathrm{d}y\,\mathrm{d}z = \mathrm{d}\sigma\mathrm{d}r$. The retarded time for the radiation from the outer surface of the shell is t_r and the retarded time for the radiation from the charge element on the inner surface of the shell is $t_\mathrm{r} - \frac{\mathrm{d}r}{c}$. From Fig. 9.1 we find the electromagnetic field observed at P at time t to originate from the fractional charges within the volume element $\mathrm{d}\sigma\mathrm{d}r$ or from the charge element $\mathrm{d}q = \rho\,\mathrm{d}\sigma\mathrm{d}r$.

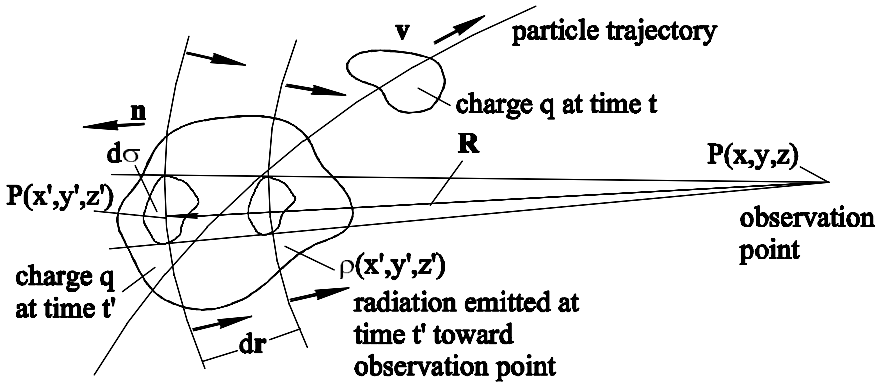

Fig. 9.1. Retarded position of a moving charge distribution

The radiation observed at point P and time t is the sum of all radiation arriving simultaneously at P. Elements of this radiation field may have been emitted by different charge elements and at different times and locations. In case of only one electrical charge moving with velocity $\boldsymbol{v}$, we have to include in the integration those charge elements that move across the inner shell surface into the volume $\mathrm{d}\sigma\mathrm{d}r$ during the time $\mathrm{d}r/c$. For a uniform charge distribution this additional charge is $\mathrm{d}q = \rho\boldsymbol{v}\boldsymbol{n}\,\mathrm{d}t\,\mathrm{d}\sigma$ where $\boldsymbol{n}$ is the vector normal to the surface of the shell and pointing away from the observer

$$\boldsymbol{n} = \frac{\boldsymbol{R}}{R}\,. \tag{9.9}$$

With $\mathrm{d}t = \mathrm{d}r/c$ and $\boldsymbol{\beta} = \boldsymbol{v}/c$, we get then for both contributions to the charge element

$$\mathrm{d}q = \rho(1 + \boldsymbol{n}\boldsymbol{\beta})\,\mathrm{d}r\,\mathrm{d}\sigma\,. \tag{9.10}$$

Depending on the direction of the velocity vector $\boldsymbol{\beta}$, we find an increase or a reduction in the radiation field from moving charges. We solve (9.10) for $\rho\,\mathrm{d}r\,\mathrm{d}\sigma$ and insert into the integrals (9.5, 9.6). Now we may use the assumption that the electrical charge is a point charge and get for the retarded potentials of a moving point charge q at time t and observation point P

$$\boldsymbol{A}(P,t) = \frac{1}{[4\pi c\epsilon_0]}\,\frac{q}{R}\frac{\boldsymbol{\beta}}{1 + \boldsymbol{n}\boldsymbol{\beta}}\bigg|_{t_\mathrm{r}} \tag{9.11}$$

and

$$\boldsymbol{\varphi}(P,t) = \frac{1}{[4\pi\epsilon_0]}\,\frac{q}{R}\frac{1}{1 + \boldsymbol{n}\boldsymbol{\beta}}\bigg|_{t_\mathrm{r}}\,. \tag{9.12}$$

These equations are known as the Liénard–Wiechert potentials and express the field potentials of a moving charge as functions of the charge parameters at the retarded time. To obtain the electric and magnetic fields we

insert the retarded potentials into (9.1, 9.2) noting that the differentiation must be performed with respect to the time t and location P of the observer while the potentials are expressed at the retarded time t_r.

In both equations for the vector and scalar potential we have the same denominator

$$r = R(1 + \boldsymbol{n}\boldsymbol{\beta}) \,. \tag{9.13}$$

It will become necessary to calculate the derivative of the retarded time with respect to the time t and since $t_\mathrm{r} = t - R/c$ the time derivative of t_r is

$$\frac{\mathrm{d}t_\mathrm{r}}{\mathrm{d}t} = 1 - \frac{1}{c}\frac{\mathrm{d}R}{\mathrm{d}t_\mathrm{r}}\frac{\mathrm{d}t_\mathrm{r}}{\mathrm{d}t} \tag{9.14}$$

The variation of the distance R with the retarded time depends on the velocity v of the moving charge and is the projection of the vector $\boldsymbol{v}\,\mathrm{d}t_\mathrm{r}$ onto the unity vector n. Therefore,

$$\mathrm{d}R = \boldsymbol{v}\boldsymbol{n}\,\mathrm{d}t_\mathrm{r} \tag{9.15}$$

and (9.14) becomes

$$\frac{\mathrm{d}t_\mathrm{r}}{\mathrm{d}t} = \frac{1}{1 + \boldsymbol{n}\boldsymbol{\beta}} = \frac{R}{r} \,. \tag{9.16}$$

The electric field (9.2) is with (9.11, 9.12) and (9.16) after a few manipulations expressed by

$$[4\pi\epsilon_0]\,\frac{\boldsymbol{E}}{q} = -\frac{1}{c}\frac{R}{r^2}\frac{\partial\boldsymbol{\beta}}{\partial t_\mathrm{r}} + \frac{\beta\boldsymbol{R}}{cr^3}\frac{\partial r}{\partial t_\mathrm{r}} + \frac{1}{r^2}\boldsymbol{\nabla}_\mathrm{r} r \,. \tag{9.17}$$

In evaluating the nabla operator and other differentials we remember that all parameters on the r.h.s. must be taken at the retarded time (9.7) which itself depends on the location of the observation point P. To distinguish between the ordinary nabla operator and the case where the dependence of the retarded time on the position $P(x, y, z)$ must be considered, we add to the nabla symbol the index $_\mathrm{r}$ like $\boldsymbol{\nabla}_\mathrm{r}$. The components of this operator are then $\frac{\partial}{\partial x}\big|_\mathrm{r} = \frac{\partial}{\partial x} + \frac{\partial t_\mathrm{r}}{\partial x}\frac{\partial}{\partial t_\mathrm{r}}$, and similar for the other components. We evaluate first

$$\boldsymbol{\nabla}_\mathrm{r} r = \boldsymbol{\nabla}_\mathrm{r} R + \boldsymbol{\nabla}_\mathrm{r}\,(\beta\boldsymbol{R}) \tag{9.18}$$

and with $\boldsymbol{\nabla} R = -\boldsymbol{n}$ from (9.8)

$$\boldsymbol{\nabla}_\mathrm{r} R = -\boldsymbol{n} + \frac{\partial R}{\partial t_\mathrm{r}}\boldsymbol{\nabla} t_\mathrm{r} \,. \tag{9.19}$$

For the gradient of the retarded time, we get

$$\boldsymbol{\nabla} t_{\rm r} = \boldsymbol{\nabla}\left[t - \frac{1}{c}R(t_{\rm r})\right] = -\frac{1}{c}\boldsymbol{\nabla}_{\rm r} R = -\frac{1}{c}\left(-\boldsymbol{n} + \frac{\partial R}{\partial t_{\rm r}}\boldsymbol{\nabla} t_{\rm r}\right) \tag{9.20}$$

and performing the differentiation we get with $\frac{\partial x_{\rm r}}{\partial t_{\rm r}} = v_x$, ...

$$\frac{\partial R}{\partial t_{\rm r}} = \frac{\partial R}{\partial x_{\rm r}}\frac{\partial x_{\rm r}}{\partial t_{\rm r}} + \frac{\partial R}{\partial y_{\rm r}}\frac{\partial y_{\rm r}}{\partial t_{\rm r}} + \frac{\partial R}{\partial z_{\rm r}}\frac{\partial z_{\rm r}}{\partial t_{\rm r}} = \boldsymbol{n}\boldsymbol{v}\,. \tag{9.21}$$

Solving (9.20) for $\boldsymbol{\nabla} t_{\rm r}$ we get

$$\boldsymbol{\nabla} t_{\rm r} = \frac{\boldsymbol{R}}{cr} \tag{9.22}$$

and (9.19) becomes finally

$$\boldsymbol{\nabla}_{\rm r} R = -\boldsymbol{n} + \frac{\boldsymbol{R}}{r}(\boldsymbol{\beta}\boldsymbol{n})\,. \tag{9.23}$$

For the second term in (9.18) we note that the velocity $\boldsymbol{v}$ does not depend on the location of the observer and with $\boldsymbol{\nabla}_{\rm r}\boldsymbol{R}{-}1$, (9.22) and

$$\frac{{\rm d}\boldsymbol{R}}{{\rm d}t_{\rm r}} = \boldsymbol{v} \tag{9.24}$$

we get for the second term in (9.18)

$$\boldsymbol{\nabla}_{\rm r}\,(\boldsymbol{\beta}\boldsymbol{R}) = -\boldsymbol{\beta} + \frac{\partial(\boldsymbol{\beta}\boldsymbol{R})}{\partial t_{\rm r}}\boldsymbol{\nabla} t_{\rm r} = -\boldsymbol{\beta} + \left(\boldsymbol{R}\frac{\partial\boldsymbol{\beta}}{\partial t_{\rm r}}\right)\frac{\boldsymbol{R}}{cr} + \beta^2\frac{\boldsymbol{R}}{r}\,. \tag{9.25}$$

To complete the evaluation of the electric field in (9.17), we express the derivative $\frac{\partial r}{\partial t_{\rm r}}$ with

$$\frac{\partial r}{\partial t_{\rm r}} = \frac{\partial R}{\partial t_{\rm r}} + \frac{\partial(\boldsymbol{\beta}\boldsymbol{R})}{\partial t_{\rm r}} = c\,\boldsymbol{n}\boldsymbol{\beta} + c\beta^2 + \boldsymbol{R}\frac{\partial\boldsymbol{\beta}}{\partial t_{\rm r}}\,, \tag{9.26}$$

where we made use of (9.21). Collecting all differential expressions required in (9.17) we get with (9.18, 9.23, 9.25, 9.26)

$$\begin{aligned}[4\pi\epsilon_0]\,\frac{\boldsymbol{E}}{q} = \frac{1}{r^2}\Bigg[&-\boldsymbol{n} - \boldsymbol{\beta} + \frac{\boldsymbol{R}}{r}\left(\boldsymbol{n}\boldsymbol{\beta} + \beta^2 + \tfrac{1}{c}\dot{\boldsymbol{\beta}}\boldsymbol{R}\right)\Bigg]_{\rm r} \\ &-\frac{R}{cr^2}\dot{\boldsymbol{\beta}} + \boldsymbol{\beta}\frac{R}{r^3}\left(\boldsymbol{n}\boldsymbol{\beta} + \beta^2 + \tfrac{1}{c}\dot{\boldsymbol{\beta}}\boldsymbol{R}\right)_{\rm r}\,,\end{aligned} \tag{9.27}$$

where $\dot{\boldsymbol{\beta}}{=}{\rm d}\boldsymbol{\beta}/{\rm d}\,t_{\rm r}$. After some manipulation and using (B.10), the equation for the electrical field of a charge q moving with velocity $\boldsymbol{v}$ becomes

$$[4\pi\epsilon_0]\,\frac{\boldsymbol{E}}{q} = \frac{1-\beta^2}{r^3}\,(\boldsymbol{R} + R\boldsymbol{\beta})_{\rm r} + \frac{1}{cr^3}\left\{\boldsymbol{R}\times\left[(\boldsymbol{R} + R\boldsymbol{\beta})_{\rm r}\times\frac{{\rm d}\boldsymbol{\beta}}{{\rm d}t_{\rm r}}\right]\right\}\Bigg|_{\rm r}\,, \tag{9.28}$$

where we have added the index $_{\rm r}$ as a remainder that all quantities on the r.h.s. of (9.28) must be taken at the retarded time $t_{\rm r}$.

This equation for the electric field of a moving charge has two distinct parts. The first part is inversely proportional to the square of the distance between radiation source and observer and depends only on the velocity of the charge. For a charge at rest β=0 this term reduces to the Coulomb field of a point charge q. The area close to the radiating charge where this term is dominant is called the Coulomb regime. The field is directed toward the observer for a positive charge at rest and tilts into the direction of propagation as the velocity of the charge increases. For highly relativistic particles we note the Coulomb field becomes very small.

We will not further consider this regime since we are interested only in the radiation field far away from the moving charge. The second term in (9.28) is inversely proportional to the distance from the charge and depends on the velocity as well as on the acceleration of the charge. This term scales linear with the distance r falling off much slower than the Coulomb term and therefore reaches out to large distances from the radiation source. We call this regime the radiation regime and the remainder of this chapter will focus on the discussion of the radiation from moving charges. The electrical field in the radiation regime is

$$[4\pi\epsilon_0]\left.\frac{\boldsymbol{E}(t)}{q}\right|_{\rm rad} = \frac{1}{cr^3}\left\{\boldsymbol{R}\times\left[(\boldsymbol{R}+R\boldsymbol{\beta})_{\rm r}\times\frac{{\rm d}\boldsymbol{\beta}}{{\rm d}t_{\rm r}}\right]\right\}\Bigg|_{\rm r} . \tag{9.29}$$

The polarization of the electric field at the location of the observer is purely orthogonal to the direction of observation $\mathbf{R}$. Similar to the derivation of the electric field, we can derive the expression for the magnetic field and get from (9.1) with (9.11)

$$\boldsymbol{B} = \boldsymbol{\nabla}_{\rm r}\times\boldsymbol{A} = q\left[\boldsymbol{\nabla}_{\rm r}\times\frac{\boldsymbol{\beta}}{r}\right] = \frac{q}{r}\left[\boldsymbol{\nabla}_{\rm r}\times\boldsymbol{\beta}\right] - \frac{q}{r^2}\left[\boldsymbol{\nabla}_{\rm r} r\times\boldsymbol{\beta}\right] , \tag{9.30}$$

where again all parameters on the r.h.s. must be evaluated at the retarded time. The evaluation of the "retarded" curl operation $\boldsymbol{\nabla}_{\rm r}\times\boldsymbol{\beta}$ becomes obvious if we evaluate one component only, for example, the x component

$$\left(\frac{\partial}{\partial y}+\frac{\partial t_{\rm r}}{\partial y}\frac{\partial}{\partial t_{\rm r}}\right)\beta_z - \left(\frac{\partial}{\partial z}+\frac{\partial t_{\rm r}}{\partial z}\frac{\partial}{\partial t_{\rm r}}\right)\beta_y = [\boldsymbol{\nabla}\times\boldsymbol{\beta}]_x + \left[\boldsymbol{\nabla}t_{\rm r}\times\frac{{\rm d}\boldsymbol{\beta}}{{\rm d}t_{\rm r}}\right]_x . \tag{9.31}$$

In a similar way, we get the other components and find with (9.22) and the fact that the particle velocity $\boldsymbol{\beta}$ does not depend on the coordinates of the observation point ($\boldsymbol{\nabla}\times\boldsymbol{\beta}=0$),

$$\left[\boldsymbol{\nabla}_{\rm r} r\times\boldsymbol{\beta}\right] = \left[\boldsymbol{\nabla}\times\boldsymbol{\beta}\right] + \left[\boldsymbol{\nabla}t_{\rm r}\times\frac{{\rm d}\boldsymbol{\beta}}{{\rm d}t_{\rm r}}\right] = \frac{1}{cr}\left[\boldsymbol{R}\times\frac{{\rm d}\boldsymbol{\beta}}{{\rm d}t_{\rm r}}\right] ,$$

The gradient $\boldsymbol{\nabla}_{\rm r} r$ has been derived earlier in (9.18) and inserting this into (9.30) we find the magnetic field of an electrical charge moving with velocity
$\mathbf{v}$

$$[4\pi c\epsilon_0]\,\frac{\boldsymbol{B}}{q} = -\frac{1}{r^2}\,(\boldsymbol{\beta}\times\boldsymbol{n}) - \frac{R}{cr^2}\left[\frac{\mathrm{d}\boldsymbol{\beta}}{\mathrm{d}t}\times\boldsymbol{n}\right]\Big|_{\mathrm{r}} + \frac{R}{r^3}\left(\boldsymbol{\beta}\boldsymbol{n}+\beta^2+\frac{1}{c}\frac{\mathrm{d}\boldsymbol{\beta}}{\mathrm{d}t}\boldsymbol{R}\right)[\boldsymbol{\beta}\times\boldsymbol{n}]\Big|_{\mathrm{r}} \,. \tag{9.32}$$

Again, there are two distinct groups of field terms. In case of the electrical field the terms that fall off like the square of the distance are the Coulomb fields. For magnetic fields such terms appear only if the charge is moving $\beta\neq 0$ and are identical to the Biot–Savart fields. Here we concentrate only on the far fields or radiation fields which decay inversely proportional to the distance from the source. The magnetic radiation field is then given by

$$[4\pi c\epsilon_0]\,\frac{\boldsymbol{B}(t)}{q}\bigg|_{\mathrm{rad}} = -\frac{R}{cr^2}\left[\frac{\mathrm{d}\boldsymbol{\beta}}{\mathrm{d}t}\times\boldsymbol{n}\right]_{\mathrm{r}} + \frac{R}{cr^3}\left(\frac{\mathrm{d}\boldsymbol{\beta}}{\mathrm{d}t}\boldsymbol{R}\right)[\boldsymbol{\beta}\times\boldsymbol{n}]_{\mathrm{r}} \tag{9.33}$$

Comparing the magnetic field (9.33) with the electrical field (9.28) reveals a very simple correlation between both fields. The magnetic field can be obtained from the electric field, and vice versa, by mere vector multiplication with the unit vector $\boldsymbol{n}$

$$\boldsymbol{B} = \tfrac{1}{|c|}\,[\boldsymbol{E}\times\boldsymbol{n}]_{\mathrm{r}} \,. \tag{9.34}$$

From this equation we can deduce special properties for the field directions by noting that the electric and magnetic fields are orthogonal to each other and both are orthogonal to the direction of observation $\boldsymbol{n}$. The existence of electric and magnetic fields can give rise to radiation for which the Poynting vector is

$$\boldsymbol{S} = [4\pi c\epsilon_0]\,\frac{c}{4\pi}\,[\boldsymbol{E}\times\boldsymbol{B}]_{\mathrm{r}} = [4\pi c\epsilon_0]\,\frac{1}{4\pi}\,[\boldsymbol{E}\times(\boldsymbol{E}\times\boldsymbol{n})]_{\mathrm{r}} \,. \tag{9.35}$$

Using again the vector relation (B.10) and noting that the electric field is normal to $\boldsymbol{n}$, we get for the Poynting vector or the radiation flux in the direction to the observer

$$\boldsymbol{S} = -\,[4\pi c\epsilon_0]\,\frac{c}{4\pi}\,\boldsymbol{E}_{\mathrm{r}}^2\boldsymbol{n}\big|_{\mathrm{r}} \,. \tag{9.36}$$

Equation (9.36) defines the energy flux density measured at the observation point P and time t in form of synchrotron radiation per unit cross section and parallel to the direction of observation $\boldsymbol{n}$. All quantities expressing this energy flux are still to be taken at the retarded time. For practical reasons it becomes desirable to express the Poynting vector at the retarded time as well. The energy flux at the observation point, in terms of the retarded time is then $\mathrm{d}W/\mathrm{d}t_{\mathrm{r}} = (\mathrm{d}W/\mathrm{d}t)\,(\mathrm{d}t/\mathrm{d}t_{\mathrm{r}})$ and instead of (9.36) we express the Poynting vector with (9.16) like

$$\boldsymbol{S}_{\mathrm{r}} = \boldsymbol{S}\frac{\mathrm{d}\,t}{\mathrm{d}\,t_{\mathrm{r}}} = -\,[4\pi c\epsilon_0]\,\frac{c}{4\pi}\boldsymbol{E}^2\,[\;(1+\boldsymbol{\beta}\boldsymbol{n})\;\boldsymbol{n}\,]_{\mathrm{r}} \,. \tag{9.37}$$

The Poynting vector in this form can be readily used for calculations like those determining the spatial distribution of the radiation power.

9.2 Total Radiation Power and Energy Loss

So far, no particular choice of the reference system has been assumed, but a particularly simple reference frame $\mathcal{L}^*$ is the one which moves uniformly with the charge before acceleration. From now on, we use a single particle with a charge e. To an observer in this reference system, the charge moves due to acceleration and the electric field in the radiation regime is from (9.29)

$$\boldsymbol{E}^*(t) = \frac{1}{[4\pi\epsilon_0]}\,\frac{e}{cR}\left[\boldsymbol{n}\times(\boldsymbol{n}\times\frac{\mathrm{d}\boldsymbol{\beta}^*}{\mathrm{d}t}\,]\right|_{\mathrm{r}}\,. \tag{9.38}$$

The synchrotron radiation power per unit solid angle and at distance R from the source is from (9.37) with $\boldsymbol{v}=0$

$$\frac{\mathrm{d}P^*}{\mathrm{d}\Omega} = -\boldsymbol{n}\boldsymbol{S}^*\,R_{\mathrm{r}}^2 = [4\pi c\epsilon_0]\,\frac{c}{4\pi}\,\boldsymbol{E}^{*2}R^2\big|_{\mathrm{r}}\,. \tag{9.39}$$

Introducing the classical particle radius $r_{\mathrm{c}}mc^2 = e^2/[4\pi\epsilon_0]$ to obtain expressions which are independent of electromagnetic units and with (9.38)

$$\frac{\mathrm{d}P^*}{\mathrm{d}\Omega} = \frac{r_{\mathrm{c}}mc^2}{4\pi c}\left|\,\boldsymbol{n}\times\left(\boldsymbol{n}\times\frac{\mathrm{d}\boldsymbol{\beta}^*}{\mathrm{d}t}\,\right)\right|_{\mathrm{r}}^2 = \frac{r_{\mathrm{c}}mc^2}{4\pi c}\,\left|\frac{\mathrm{d}\boldsymbol{\beta}^*}{\mathrm{d}t}\right|_{\mathrm{r}}^2\sin^2\vartheta_{\mathrm{r}}\,, \tag{9.40}$$

where ϑ_{r} is the retarded angle between the direction of acceleration and the direction of observation $\boldsymbol{n}$. Integration over all solid angles gives the total radiated power. With $\mathrm{d}\Omega = \sin\vartheta_{\mathrm{r}}\mathrm{d}\vartheta_{\mathrm{r}}\mathrm{d}\phi$, where ϕ is the azimuthal angle with respect to the direction of acceleration, the total radiation power is in agreement with (3.1)

$$P^* = \frac{2}{3}r_{\mathrm{c}}mc\left|\frac{\mathrm{d}\boldsymbol{\beta}^*}{\mathrm{d}t}\right|_{\mathrm{r}}^2\,. \tag{9.41}$$

This equation has been derived first by Larmor [49] within the realm of classical electrodynamics. The emission of a quantized photon, however, exerts a recoil on the electron varying its energy slightly. Schwinger [50] investigated this effect and derived a correction to the radiation power like

$$P^* = P^*_{\mathrm{classical}}\left(1-\tfrac{55}{16\sqrt{3}}\frac{\epsilon_{\mathrm{c}}}{E}\right)\,, \tag{9.42}$$

where ϵ_{c} is the critical photon energy and E the electron energy. The correction is generally very small and we ignore therefore this quantum mechanical effect in our discussions.

9.2.1 Transition Radiation

Digressing slightly from the discussion of synchrotron radiation we turn our attention to the solution of (9.39). Generally, we do not know the fields $\boldsymbol{E}^*$

and to solve (9.40) we need to know more about the particular trajectory of the particle motion. In the case of transition radiation, we have, however, all information to formulate a solution. Transition radiation is emitted when a charged particle passes through the boundary of two media with different dielectric constant. We will not go into the detailed general theory of transition radiation but concentrate on the case where a charged particle passes through a thin metallic foil in vacuum. As the particle passes through the foil backward transition radiation is emitted when the particle enters the foil and forward radiation is emitted when it appears on the other side. The emitted radiation energy can be derived directly from (9.39) .First, we replace the electric radiation field by the magnetic field component and (9.39) becomes simply

$$\frac{\mathrm{d}\varepsilon(t)}{\mathrm{d}t} = [4\pi c\epsilon_0]\,\frac{c}{4\pi}\,\boldsymbol{B}^{*2}(t)R^2\big|_{\mathrm{r}}\,\mathrm{d}\Omega\,. \tag{9.43}$$

From Parceval's theorem $(B.32)$ we know that

$$\int_{-\infty}^{\infty} B^2(t)\,\mathrm{d}t = \frac{1}{2\pi}\int_{-\infty}^{\infty} B^2(\omega)\,\mathrm{d}\omega\,, \tag{9.44}$$

where $B(t) = \frac{1}{2\pi}\int B(\omega)\,\mathrm{e}^{-\mathrm{i}\omega t}\,\mathrm{d}\omega$ and $B(\omega) = \int B(t)\,\mathrm{e}^{\mathrm{i}\omega t}\,\mathrm{d}t$. The emission of transition radiation occurs in a very short time $\tau = \omega_{\mathrm{p}}^{-1}$, where ω_{p} is the plasma frequency. For this reason, the transition radiation frequency reaches into the x-ray regime. We limit ourselves here to frequencies ω, which are much lower such that $\tau \ll \omega^{-1}$. The magnetic field is nonzero only during the emission process and we can therefore set

$$B(\omega) = \int_{-\infty}^{\infty} B(t)\,e^{\mathrm{i}\omega t}\,\mathrm{d}t \approx \int_{-\tau/2}^{\tau/2} B(t)\,\mathrm{d}t\,. \tag{9.45}$$

To solve this integral we recall the definition of the vector potential $\boldsymbol{B}(t) = \nabla \times \boldsymbol{A}_{\mathrm{r}}$ and keep in mind that all quantities are to be taken at the retarded time. Expressing in component form $\nabla \times \boldsymbol{A}_{\mathrm{r}} = \left\{\frac{\partial A_z}{\partial y} - \frac{\partial A_y}{\partial z}, \frac{\partial A_x}{\partial z} - \frac{\partial A_z}{\partial x}, \frac{\partial A_y}{\partial z} - \frac{\partial A_z}{\partial x}\right\}_{t_{\mathrm{r}} = t - \frac{1}{c}R(t)}$ the derivatives are $\frac{\partial A_z}{\partial y} = \frac{\partial A_z}{\partial t_{\mathrm{r}}}\frac{\partial t_{\mathrm{r}}}{\partial y}$ etc. With $\frac{\partial t_{\mathrm{r}}}{\partial y} = \frac{1}{c}\frac{y_{\mathrm{r}} - y}{R} = \frac{n_y}{c}$ we get $\frac{\partial A_z}{\partial y} - \frac{\partial A_y}{\partial z} = \frac{1}{c}\frac{\partial A_z}{\partial t_{\mathrm{r}}}n_y - \frac{1}{c}\frac{\partial A_y}{\partial t_{\mathrm{r}}}n_z$ or finally

$$\boldsymbol{B}(t) = \nabla \times \boldsymbol{A}_{\mathrm{r}} = \frac{1}{c}\boldsymbol{n}_{\mathrm{r}} \times \frac{\partial}{\partial t_{\mathrm{r}}}\boldsymbol{A}_{\mathrm{r}} = \frac{1}{c}\frac{\partial}{\partial t_{\mathrm{r}}}\left[\boldsymbol{n} \times \boldsymbol{A}\right]_{\mathrm{r}}\,. \tag{9.46}$$

The magnetic field spectrum (9.45) becomes then simply

$$B(\omega) = \int_{-\tau/2}^{\tau/2} B(t)\,\mathrm{d}t = \frac{1}{c}\left[\boldsymbol{n} \times \boldsymbol{A}\right]_{\mathrm{r}}\Big|_{\mathrm{initial}}^{\mathrm{final}}\,. \tag{9.47}$$

Initially, while the electron has not yet vanished into the metallic foil, the vector potential is made up of the Lièнard–Wiechert potentials of a free electron and its image charge (a positron) moving in the opposite direction. The vector potential is therefore

$$\boldsymbol{A} = \underbrace{\frac{e\boldsymbol{\beta}}{R(1+\boldsymbol{\beta}\boldsymbol{n})}}_{\text{electron}} + \underbrace{\frac{e\boldsymbol{\beta}}{R(1-\boldsymbol{\beta}\boldsymbol{n})}}_{\text{positron}} . \tag{9.48}$$

Instead of (9.43) we use the spectral radiation energy $\mathrm{d}\varepsilon(\omega) = [4\pi c\epsilon_0]\,\frac{c}{4\pi}R^2\mathrm{d}\Omega\,\frac{1}{2\pi}\boldsymbol{B}_{\mathrm{r}}^{*2}(t)\,\mathrm{d}\omega\,2$, where the extra factor of two comes from using only positive frequencies $\omega > 0$, and get with (9.48) and $e^2 = r_{\mathrm{e}}mc^2$

$$\begin{aligned}\frac{\mathrm{d}^2\varepsilon}{\mathrm{d}\omega\mathrm{d}\Omega} &= \frac{1}{4\pi^2}\frac{r_{\mathrm{e}}mc^2}{c}\left\{\frac{\boldsymbol{n}\times\boldsymbol{\beta}}{1+\boldsymbol{\beta}\boldsymbol{n}} + \frac{\boldsymbol{n}\times\boldsymbol{\beta}}{1-\boldsymbol{\beta}\boldsymbol{n}}\right\}^2 \\ &= \frac{r_{\mathrm{e}}mc^2}{\pi^2 c}\underbrace{|\boldsymbol{n}\times\boldsymbol{z}|^2}_{\sin^2\vartheta}\left(\frac{\beta}{1-\beta^2\underbrace{(\boldsymbol{n}\boldsymbol{z})^2}_{\cos^2\vartheta}}\right)^2 ,\end{aligned}$$

where we used $\boldsymbol{\beta} \approx \beta\boldsymbol{z}$ and where $\boldsymbol{z}$ is the unit vector along the z-axis. The emission angle ϑ is taken with respect to the z-axis. The spectral and spatial transition radiation distribution from a single electron is finally

$$\frac{\mathrm{d}^2\varepsilon}{\mathrm{d}\omega\mathrm{d}\Omega} = \frac{r_{\mathrm{e}}mc^2}{\pi^2 c}\frac{\beta^2\sin^2\vartheta}{\left(1-\beta^2\cos^2\vartheta\right)^2} . \tag{9.49}$$

The spatial radiation distribution of transition radiation is shown in Fig. 9.2. No radiation is emitted along the axis $\vartheta = 0$ while the radiation intensity reaches a maximum at an emission angle of $1/\gamma$. Equation (9.49) does not exhibit any frequency dependence, which is due to the fact that the emission process occurs in a very short time generating a uniform spectrum. Very high frequencies in the x-ray regime, where the spectral intensity is expected to drop, have been excluded in this derivation.

Integrating (9.49) over a half space, we get

$$\begin{aligned}\frac{\mathrm{d}\varepsilon}{\mathrm{d}\omega} &= \frac{2r_{\mathrm{e}}mc^2}{\pi c}\int_0^{\pi/2}\frac{\beta^2\sin^2\vartheta}{\left(1-\beta^2\cos^2\vartheta\right)^2}\sin\vartheta\,\mathrm{d}\vartheta \\ &= \frac{2r_{\mathrm{e}}mc^2}{\pi c}\frac{1}{4\beta}\left[\left(1+\beta^2\right)\ln\frac{1+\beta}{1-\beta} - 2\beta\right] ,\end{aligned} \tag{9.50}$$

which is for relativistic particles $\gamma \gg 1$

$$\frac{\mathrm{d}\varepsilon(\omega)}{\mathrm{d}\omega} \approx \frac{2r_{\mathrm{e}}mc^2}{\pi c}\ln\gamma . \tag{9.51}$$

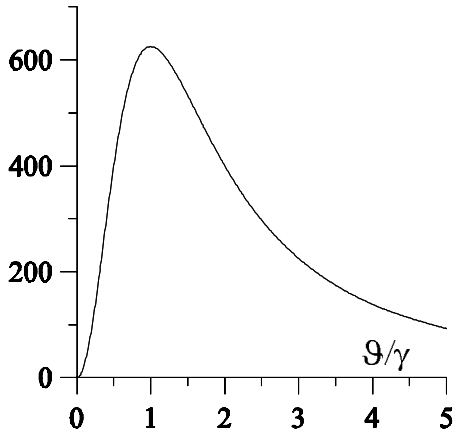

Fig. 9.2. Intensity distribution $\frac{\mathrm{d}^2\varepsilon}{\mathrm{d}\omega\mathrm{d}\Omega}\frac{\pi^2 c}{r_\mathrm{c}mc^2}$ of transition radiation

The spectral energy emitted into one half space by a single electron in form of transition radiation is uniform for all frequencies reaching up into the soft x-ray regime and depends only logarithmically on the particle energy.

9.2.2 Synchrotron Radiation Power

Coming back to synchrotron radiation we must define the electron motion in great detail. It is this motion which determines many of the photon beam characteristics. The radiation power and spatial distribution in the electron system is identical to that from a linear microwave antenna being emitted normal to the direction of acceleration with a $\sin^2$-distribution.

In Section C.8 we have shown that the radiation power is invariant to Lorentz transformations, we may set $P = P^*$ and the total radiation power in the laboratory system is

$$P = \tfrac{2}{3}\, r_\mathrm{c} mc\, \gamma^6 \left[\dot{\boldsymbol{\beta}}^2 - (\boldsymbol{\beta}\times\dot{\boldsymbol{\beta}})^2\right] . \tag{9.52}$$

which has been discussed before leading to (3.2). Equation (9.52) expresses the radiation power in a simple way and allows us to calculate other radiation characteristics based on beam parameters in the laboratory system. Specifically, we will distinguish between acceleration parallel $\left.\frac{\mathrm{d}\boldsymbol{\beta}}{\mathrm{d}t}\right|_\parallel$ and perpendicular $\left.\frac{\mathrm{d}\boldsymbol{\beta}}{\mathrm{d}t}\right|_\perp$ to the propagation $\boldsymbol{\beta}$ of the charge and set therefore

$$\frac{\mathrm{d}\boldsymbol{\beta}}{\mathrm{d}t} = \left.\frac{\mathrm{d}\boldsymbol{\beta}}{\mathrm{d}t}\right|_\parallel + \left.\frac{\mathrm{d}\boldsymbol{\beta}}{\mathrm{d}t}\right|_\perp . \tag{9.53}$$

Insertion into (9.52) shows the total radiation power to consist of separate contributions from parallel and orthogonal acceleration. Separating both contributions, we get the synchrotron radiation power for both parallel and transverse acceleration, respectively

$$P_{\parallel} = \tfrac{2}{3} r_{\mathrm{c}} mc\, \gamma^6 \left.\frac{\mathrm{d}\boldsymbol{\beta}}{\mathrm{d}t}\right|_{\parallel}^{2}, \tag{9.54}$$

$$P_{\perp} = \tfrac{2}{3} r_{\mathrm{c}} mc\, \gamma^4 \left.\frac{\mathrm{d}\boldsymbol{\beta}}{\mathrm{d}t}\right|_{\perp}^{2}. \tag{9.55}$$

Expressions have been derived that define the radiation power for parallel acceleration like in a linear accelerator or orthogonal acceleration found in circular accelerators or deflecting systems. We note a similarity for both contributions except for the energy dependence. At relativistic energies, the same acceleration force leads to much less radiation if the acceleration is parallel to the motion of the particle compared to orthogonal acceleration. Parallel acceleration is related to the accelerating force $F_{\parallel}$ by $\boldsymbol{v}_{\parallel} = \frac{1}{\gamma^3}\frac{\mathrm{d}\boldsymbol{p}_{\parallel}}{\mathrm{d}t}$ and after insertion into (9.54) the radiation power due to parallel acceleration becomes

$$P_{\parallel} = \frac{2}{3}\frac{r_{\mathrm{c}}\, c}{mc^2}\left(\frac{\mathrm{d}\boldsymbol{p}_{\parallel}}{\mathrm{d}t}\right)^2. \tag{9.56}$$

The radiation power for acceleration along the propagation of the charged particle is therefore independent of the energy of the particle and depends only on the accelerating force or with $\mathrm{d}\boldsymbol{p}_{\parallel}/\mathrm{d}t = \beta c\, \mathrm{d}E/\mathrm{d}x$ on the energy increase per unit length, $\mathrm{d}E/\mathrm{d}x$, of the accelerator.

In contrast, we find very different radiation characteristics for transverse acceleration as it happens, for example, during the transverse deflection of a charged particle in a magnetic field. The transverse acceleration $\boldsymbol{v}_{\perp}$ is expressed by the Lorentz force

$$\frac{\mathrm{d}\,\boldsymbol{p}_{\perp}}{\mathrm{d}\,t} = \gamma m \dot{\boldsymbol{v}}_{\perp} = [c]\; e\,[\boldsymbol{\beta}\times\boldsymbol{B}] \tag{9.57}$$

and after insertion into (9.55) the radiation power from transversely accelerated particles becomes

$$P_{\parallel} = \tfrac{2}{3}\, r_{\mathrm{c}} mc\, \gamma^2 \left(\frac{\mathrm{d}\,\boldsymbol{p}_{\perp}}{\mathrm{d}\,t}\right)^2. \tag{9.58}$$

Comparing (9.56) with (9.58) we find that the same accelerating force leads to a much higher radiation power by a factor γ^2 for transverse acceleration with respect to longitudinal acceleration. For all practical purposes technical limitations prevent the occurrence of sufficient longitudinal acceleration to generate noticeable radiation. We express the deflecting magnetic field $\boldsymbol{B}$ by the bending radius ρ and get the instantaneous synchrotron radiation power

$$P_\gamma = \tfrac{2}{3}\, r_\mathrm{c} mc^2\, \frac{c\,\beta^4\gamma^4}{\rho^2}, \tag{9.59}$$

or in more practical units

$$P_\gamma(\mathrm{GeV/s}) = \frac{c\,C_\gamma}{2\pi}\,\frac{E^4}{\rho^2}\,, \tag{9.60}$$

where we use *Sands'* definition of the radiation constant [14]

$$C_\gamma = \frac{4\pi}{3}\frac{r_\mathrm{c}}{(mc^2)^3} = 8.8575\ \times 10^{-5}\quad \mathrm{m/GeV^3}\,. \tag{9.61}$$

This numerical value is correct for relativistic electrons and positrons and must be modified for other particles.

From here on we will stop considering longitudinal acceleration unless specifically mentioned and replace therefore the index $_\perp$ by setting $P_\perp = P_\gamma$. We also restrict from now on the discussion to singly charged particles and set $q = e$ ignoring extremely high energies where multiple charged ions start to radiate.

The electromagnetic radiation of charged particles in transverse magnetic fields is proportional to the fourth power of the particle momentum $\beta\gamma$ and inversely proportional to the square of the bending radius ρ. The radiation emitted by charged particles being deflected in magnetic fields is called synchrotron radiation. The synchrotron radiation power increases very fast for high energy particles and provides the most severe limitation to the maximum energy achievable in circular accelerators. We note also a strong dependence on the kind of particles involved in the process of radiation. Because of the much heavier mass of protons compared to the lighter electrons, we find appreciable synchrotron radiation only in circular electron accelerators. The radiation power of protons actually is smaller compared to that for electrons by the fourth power of the mass ratio or by the factor

$$\frac{P_\mathrm{e}}{P_\mathrm{p}} = 1836^4 = 1.36\ \ 10^{13}\,. \tag{9.62}$$

In spite of this enormous difference measurable synchrotron radiation has been predicted by Coisson [15] and was indeed detected at the 400 GeV proton synchrotron SPS at CERN [16, 17]. Substantial synchrotron radiation is expected in circular proton accelerators at a beam energy of 10 TeV and more.

The knowledge of the synchrotron radiation power allows us now to calculate the energy loss of a particle per turn in a circular accelerator by integrating the radiation power along the circumference L_0 of the circular accelerator

$$\Delta E = \oint P_\gamma\,\mathrm{d}t = \tfrac{2}{3}\, r_\mathrm{c}\, mc^2\beta^3\gamma^4 \int\limits_{L_0} \frac{\mathrm{d}s}{\rho^2}\,. \tag{9.63}$$

If we assume an isomagnetic lattice where the bending radius is the same for all bending magnets $\rho = \text{const}$, and integrate around a circular accelerator, the energy loss per turn due to synchrotron radiation is given by

$$\Delta E = \tfrac{4\pi}{3} r_\mathrm{c}\, mc^2 \beta^3 \frac{\gamma^4}{\rho}\,. \tag{9.64}$$

The integration obviously is to be performed only along those parts of the circular accelerator where synchrotron radiation occurs or along bending magnets only. In more practical units, the energy loss of relativistic electrons per revolution in a circular accelerator with an isomagnetic lattice and a bending radius ρ is given by

$$\Delta E = C_\gamma \frac{E^4}{\rho}\,. \tag{9.65}$$

From this energy loss per particle in each turn we calculate the total synchrotron radiation power for a beam of N_e particles. The total synchrotron radiation power for a single particle is its energy loss multiplied by the revolution frequency of the particle around the circular orbit. If L_0 is the circumference of the orbit we have for the revolution frequency $f_\mathrm{rev} = \beta c / L_0$ and for the circulating particle current $I = e f_\mathrm{rev} N_e$. The total synchrotron radiation power is then

$$P_\gamma(\mathrm{MW}) = C_\gamma \frac{E^4(\mathrm{GeV})}{\rho(\mathrm{m})}\, I(\mathrm{A})\,. \tag{9.66}$$

The total synchrotron radiation power scales like the fourth power of energy and is inversely proportional to the bending radius. The strong dependence of the radiation on the particle energy causes severe practical limitations on the maximum achievable energy in a circular accelerator.

9.3 Radiation Lobes

Expressions for the radiation fields and Poynting vector exhibit strong vectorial dependencies on the directions of motion and acceleration of the charged particles and on the direction of observation. These vectorial dependencies indicate that the radiation may not be emitted isotropic but rather into specific directions forming characteristic radiation patterns. In this section we will derive these spatial radiation characteristics and determine the direction of preferred radiation emission.

In (9.40) the radiation power per unit solid angle is expressed in the reference frame of the particle

$$\frac{\mathrm{d}P}{\mathrm{d}\Omega} = \frac{r_\mathrm{c} mc}{4\pi} \dot{\beta}_\mathrm{r}^{*2} \sin^2 \Theta \tag{9.67}$$

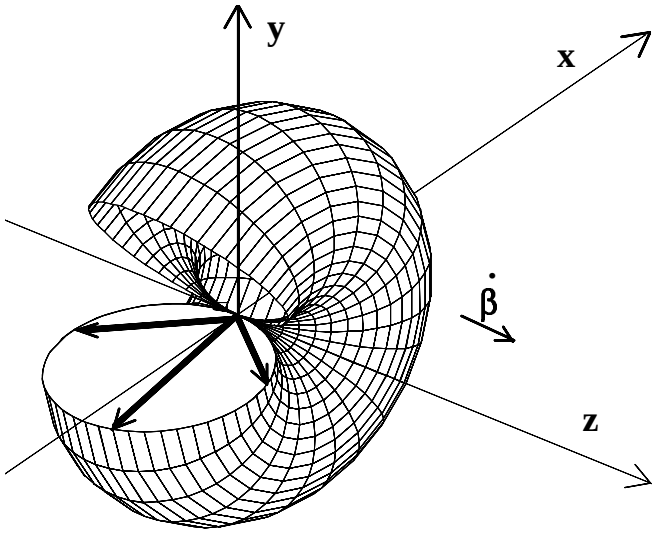

Fig. 9.3. Radiation pattern in the particle frame of reference or for nonrelativistic particles in the laboratory system

showing a particular directionality of the radiation as shown in Fig. 9.3. The radiation power is mainly concentrated in the x, y-plane and is proportional to $\sin^2 \Theta$ where Θ is the angle between the direction of acceleration, in this case the z-axis, and the direction of observation $\boldsymbol{n}$. The radiation pattern in Fig. 9.3 is formed by the end points of vectors with the length $\mathrm{d}P/\mathrm{d}\Omega$ and angles Θ with respect to the z-axis. Because of symmetry, the radiation is isotropic with respect to the polar angle φ and therefore, the radiation pattern is rotation symmetric about the direction of acceleration or in this case about the z-axis.

This pattern is the correct representation of the radiation for the reference frame of the radiating particle. We may, however, also consider this pattern as the radiation pattern from non relativistic particles like that from a linear radio antenna. For relativistic particles the radiation pattern differs significantly from the non relativistic case. The Poynting vector in the form of (9.37) can be used to calculate the radiation power per unit solid angle in the direction to the observer $-\boldsymbol{n}$

$$\frac{\mathrm{d}P}{\mathrm{d}\Omega} = -\left.\boldsymbol{n}\boldsymbol{S}\,R^2\right|_{\mathrm{r}} = [4\pi c\epsilon_0]\,\frac{c}{4\pi}\left.\boldsymbol{E}^2\,(1+\boldsymbol{\beta}\boldsymbol{n})\,R^2\right|_{\mathrm{r}} . \tag{9.68}$$

We calculate the spatial distribution of the synchrotron radiation for the case of acceleration orthogonal to the propagation of the particle as it happens in beam transport systems where the particles are deflected by a transverse magnetic fields. The particle is assumed to be located at the origin of a right-handed coordinate system as shown in Fig. 9.4 propagating in the z-direction

and the orthogonal acceleration in this coordinate system occurs along the x-axis.

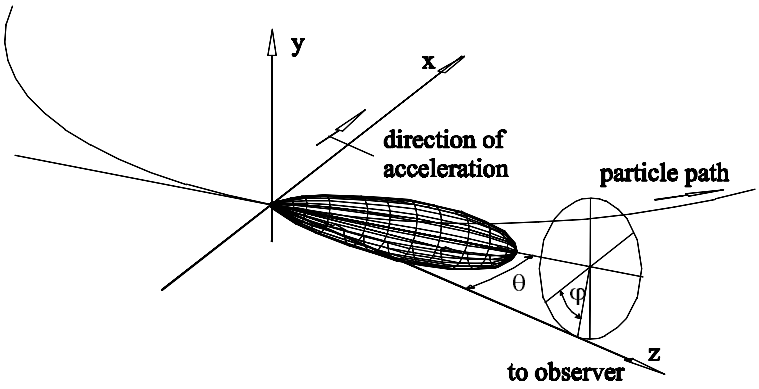

Fig. 9.4. Radiation geometry in the laboratory frame of reference for highly relativistic particles

With the expression (9.29) for the electric fields in the radiation regime the spatial radiation power distribution (9.68) becomes

$$\frac{\mathrm{d}P}{\mathrm{d}\Omega} = \frac{c}{4\pi} r_\mathrm{e} mc^2 \frac{R^5}{c^3 r^5} \left\{ \boldsymbol{n} \times \left[(\boldsymbol{n} + \boldsymbol{\beta}) \times \dot{\boldsymbol{\beta}} \right] \right\}^2 . \tag{9.69}$$

We will now replace all vectors by their components to obtain the directional dependency of the synchrotron radiation. The vector $\boldsymbol{n}$ pointing from the observation point to the source point of the radiation has from Fig. 9.4 the components

$$\boldsymbol{n} = (-\sin\theta\, \cos\varphi, -\sin\theta\, \sin\varphi, \cos\theta) , \tag{9.70}$$

where the angle θ is the angle between the direction of particle propagation and the direction of emission of the synchrotron light $-\boldsymbol{n}$. The x-component of the acceleration can be derived from the Lorentz equation

$$\gamma m \dot{\boldsymbol{v}}_x = \frac{\mathrm{d}p_x}{\mathrm{d}t} = [c]\; e\beta_z B_y . \tag{9.71}$$

With $v_z \approx v$ we have $1/\rho = [c]\; eB_y/cp = [c]\; eB_y/(\gamma mcv)$ and the acceleration vector is

$$\dot{\boldsymbol{v}}_\perp = (\dot{v}, 0, 0) = \left(\frac{v^2}{\rho}, 0, 0 \right) . \tag{9.72}$$

The velocity vector is

$$\boldsymbol{v} = (0, 0, v) \tag{9.73}$$

and after replacing the double vector product in (9.69) by a single vector sum

$$\boldsymbol{n}\times[(\boldsymbol{n}+\boldsymbol{\beta})\times\boldsymbol{\beta}] = (\boldsymbol{n}+\boldsymbol{\beta})\,(\boldsymbol{n}\,\boldsymbol{\beta}) - \boldsymbol{\beta}(\mathbf{1}+\boldsymbol{n}\,\boldsymbol{\beta})\,, \tag{9.74}$$

we may now square the r.h.s. of (9.69) and replace all vectors by their components. The denominator in (9.69) then becomes

$$r^5 = R^5(1+\boldsymbol{n}\boldsymbol{\beta})^5 = R^5(1-\beta\cos\theta)^5\,, \tag{9.75}$$

and the full expression for the radiation power exhibiting the spatial distribution is finally

$$\frac{\mathrm{d}P}{\mathrm{d}\Omega} = \frac{r_\mathrm{e} mc^2 c}{4\pi}\frac{\beta^4}{\rho^2}\frac{(1-\beta\cos\theta)^2 - (1-\beta^2)\sin^2\theta\cos^2\varphi}{(1-\beta\cos\theta)^5}\,. \tag{9.76}$$

This equation describes the instantaneous synchrotron radiation power per unit solid angle from charged particles moving with velocity v and being accelerated normal to the propagation by a magnetic field. The angle θ is the angle between the direction of observation $-\boldsymbol{n}$ and propagation $\boldsymbol{v}/v$. Integration over all angles results again in the total synchrotron radiation power (9.59).

In Fig. 9.5 the radiation power distribution is shown in real space as derived from (9.76). We note that the radiation is highly collimated in the forward direction along the z-axis which is also the direction of particle propagation. Synchrotron radiation in particle accelerators or beam lines is emitted whenever there is a deflecting electromagnetic field and emerges mostly tangentially from the particle trajectory. An estimate of the typical opening angle can be derived from (9.76). We set $\varphi = 0$ and expand the cosine function for small angles $\cos\theta \approx 1 - \frac{1}{2}\theta^2$. With $\beta \approx 1 - \frac{1}{2}\gamma^{-2}$ we find the radiation power to scale like $(\gamma^{-2}+\theta^2)^{-3}$. The radiation power therefore is reduced to about one eighth the peak intensity at an emission angle of $\theta_\gamma = 1/\gamma$ or virtually all synchrotron radiation is emitted within an angle of

$$\theta_\gamma = \pm\frac{1}{\gamma} \tag{9.77}$$

with respect to the direction of the particle propagation.

From Fig. 9.5 we observe a slightly faster fall off for an azimuthal angle of $\varphi = 0$ which is in the plane of particle acceleration and propagation. Although the synchrotron radiation is emitted symmetrically within a small angle of the order of $\pm\frac{1}{\gamma}$ with respect to the direction of particle propagation, the radiation pattern from a relativistic particle as observed in the laboratory is very different in the deflecting plane from that in the nondeflecting plane. While the particle radiates from every point along its path, the direction of this path changes in the deflecting plane but does not in the nondeflecting

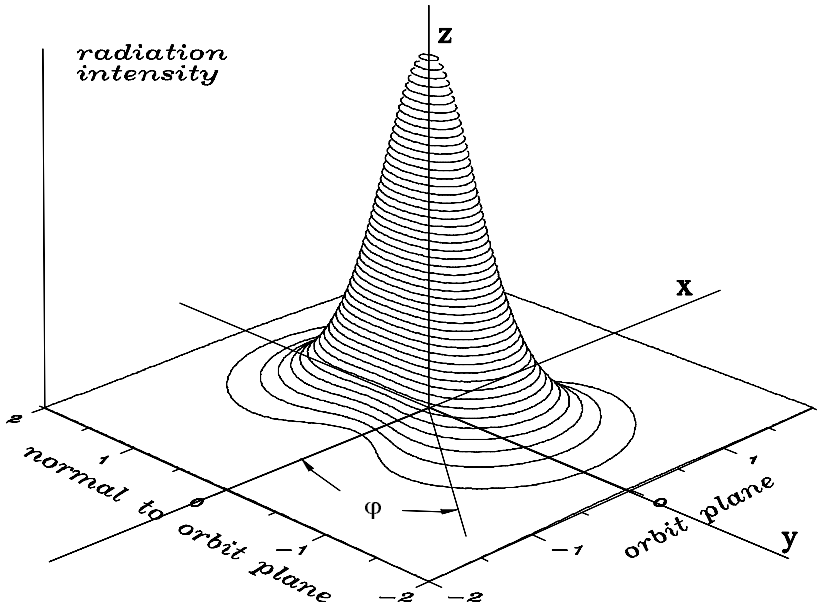

Fig. 9.5. Spatial synchrotron radiation distribution

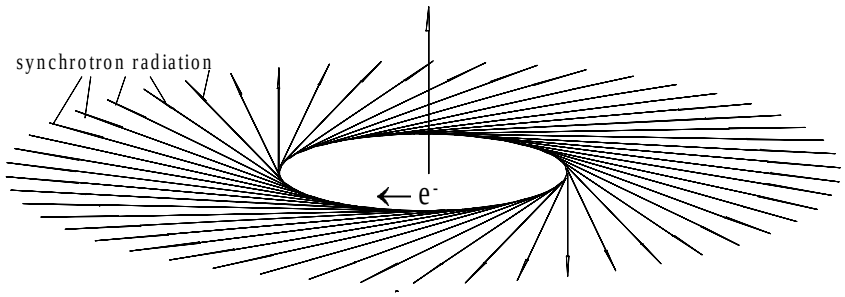

Fig. 9.6. Synchrotron radiation from a circular particle accelerator

plane. The synchrotron radiation pattern from a bending magnet therefore resembles the form of a swath where the radiation is emitted evenly and tangentially from every point of the particle trajectory as shown in Fig. 9.6.

The extreme collimation of the synchrotron radiation and its high intensity in high energy electron accelerators can cause significant heating problems as well as desorption of gas molecules from the surface of the vacuum chamber. In addition, the high density of thermal energy deposition on the vacuum chamber walls can cause significant mechanical stresses causing cracks in the material. A careful design of the radiation absorbing surfaces

to avoid damage to the integrity of the material is required. On the other hand, this same radiation is a valuable source of photons for a wide variety of research applications where, specifically, the collimation of the radiation together with the small source dimensions are highly desired features of the radiation.

9.4 Synchrotron Radiation Spectrum

Synchrotron radiation from relativistic charged particles is emitted over a wide spectrum of photon energies. The basic characteristics of this spectrum can be derived from simple principles as suggested in [19] and discussed in Chap. 3. The spectrum extends from very low photon energies up to about the critical photon energy

$$\varepsilon_{\mathrm{c}} = \tfrac{3}{2}\hbar c\frac{\gamma^3}{\rho}\,. \tag{9.78}$$

The significance of the critical photon energy is its definition for the upper bound for the synchrotron radiation spectrum. The spectral intensity falls off rapidly for photon energies above the critical photon energy. In practical units, the critical photon energy is

$$\epsilon_{\mathrm{c}}(\mathrm{keV}) = 2.218\,\frac{E^3(\mathrm{GeV})}{\rho(\mathrm{m})} = 0.665\,E^2(\mathrm{GeV})\,B(\mathrm{T})\,. \tag{9.79}$$

The synchrotron radiation spectrum from relativistic particles in a circular accelerator is made up of harmonics of the particle revolution frequency ω_0 and extends to values up to and beyond the critical frequency (9.78). Generally, a real synchrotron radiation beam from say a storage ring will not display this harmonic structure. The distance between the harmonics is extremely small compared to the extracted photon frequencies in the VUV and x-ray regime while the line width is finite due to the energy spread in a beam of many particles and the spectrum becomes therefore continuous. For a single pass of particles through a bending magnet in a beam transport line, we observe the same spectrum, although now genuinely continuous as can be derived with the use of Fourier transforms of a single light pulse. Specifically, the maximum frequency is the same assuming similar parameters.

9.5 Radiation Field in the Frequency Domain

Synchrotron radiation is emitted within a wide range of frequencies. As we have seen in the previous paragraph, a particle orbiting in a circular accelerator emits light flashes at the revolution frequency. We expect therefore in

the radiation frequency spectrum all harmonics of the revolution frequency up to very high frequencies limited only by the very short duration of the radiation pulse being sent into a particular direction toward the observer. The number of harmonics increases with beam energy and reaches at the critical frequency the order of γ^3.

The frequency spectrum of synchrotron radiation has been derived by many authors. In this text, we will stay closer to the derivation by Jackson [19] than others. The general method to derive the frequency spectrum is to transform the electric field from the time domain to the frequency domain by the use of Fourier transforms. Applying this method, we will determine the radiation characteristics of the light emitted by a single pass of a particle in a circular accelerator at the location of the observer. The electric field at the observation point has a strong time dependence and is given by (9.29) while the total radiation energy for one pass is from (9.38)

$$\frac{\mathrm{d}W}{\mathrm{d}\Omega} = -\int\limits_{-\infty}^{\infty} \frac{\mathrm{d}P}{\mathrm{d}\Omega}\,\mathrm{d}t = \int\limits_{-\infty}^{\infty} \boldsymbol{S}_\mathrm{r}\,\boldsymbol{n}\,R^2\mathrm{d}t = [4\pi c\epsilon_0]\,\frac{cR^2}{4\pi}\int\limits_{-\infty}^{\infty} \boldsymbol{E}_\mathrm{r}^2(t)\,\mathrm{d}t\,. \qquad (9.80)$$

The transformation from the time domain to the frequency domain is performed by a Fourier transform or an expansion into Fourier harmonics. This is the point where the particular characteristics of the transverse acceleration depend on the magnetic field distribution and are, for example, different in a single bending magnet as compared to an oscillatory wiggler magnet. We use here the method of Fourier transforms to describe the electric field of a single particle passing only once through a homogeneous bending magnet. In case of a circular accelerator the particle will appear periodically with the period of the revolution time and we expect a correlation of the frequency spectrum with the revolution frequency. This is indeed the case and we will later discuss the nature of this correlation. Expressing the electrical field $\mathbf{E}_\mathrm{r}(t)$ by its Fourier transform, we set

$$\boldsymbol{E}_\mathrm{r}(\omega) = \int_{-\infty}^{\infty} \boldsymbol{E}_\mathrm{r}(t)\,\mathrm{e}^{-\mathrm{i}\omega t}\mathrm{d}t\,, \qquad (9.81)$$

where $-\infty < \omega < \infty$. Applying Parseval's theorem we have

$$\int_{-\infty}^{\infty} |\boldsymbol{E}_\mathrm{r}(\omega)|^2\,\mathrm{d}\omega = 2\pi\int_{-\infty}^{\infty} |\boldsymbol{E}_\mathrm{r}(t)|^2\,\mathrm{d}t \qquad (9.82)$$

and the total absorbed radiation energy from a single pass of a particle is therefore

$$\frac{\mathrm{d}W}{\mathrm{d}\Omega} = [4\pi c\epsilon_0]\,\frac{cR^2}{8\pi^2}\int_{-\infty}^{\infty} |\boldsymbol{E}_\mathrm{r}(\omega)|^2\,\mathrm{d}\omega\,. \qquad (9.83)$$

Evaluating the electrical field by its Fourier components, we derive an expression for the spectral distribution of the radiation energy

$$\frac{\mathrm{d}^2W}{\mathrm{d}\Omega\mathrm{d}\omega} = [4\pi c\epsilon_0]\,\frac{c}{4\pi^2}\,|\boldsymbol{E}_\mathrm{r}(\omega)|^2\,R_\mathrm{r}^2\,, \tag{9.84}$$

where we have implicitly used the fact that $\boldsymbol{E}_\mathrm{r}(\omega) = \boldsymbol{E}_\mathrm{r}(-\omega)$ since $\boldsymbol{E}_\mathrm{r}(t)$ is real. To calculate the Fourier transform, we use (9.29) and note that the electrical field is expressed in terms of quantities at the retarded time. The calculation is simplified if we express the whole integrand in (9.81) at the retarded time and get with $t_\mathrm{r} = 1 - \frac{1}{c}R(t_\mathrm{r})$ and $\mathrm{d}t_\mathrm{r} = \frac{R(t_\mathrm{r})}{r}\mathrm{d}t$ instead of (9.81)

$$\boldsymbol{E}_\mathrm{r}(\omega) = \frac{1}{[4\pi\epsilon_0]}\frac{e}{c}\int\limits_{-\infty}^{\infty} \left.\frac{\boldsymbol{R}\times\left[(\boldsymbol{R}+\boldsymbol{\beta}R)\times\dot{\boldsymbol{\beta}}\right]}{r^2R}\right|_\mathrm{r} \mathrm{e}^{-\mathrm{i}\,\omega\left(t_\mathrm{r}+\frac{R_\mathrm{r}}{c}\right)}\,\mathrm{d}t_\mathrm{r}\,. \tag{9.85}$$

We require now that the radiation be observed at a point sufficiently far away from the source that during the time of emission the vector $\boldsymbol{R}(t_\mathrm{r})$ does not change appreciably in direction. This assumption is generally justified since the duration of the photon emission is of the order of $1/(\omega_\mathrm{L}\gamma)$, where $\omega_\mathrm{L} = c/\rho$ is the Larmor frequency. The observer therefore should be at a distance from the source large compared to ρ/γ. Equation (9.85) together with (9.14) may then be written like

$$\boldsymbol{E}_\mathrm{r}(\omega) = \frac{1}{[4\pi\epsilon_0]}\frac{e}{cR}\int\limits_{-\infty}^{\infty} \left.\frac{\boldsymbol{n}\times\left[(\boldsymbol{n}+\boldsymbol{\beta})\times\dot{\boldsymbol{\beta}}\right]}{(1+\boldsymbol{n}\,\boldsymbol{\beta})^2}\right|_\mathrm{r} \mathrm{e}^{-\mathrm{i}\,\omega\left(t_\mathrm{r}+\frac{R_\mathrm{r}}{c}\right)}\,\mathrm{d}t_\mathrm{r}\,. \tag{9.86}$$

With

$$\frac{\boldsymbol{n}\times\left[(\boldsymbol{n}+\boldsymbol{\beta})\times\dot{\boldsymbol{\beta}}\right]}{(1+\boldsymbol{n}\,\boldsymbol{\beta})^2} = \frac{\mathrm{d}}{\mathrm{d}t_\mathrm{r}}\frac{\boldsymbol{n}\times(\boldsymbol{n}\times\boldsymbol{\beta})}{1+\boldsymbol{n}\,\boldsymbol{\beta}}\,, \tag{9.87}$$

we integrate (9.86) by parts while noting that the integrals vanish at the boundaries and get

$$\boldsymbol{E}_\mathrm{r}(\omega) = \frac{1}{[4\pi\epsilon_0]}\frac{-\mathrm{i}\,e\omega}{cR}\int\limits_{-\infty}^{\infty} [\boldsymbol{n}\times(\boldsymbol{n}\times\boldsymbol{\beta})]_\mathrm{r}\,\mathrm{e}^{-\mathrm{i}\,\omega\left(t_\mathrm{r}+\frac{R_\mathrm{r}}{c}\right)}\,\mathrm{d}t_\mathrm{r}\,. \tag{9.88}$$

After insertion into (9.84) the spectral and spatial intensity distribution is

$$\frac{\mathrm{d}^2W}{\mathrm{d}\Omega\,\mathrm{d}\omega} = \frac{r_\mathrm{c}mc^2}{4\pi c}\omega^2\left|\int\limits_{-\infty}^{\infty} [\boldsymbol{n}\times(\boldsymbol{n}\times\boldsymbol{\beta})]\,\mathrm{e}^{-\mathrm{i}\,\omega\left(t_\mathrm{r}+\frac{R_\mathrm{r}}{c}\right)}\,\mathrm{d}t_\mathrm{r}\right|_\mathrm{r}^2\,. \tag{9.89}$$

The spectral and spatial radiation distribution depends on the Fourier transform of the particle trajectory which itself is a function of the magnetic

field distribution. The trajectory in a uniform dipole field is different from say the step function of real lumped bending magnets or oscillating deflecting fields from wiggler magnets and the radiation characteristics may therefore be different. In this chapter, we will concentrate only on a uniform dipole field and postpone the discussion of specific radiation characteristics for insertion devices to Chap. 10.

The integrand in (9.89) can be expressed in component form to simplify integration. For that we consider a fixed coordinate system (x, y, z) as shown in Fig. 9.7. The observation point is far away from the source point and we focus on the radiation that is centered about the tangent to the orbit at the source point. The observation point P and the vectors $\boldsymbol{R}$ and $\boldsymbol{n}$ are therefore within the (y, z)-plane and radiation is emitted at angles θ with respect to the z-axis.

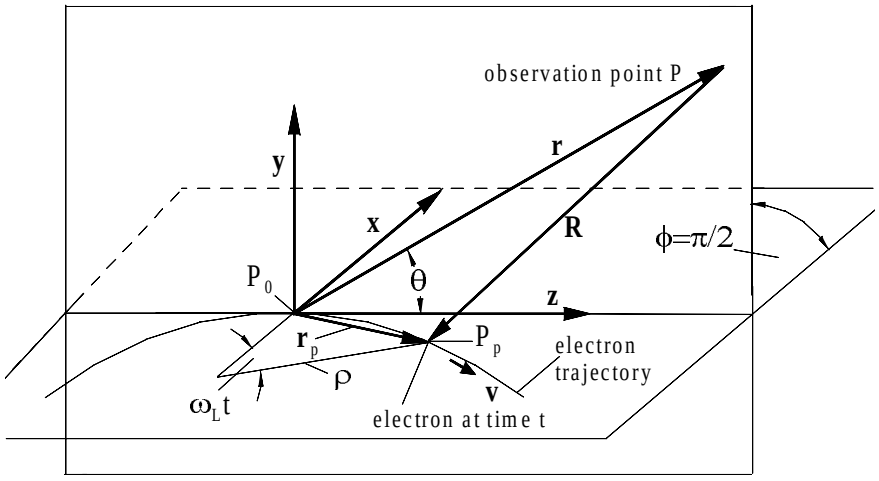

Fig. 9.7. Radiation geometry

The vector from the origin of the coordinate system P_0 to the observation point P is $\boldsymbol{r}$, the vector $\boldsymbol{R}$ is the vector from P to the particle at P_p and $\boldsymbol{r}_\mathrm{p}$ is the vector from the origin to P_p. With this we have

$$\boldsymbol{r} = \boldsymbol{r}_\mathrm{p} - \boldsymbol{R}\,(t_\mathrm{r}) \ , \tag{9.90}$$

where $\boldsymbol{r}_\mathrm{p}$and $\boldsymbol{R}_\mathrm{r}$ are taken at the retarded time. The exponent in (9.89) is then

$$\omega(t_\mathrm{r} + R_\mathrm{r}/c) = \omega(t_\mathrm{r} + \boldsymbol{n}\boldsymbol{R}_\mathrm{r}/c) = \omega\left(t_\mathrm{r} + \frac{\boldsymbol{n}\boldsymbol{r}_\mathrm{p}}{c} - \frac{\boldsymbol{n}\boldsymbol{r}}{c}\right) \tag{9.91}$$

and the term $-\omega\frac{\boldsymbol{n}\boldsymbol{r}}{c}$ is independent of the time generating only a constant phase factor which is completely irrelevant for the spectral distribution and may therefore be ignored.

In determining the vector components, we note from Fig. 9.7 that now the coordinate system is fixed in space. Following the above discussion the azimuthal angle is constant and set to $\varphi = \frac{1}{2}\,\pi$ because we are interested only in the vertical radiation distribution. the horizontal distribution is uniform by virtue of the tangential emission along the orbit. With these assumptions, we get the vector components for the vector $\boldsymbol{n}$ from (9.70)

$$\boldsymbol{n} = (0, -\sin\theta, -\cos\theta)\,. \tag{9.92}$$

The vector $\mathbf{r}_\mathrm{p}$ is defined by Fig. 9.7 and depends on the exact variation of the deflecting magnetic field along the path of the particles. Here we assume a constant bending radius ρ and have

$$\boldsymbol{r}_\mathrm{p} = [-\rho\cos(\omega_\mathrm{L} t_\mathrm{r}), 0, \rho\sin(\omega_\mathrm{L} t_\mathrm{r})]\ , \tag{9.93}$$

where $\omega_\mathrm{L} = \beta c/\rho$ is the Larmor frequency. From these component representations the vector product

$$\frac{\boldsymbol{n}\boldsymbol{r}_\mathrm{p}}{c} = -\frac{\rho}{c}\sin(\omega_\mathrm{L} t_\mathrm{r})\cos\theta \tag{9.94}$$

Noting that both arguments of the trigonometric functions in (9.94) are very small, we may expand the r.h.s. of (9.94) up to third order in t_r and the factor $t_\mathrm{r} + \boldsymbol{n}\boldsymbol{r}_\mathrm{p}/c$ in (9.91) becomes

$$t_\mathrm{r} + \frac{\boldsymbol{n}\boldsymbol{r}_\mathrm{p}}{c} = t_\mathrm{r} - \frac{\rho}{c}\left[\omega_\mathrm{L} t_\mathrm{r} - \tfrac{1}{6}(\omega_\mathrm{L} t_\mathrm{r})^3\left(1 - \tfrac{1}{2}\,\theta^2\right)\right]\ . \tag{9.95}$$

With $\omega_\mathrm{L} = \beta c/\rho$ we get $t_\mathrm{r}(1 - \rho\,\omega_\mathrm{L}/c) = (1-\beta)\,t_\mathrm{r} \approx t_\mathrm{r}/(2\gamma^2)$. Keeping only up to third order terms in $\omega_\mathrm{L} t_\mathrm{r}$ and θ we have finally for high energetic particles $\beta \approx 1$

$$t_\mathrm{r} + \frac{\boldsymbol{n}\boldsymbol{r}_\mathrm{p}}{c} = \tfrac{1}{2}\,\left(\gamma^{-2} + \theta^2\right)\,t_\mathrm{r} + \tfrac{1}{6}\omega_\mathrm{L}^2 {t_\mathrm{r}}^3\,. \tag{9.96}$$

The triple vector product in (9.89) can be evaluated in a similar way. For the velocity vector we derive from Fig. 9.7

$$\boldsymbol{\beta} = \beta\ [-\mathrm{sign}(1/\rho)\ \sin(\omega_\mathrm{L} t_\mathrm{r}), 0, \cos(\omega_\mathrm{L} t_\mathrm{r})]\ . \tag{9.97}$$

Consistent with the definition of the curvature in (6.7), the sign of the curvature $\mathrm{sign}(1/\rho)$ is positive for a positive charge and a positive magnetic field vector B_y. The vector relation (B.10) and (9.92, 9.97) can be used to express the triple vector product in terms of its components

$$\boldsymbol{n}\times(\boldsymbol{n}\times\boldsymbol{\beta}) = \beta\,\left[\mathrm{sign}(1/\rho)\ \sin(\omega_\mathrm{L} t_\mathrm{r}), \tfrac{1}{2}\sin 2\theta\ \cos(\omega_\mathrm{L} t_\mathrm{r}), -\sin^2\theta\ \cos(\omega_\mathrm{L} t_\mathrm{r})\right]\ .$$

(9.98)

Splitting this three-dimensional vector into two parts will allow us to characterize the polarization states of the radiation. To do this, we take the unit vector $\boldsymbol{u}_\perp$ in the x-direction and $\boldsymbol{u}_\parallel$ a unit vector normal to $\boldsymbol{u}_\perp$ and normal to $\boldsymbol{r}$. The y and z – components of (9.98) are then also the components of $\boldsymbol{u}_\parallel$ and we may express the vector (9.98) by

$$\boldsymbol{n}\times(\boldsymbol{n}\times\boldsymbol{\beta}) = \beta\,\mathrm{sign}(1/\rho)\sin(\omega_\mathrm{L}t_\mathrm{r})\,\boldsymbol{u}_\perp + \beta\sin\theta\,\cos(\omega_\mathrm{L}t_\mathrm{r})\boldsymbol{u}_\parallel\,, \tag{9.99}$$

Inserting (9.96) and (9.99) into the integrand (9.88) we get with $\beta\approx 1$

$$\boldsymbol{E}_\mathrm{r}(\omega) = \frac{-1}{[4\pi\epsilon_0]}\frac{e\omega}{cR}\int_{-\infty}^{\infty}\left[\mathrm{sign}(1/\rho)\sin(\omega_\mathrm{L}t_\mathrm{r})\,\boldsymbol{u}_\perp + \sin\theta\,\cos(\omega_\mathrm{L}t_\mathrm{r})\,\boldsymbol{u}_\parallel\right]\mathrm{e}^X\,\mathrm{d}t_\mathrm{r}\,, \tag{9.100}$$

where

$$X = -\mathrm{i}\,\frac{\omega}{2\gamma^2}\left[(1+\gamma^2\theta^2)\,t_\mathrm{r} + \tfrac{1}{3}\gamma^2\omega_\mathrm{L}^2 t_\mathrm{r}^3\right]\,.$$

Two polarization directions have been defined for the electric radiation field. One of which, $\boldsymbol{u}_\perp$, is in the plane of the particle path being perpendicular to the particle velocity and to the deflecting magnetic field. Following Sokolov and Ternov [51] we call this the σ-mode ($\boldsymbol{u}_\perp = \boldsymbol{u}_\sigma$). The other polarization direction in the plane containing the deflecting magnetic field and the observation point is perpendicular to $\boldsymbol{n}$ and is called the π-mode ($\boldsymbol{u}_\parallel = \boldsymbol{u}_\pi$). Since the emission angle θ is very small, we find this polarization direction to be mostly parallel to the magnetic field. Noting that most accelerators or beam lines are constructed in the horizontal plane, the polarizations are also often referred to as the horizontal polarization for the σ-mode and as the vertical polarization for the π-mode.

9.5.1 Spectral Distribution in Space and Polarization

As was pointed out by Jackson [19], the mathematical need to extend the integration over infinite times does not invalidate our expansion of the trigonometric functions where we assumed the argument $\omega_\mathrm{L}t_\mathrm{r}$ to be small. Although the integral (9.100) extends over all past and future times, the integrand oscillates rapidly for all but the lowest frequencies and therefore only times of the order $ct_\mathrm{r} = \pm\,\rho/\gamma$ centered about t_r contribute to the integral. This is a direct consequence of the fact that the radiation is emitted in the forward direction and therefore only photons from a very small segment of the particle trajectory reach the observation point. For very small frequencies of the order of the Larmor frequency, however, we must expect considerable deviations from our results. In practical circumstances such low harmonics will,

however, not propagate in the vacuum chamber [27] and the observed photon spectrum therefore is described accurately for all practical purposes.

The integral in (9.100) can be expressed by modified Bessel's functions in the form of Airy's integrals as has been pointed out by Schwinger [21]. Since the deflection angle $\omega_{\mathrm{L}} t_{\mathrm{r}}$ is very small, we may use linear expansions $\sin(\omega_{\mathrm{L}} t_{\mathrm{r}}) \approx \omega_{\mathrm{L}} t_{\mathrm{r}}$ and $\cos(\omega_{\mathrm{L}} t_{\mathrm{r}}) \approx 1$. Inserting the expression for the electric field (9.100) into (9.83) we note that cross terms of both polarizations vanish $\boldsymbol{u}_{\perp} \boldsymbol{u}_{\parallel} = 0$ and the radiation intensity can therefore be expressed by two separate orthogonal polarization components. Introducing in (9.100) the substitutions [21]

$$\omega_{\mathrm{L}} t_{\mathrm{r}} = \sqrt{\frac{1}{\gamma^2} + \theta^2}\, x \,, \tag{9.101}$$

$$\xi = \tfrac{1}{3} \frac{\omega}{\omega_{\mathrm{L}}} \frac{1}{\gamma^3} (1 + \gamma^2 \theta^2)^{3/2} = \tfrac{1}{2} \frac{\omega}{\omega_{\mathrm{c}}} (1 + \gamma^2 \theta^2)^{3/2} \,, \tag{9.102}$$

where $\hbar\omega_{\mathrm{c}}$ is the critical photon energy, the argument in the exponential factor of (9.100) becomes

$$\frac{\omega}{2\gamma^2} \left[(1 + \gamma^2 \theta^2)\, t_{\mathrm{r}} + \tfrac{1}{3} \gamma^2 \omega_{\mathrm{L}}^2 t_{\mathrm{r}}^3 \right] = \tfrac{1}{2}\, \xi (3x + x^3) \,. \tag{9.103}$$

With these substitutions, (9.100) can be evaluated noting that only even terms contribute to the integral. With $\omega_{\mathrm{L}} t_{\mathrm{r}}$ and θ being small quantities we get integrals of the form [52]

$$\int_0^{\infty} \cos \left[\tfrac{1}{2}\, \xi (3x + x^3) \right] \mathrm{d}x = \tfrac{1}{\sqrt{3}} K_{1/3}(\xi) \,, \tag{9.104a}$$

$$\int_0^{\infty} \sin \left[\tfrac{1}{2}\, \xi (3x + x^3) \right] \mathrm{d}x = \tfrac{1}{\sqrt{3}} K_{2/3}(\xi) \,, \tag{9.104b}$$

where the functions K_{ν} are modified Bessels's functions of the second kind. These functions assume finite values for small arguments but vanish exponentially for large arguments as shown in Fig. 9.8. Fast converging series for these modified Bessels's functions with fractional index have been derived by Kostroun [53]. The Fourier transform of the electrical field (9.100) finally becomes

$$\boldsymbol{E}_{\mathrm{r}}(\omega) = \frac{-1}{[4\pi\epsilon_0]} \frac{\sqrt{3} e}{cR} \frac{\omega}{\omega_{\mathrm{c}}} \gamma (1 + \gamma^2 \theta^2) \left[\mathrm{sign}(1/\rho)\, K_{2/3}(\xi)\, \boldsymbol{u}_{\sigma} - \mathrm{i}\, \frac{\gamma \theta K_{1/3}(\xi)}{\sqrt{1 + \gamma^2 \theta^2}}\, \boldsymbol{u}_{\pi} \right] , \tag{9.105}$$

describing the spectral radiation field far from the source for particles traveling through a uniform magnetic dipole field. Later, we will modify this expression to make it suitable for particle motion in undulators or other nonuniform fields.

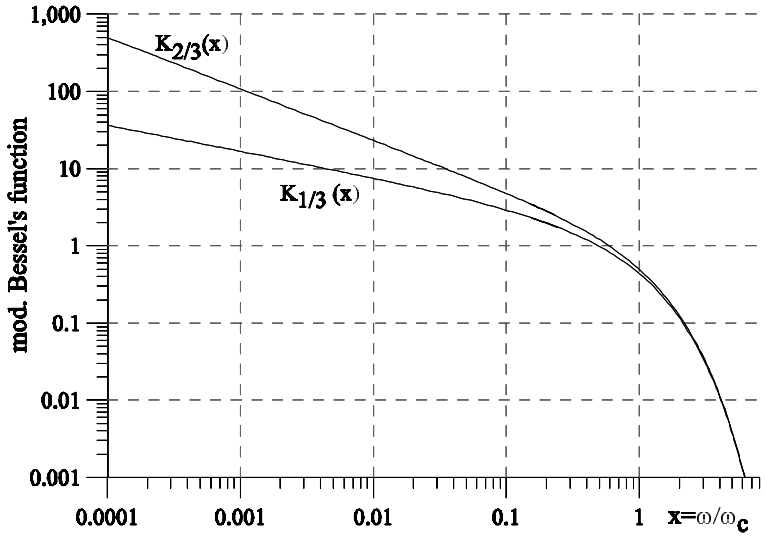

Fig. 9.8. Modified Bessel's functions $K_{1/3}(x)$ and $K_{2/3}(x)$

The spectral synchrotron radiation energy emitted by one electron per pass is proportional to the square of the electrical field (9.105) and is from (9.84)

$$\frac{\mathrm{d}^2W}{\mathrm{d}\Omega\mathrm{d}\omega} = \frac{3\,r_\mathrm{c}mc}{4\pi^2}\gamma^2\left(\frac{\omega}{\omega_\mathrm{c}}\right)^2(1+\gamma^2\theta^2)^{\,2}\left[K_{2/3}^2(\xi)\,\boldsymbol{u}_\sigma^2+\frac{\gamma^2\theta^2K_{1/3}^2(\xi)}{1+\gamma^2\theta^2}\boldsymbol{u}_\pi^2\right]. \tag{9.106}$$

The radiation spectrum has two components of orthogonal polarization, one in the plane of the particle trajectory and the other almost parallel to the deflecting magnetic field. In (9.105) both polarizations appear explicitly through the orthogonal unit vectors. Forming the square of the electrical field to get the radiation intensity, cross terms disappear because of the orthogonality of the unit vectors $\boldsymbol{u}_\sigma$and $\boldsymbol{u}_\pi$. The expression for the radiation intensity therefore preserves separately the two polarization modes in the square brackets of (9.106) representing the σ-mode and π-mode of polarization, respectively.

It is interesting to study the spatial distribution for the two polarization modes in more detail. Not only are the intensities very different but the spatial distribution is different too. The spatial distribution of the σ-mode is directed mainly in the forward direction while the π-mode radiation is emitted into two lobes at finite angles and zero intensity in the forward direction $\theta = 0$. In Fig. 9.9 the instantaneous radiation lobes are shown for both the σ- and the

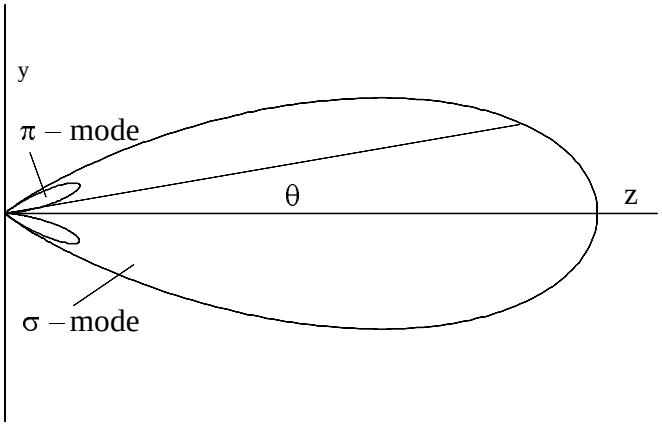

Fig. 9.9. Radiation lobes for $\sigma-$ and $\pi-$mode polarization

π-mode at the critical photon energy and being emitted tangentially from the orbit at the origin of the coordinate system. A more detailed discussion of elliptical polarization properties can be found in Sect. 10.3.

9.5.2 Spectral and Spatial Photon Flux

The radiation intensity W from a single electron and for a single pass may not always be the most useful parameter. A more useful parameter is the spectral photon flux per unit solid angle into a frequency bin $\Delta\omega/\omega$ and for a circulating beam current I

$$\frac{\mathrm{d}^2\dot{N}_{\mathrm{ph}}\,(\omega)}{\mathrm{d}\,\theta\,\mathrm{d}\,\psi} = \frac{\mathrm{d}W\,(\omega)}{\mathrm{d}\omega\,\mathrm{d}\,\Omega}\frac{1}{\hbar}\frac{I}{e}\frac{\Delta\omega}{\omega}\,. \tag{9.107}$$

Here we have replaced the solid angle by its components, the vertical angle θ and the bending angle ψ. In more practical units the differential photon flux is

$$\frac{\mathrm{d}^2\dot{N}_{\mathrm{ph}}\,(\omega)}{\mathrm{d}\theta\,\mathrm{d}\psi} = C_\Omega E^2 I\,\frac{\Delta\omega}{\omega}\left(\frac{\omega}{\omega_{\mathrm{c}}}\right)^2 K^2_{2/3}(\xi)\,F(\xi,\theta)\,, \tag{9.108}$$

where

$$C_\Omega = \frac{3\alpha}{4\pi^2 e(mc^2)^2} = 1.3273\ 10^{16}\ \frac{\text{photons}}{\text{s mrad}^2\ \text{GeV}^2\text{A}}\,, \tag{9.109}$$

I the circulating particle beam current, α the fine structure constant, and

$$F(\xi,\theta) = (1+\gamma^2\theta^2)^{\,2}\left[1+\frac{\gamma^2\theta^2}{1+\gamma^2\theta^2}\frac{K^2_{1/3}(\xi)}{K^2_{2/3}(\xi)}\right]. \tag{9.110}$$

For approximate numerical calculations of photon fluxes, we may use the graphic representation in Fig. 9.8 of the modified Bessel's function.

The spatial radiation pattern varies with the frequency of the radiation. Specifically, the angular distribution concentrates more and more in the forward direction as the radiation frequency increases. The radiation distribution in frequency and angular space is shown for both the σ-(Fig. 9.10) and the π-mode (Fig. 9.11) at the fundamental frequency. The high collimation of synchrotron radiation in the forward direction makes it a prime research tool to probe materials and its atomic and molecular properties

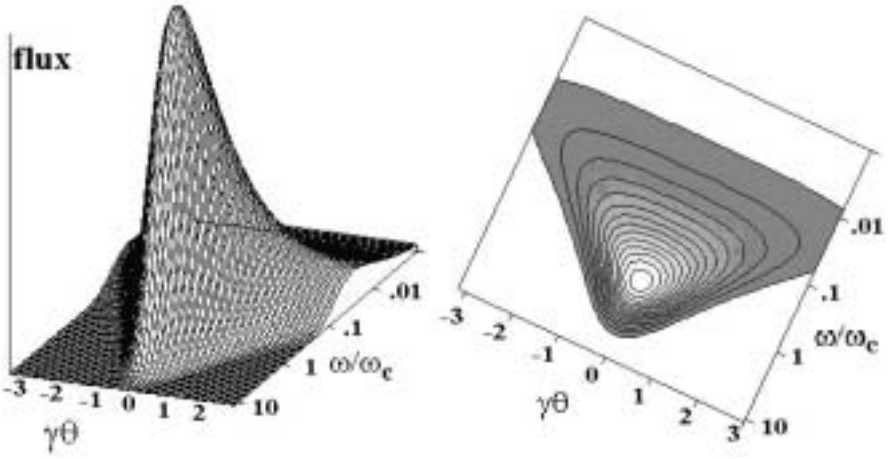

Fig. 9.10. Distribution in frequency and angular space for $\sigma-$mode radiation

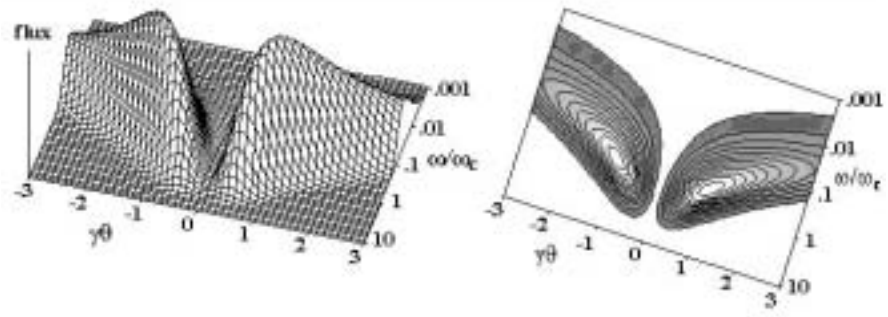

Fig. 9.11. Distribution in frequency and angular space for π-mode radiation

9.5.3 Harmonic Representation

Expression (9.106) can be transformed into a different formulation emphasizing the harmonic structure of the radiation spectrum. The equivalence between both formulations has been shown by Sokolov and Ternov [51] expressing the modified Bessel's functions $K_{1/3}$ and $K_{2/3}$ by regular Bessel's functions of high order. With $\nu = \frac{\omega}{\omega_{\mathrm{L}}}$ the asymptotic formulas for $\nu \gg 1$ are

$$K_{1/3}(\xi) = \frac{\sqrt{3}\pi}{\sqrt{1-\beta^2\cos^2\theta}} J_\nu(\nu\beta\cos\theta)\,, \tag{9.111}$$

$$K_{2/3}(\xi) = \frac{\sqrt{3}\pi}{1-\beta^2\cos^2\theta}\, J'_\nu(\nu\beta\cos\theta)\,, \tag{9.112}$$

where $\xi = \frac{\nu}{3}\left(1-\beta^2\cos^2\theta\right)^{3/2} \approx \frac{\nu}{3}\left(\gamma^{-2}+\beta^2\theta^2\right)^{3/2}$ for small angles. These approximations are justified since we are only interested in very large harmonics of the revolution frequency. The harmonic number ν for the critical photon frequency, for example, is given by $\nu_{\mathrm{c}} = \omega_{\mathrm{c}}/\omega_{\mathrm{L}} = \frac{3}{2}\gamma^3$ which for practical cases is generally a very large number. Inserting these approximations into (9.106) gives the the formulation that has been derived first by Schott [3, 4, 5] in 1907 long before synchrotron radiation was discovered in an attempt to calculate the radiation intensity of atomic spectral lines

$$\frac{\mathrm{d}^2P}{\mathrm{d}\Omega\mathrm{d}\nu} = \frac{r_{\mathrm{c}}mc^3}{2\pi\rho^2}\nu^2\left[J'^2_\nu(\nu\cos\theta) + \theta^2 J^2_\nu(\nu\cos\theta)\right]\,, \tag{9.113}$$

where we have introduced the radiation power $P = W\frac{c}{2\pi\rho}$. This form still exhibits the separation of the radiation into the two polarization modes.

9.6 Spatial Radiation Power Distribution

Integrating over all frequencies we obtain the angular distribution of the synchrotron radiation. From (9.106) we note the need to perform integrals of the form $\int_{-\infty}^{\infty}\omega^2 K_\mu^2(a\omega)\,\mathrm{d}\,\omega$, where $a\omega = \xi$. The solution can be found in the integral tables of Gradshteyn and Ryzhik [54] as solution number GR(6.576.4)[1]

$$\int_0^\infty \omega^2 K_\mu^2(a\omega)\,d\omega = \frac{\pi^2}{32a^3}\frac{1-4\mu}{\cos\pi\mu}\,. \tag{9.114}$$

Applying this solution to (9.106) and integrating over all frequencies, we get for the angular distribution of the synchrotron radiation

[1] In this chapter we will need repeatedly results from mathematical tables. We abbreviate such solutions with the first letters of the authors names and the formula number.

$$\frac{\mathrm{d}W}{\mathrm{d}\Omega} = \frac{21}{32}\frac{r_\mathrm{c} mc^2}{\rho}\frac{\gamma^5}{(1+\gamma^2\theta^2)^{5/2}}\left(1+\frac{5}{7}\frac{\gamma^2\theta^2}{1+\gamma^2\theta^2}\right). \tag{9.115}$$

This result is consistent with the angular radiation power distribution (9.76) where we found that the radiation is collimated very much in the forward direction with most of the radiation energy being emitted within an angle of $\pm 1/\gamma$. There are two contributions to the total radiation intensity, the σ-mode and the π-mode. The σ-mode has a maximum intensity in the forward direction, while the maximum intensity for the π-mode occurs at an angle of $\theta_\pi = 1/(\sqrt{5/2}\ \gamma)$. The quantity W is the radiation energy per unit solid angle from a single electron and a single pass and the average radiation power is therefore $P_\gamma = W\,/\,T_\mathrm{rev}$ or (9.115) becomes

$$\frac{\mathrm{d}P_\gamma}{\mathrm{d}\Omega} = \frac{2r_\mathrm{c} mc^3}{6\pi\rho^2}\frac{\gamma^5}{(1+\gamma^2\theta^2)^{5/2}}\left(1+\frac{5}{7}\frac{\gamma^2\theta^2}{1+\gamma^2\theta^2}\right). \tag{9.116}$$

Integrating (9.116) over all angles θ we find the synchrotron radiation power into both polarization modes, the σ-mode perpendicular to the magnetic field and the π-mode parallel to the magnetic field. In doing so, we note first that (9.116) can be simplified with (9.59) and $\beta = 1$

$$\frac{\mathrm{d}P_\gamma}{\mathrm{d}\Omega} = \frac{21}{32}\frac{P_\gamma}{2\pi}\frac{\gamma}{(1+\gamma^2\theta^2)^{5/2}}\left(1+\frac{5}{7}\frac{\gamma^2\theta^2}{1+\gamma^2\theta^2}\right). \tag{9.117}$$

This result is consistent with (9.76) although it should be noted that (9.117) gives the average radiation power from a circular accelerator with uniform intensity in ψ, while (9.76) is the instantaneous power into the forward lobe. Equation (9.117) exhibits the power into each polarization mode for which the total power can be obtained by integration over all angles. First, we integrate over all points along the circular orbit and get a factor 2π since the observed radiation power does not depend on the location along the orbit. Continuing the integration over all angles of θ, we find the contributions to the integral to become quickly negligible for angles larger than $1/\gamma$. If it were not so, we could not have used (9.117) where the trigonometric functions have been replaced by their small arguments. Both terms in (9.117) can be integrated readily and the first term becomes with GR(2.271.6) [54]

$$\int_{\theta_\mathrm{max}\gamma\ll 1}^{\theta_\mathrm{max}\gamma\gg 1}\frac{\gamma\,\mathrm{d}\theta}{(1+\gamma^2\theta^2)^{5/2}} = \frac{4}{3}. \tag{9.118}$$

The second term is with GR[2.272.7] [54]

$$\int_{\theta_\mathrm{max}\gamma\ll 1}^{\theta_\mathrm{max}\gamma\gg 1}\frac{\gamma^3\theta^2\,\mathrm{d}\theta}{(1+\gamma^2\theta^2)^{7/2}} = \frac{4}{15}. \tag{9.119}$$

With these integrals and (9.117) we express the radiation power into the σ-and π-mode with P_γ from (9.59) by

$$P_\sigma = \tfrac{7}{8} P_\gamma \,, \tag{9.120a}$$

$$P_\pi = \tfrac{1}{8} P_\gamma \,. \tag{9.120b}$$

The horizontally polarized component of synchrotron radiation greatly dominates the photon beam characteristics and only 12.5% of the total intensity is polarized in the vertical plane. In the forward direction the σ-polarization even approaches 100%. Obviously, the sum of both components is equal to the total radiation power. This high polarization of the radiation provides a valuable characteristic for experimentation with synchrotron radiation. In addition, the emission of polarized light generates a slow polarizing reaction on the particle beam orbiting in a circular accelerator like in a storage ring [55].

9.6.1 Asymptotic Solutions

Expressions for the radiation distribution can be greatly simplified if we restrict the discussion to very small or very large arguments of the modified Bessel's functions for which approximate expressions exist [24]. Knowledge of the radiation distribution at very low photon frequencies becomes important for experiments using such radiation or for beam diagnostics where the beam cross section is being imaged to a TV camera using the visible part of the radiation spectrum. To describe this visible part of the spectrum, we may in most cases assume that the photon frequency is much lower than the critical photon frequency.

Low frequencies and small observation angles. For very small arguments or low frequencies and small angles, we find the following approximations AS(9.6.9) [24]

$$K_{1/3}(\xi \longrightarrow 0) \approx \frac{\Gamma^2(1/3)}{2^{2/3}} \left(\frac{\omega}{\omega_\mathrm{c}}\right)^{-2/3} \frac{1}{1+\gamma^2\theta^2} \,, \tag{9.121a}$$

$$K_{2/3}(\xi \longrightarrow 0) \approx 2^{2/3}\Gamma^2(2/3) \left(\frac{\omega}{\omega_\mathrm{c}}\right)^{-4/3} \frac{1}{(1+\gamma^2\theta^2)^2} \,, \tag{9.121b}$$

where the Gamma functions $\Gamma(1/3) = 2.6789385$ and $\Gamma(2/3) = 1.351179$ and from (9.103)

$$\xi = \frac{1}{2} \frac{\omega}{\omega_\mathrm{c}} (1+\gamma^2\theta^2)^{3/2} \,. \tag{9.122}$$

Inserting this into (9.108) the photon flux spectrum in the forward direction becomes for $\theta = 0$ and $\frac{\omega}{\omega_\mathrm{c}} \ll 1$

$$\frac{\mathrm{d}^2 \dot{N}_\mathrm{ph}}{\mathrm{d}\theta \mathrm{d}\psi} \approx C_\Omega \, E^2 I \; \Gamma^2(2/3) \left(\frac{2\omega}{\omega_\mathrm{c}}\right)^{2/3} \frac{\Delta\omega}{\omega} \,. \tag{9.123}$$

The photon spectrum at very low frequencies is independent of the particle energy since $\omega_c \propto E^3$. Clearly, in this approximation there is no angular dependence for the σ-mode radiation and the intensity increases with frequency. The π-mode radiation on the other hand is zero for $\theta = 0$ and increases in intensity with the square of θ as long as the approximation is valid.

High frequencies or large observation angles. For large arguments of the modified Bessel's functions or for high frequencies and large emission angles different approximations hold. In this case, the approximate expressions are actually the same for both Bessel's functions indicating the same exponential drop off for high energetic photons AS(9.7.2)

$$K_{1/3}^2(\xi \longrightarrow \infty) \approx \frac{\pi}{2}\frac{\mathrm{e}^{-2\xi}}{\xi}\,, \tag{9.124a}$$

$$K_{2/3}^2(\xi \longrightarrow \infty) \approx \frac{\pi}{2}\frac{\mathrm{e}^{-2\xi}}{\xi}\,. \tag{9.124b}$$

The photon flux distribution in this approximation becomes from (9.106)

$$\frac{\mathrm{d}^2 N_{\mathrm{ph}}}{\mathrm{d}\theta \mathrm{d}\psi} \approx \frac{3 r_c m c^2}{4\pi\hbar c}\gamma^2 \frac{\omega}{\omega_c}\mathrm{e}^{-2\xi}\sqrt{1+\gamma^2\theta^2}\frac{\Delta\omega}{\omega}\,, \tag{9.125}$$

where N_{ph} is the number of photons emitted per pass. The spatial radiation distribution is greatly determined by the exponential factor and the relative amplitude with respect to the forward direction scales therefore like

$$\exp\left\{-\frac{\omega}{\omega_c}\left[\left(1+\gamma^2\theta^2\right)^{3/2}-1\right]\right\}\,. \tag{9.126}$$

We look now for the specific angle for which the intensity has fallen to $1/e$. Since $\omega \gg \omega_c$, this angle must be very small $\gamma\theta \ll 1$ and we can ignore other θ-dependent factors. The exponential factor becomes equal to $1/e$ for

$$\tfrac{3}{2}\frac{\omega}{\omega_c}\gamma^2\theta_{1/e}^2 \approx 1 \tag{9.127}$$

and solving for $\theta_{1/e}$ we get finally

$$\theta_{1/e} = \sqrt{\tfrac{2}{3}}\frac{1}{\gamma}\frac{\omega_c}{\omega} \qquad \text{for} \quad \omega \gg \omega_c\,. \tag{9.128}$$

The high energy end of the synchrotron radiation spectrum is more and more collimated into the forward direction. The angular distribution is graphically illustrated for both polarization modes in Figs. 9.10 and 9.11.

9.7 Angle-Integrated Spectrum

Synchrotron radiation is emitted over a wide range of frequencies and it is of great interest to know the exact frequency distribution of the radiation.

Since the radiation is very much collimated in the forward direction, it is useful to integrate over all angles of emission to obtain the total spectral photon flux that might be accepted by a beam line with proper aperture. To that goal, (9.106) will be integrated with respect to the emission angles to obtain the frequency spectrum of the radiation. The emission angle θ appears in (9.106) in a rather complicated way which makes it difficult to perform the integration directly. We replace therefore the modified Bessel's functions by Airy's functions defined by AS(10.4.14) and AS(10.4.31) [24]

$$\mathcal{A}i\,(z) = \frac{\sqrt{z}}{\sqrt{3}\pi} K_{1/3}(\xi)\,, \tag{9.129a}$$

$$\mathcal{A}'\mathrm{i}\,(z) = -\frac{z}{\sqrt{3}\pi} K_{2/3}(\xi)\,. \tag{9.129b}$$

With the definition

$$\eta = \tfrac{3}{4}\frac{\omega}{\omega_\mathrm{c}} \tag{9.130}$$

we get from (9.103)

$$z = \left(\tfrac{3}{2}\xi\right)^{2/3} = \eta^{2/3}\left(1+\gamma^2\theta^2\right)\,. \tag{9.131}$$

We apply this to the periodic motion of particles orbiting in a circular accelerator. In this case the spectral distribution of the radiation power can be obtained by noting that the differential radiation energy (9.106) is emitted every time the particle passes by the source point. A short pulse of radiation is sent towards the observation point at periodic time intervals equal to the revolution time $T_\mathrm{rev} = \frac{c}{2\pi\rho}$. The spectral power distribution (9.106) expressed by Airy functions is

$$\frac{\mathrm{d}^2 P_\gamma}{\mathrm{d}\omega\,\mathrm{d}\Omega} = \frac{9P_\gamma}{2\pi}\frac{\gamma}{\omega_\mathrm{c}}\left[\eta^{2/3}\mathcal{A}'i^2\,(z) + \eta^{4/3}\gamma^2\theta^2\mathcal{A}i^2\,(z)\right]\,. \tag{9.132}$$

To obtain the photon frequency spectrum, we integrate over all angles of emission which is accomplished by integrating along the orbit contributing a mere factor of 2π and over the angle θ. Although this latter integration is to be performed between -π and $+\pi$, we choose the mathematically easier integration from $-\infty$ to $+\infty$ because the Airy functions fall off very fast for large arguments. In fact, we have seen already that most of the radiation is emitted within a very small angle of $\pm 1/\gamma$. The integrals to be solved are of the form $\int_0^\infty \theta^n \mathcal{A}i^2\left[\eta^{2/3}(1+\gamma^2\theta^2\right]\mathrm{d}\,\theta$ where $n = 0$ or 2. We concentrate first on the second term in (9.132), and form with (9.104) and (9.129a) the square of the Airy function

$$\theta^2\mathcal{A}i^2(z) = \frac{1}{\pi^2}\int_0^\infty \theta^2\cos\left[\tfrac{1}{3}x^3 + zx\right]\,\mathrm{d}x \int_0^\infty \theta^2\cos\left[\tfrac{1}{3}\,y^3 + z\,y\right]\,\mathrm{d}y\,. \tag{9.133}$$

We solve these integrals by making use of the trigonometric relation

$$\cos(\alpha + \tfrac{1}{2}\beta)\,\cos(\alpha - \tfrac{1}{2}\beta) = \cos\alpha\,\cos\beta\,. \tag{9.134}$$

After introducing the substitutions $x + y = s$ and $x - y = t$, we obtain integrals over two terms which are symmetric in s and t and therefore can be set equal to get

$$\theta^2 \mathcal{A}i^2(z) = \frac{1}{2\pi^2}\int_0^\infty \int_0^\infty \theta^2 \cos\left[\tfrac{1}{12}s^3 + 3\,s\,t^2 + z\,s\right] \mathrm{d}s\,\mathrm{d}y\,, \tag{9.135}$$

where the factor $\frac{1}{2}$ comes from the transformation of the area element $\mathrm{d}s\,\mathrm{d}y = \frac{\mathrm{d}s}{\sqrt{2}}\frac{\mathrm{d}t}{\sqrt{2}}$. In our problem we replace the argument z by the expression $z = \eta^{2/3}\left(1 + \gamma^2\theta^2\right)$ and integrate over the angle θ

$$\pi^2 \int_{-\infty}^{\infty} \theta^2 \mathcal{A}i^2(z)\;\mathrm{d}\theta = \int_{-\infty}^{\infty}\int_{-\infty}^{\infty}\int_{-\infty}^{\infty} \theta^2 \cos\left[\tfrac{1}{12}s^3 + 3\,s\,t^2 + s\,\eta^{2/3}\left(1 + \gamma^2\theta^2\right)\right] \mathrm{d}s\,\mathrm{d}y\,\mathrm{d}\theta\,. \tag{9.136}$$

The integrand is symmetric with respect to θ and the integration therefore needs to be performed only from 0 to ∞ with the result being doubled. We also note that the integration is taken over only one quadrant of the (s,t)-space. Further simplifying the integration, the number of variables in the argument of the cosine function can be reduced in the following way. We note the coefficient $\frac{1}{4}t^2 + \eta^{2/3}\gamma^2\theta^2$ which is the sum of squares. Setting $\frac{1}{2}t = r\cos\varphi$ and $\eta^{1/3}\gamma\theta = r\sin\varphi$ this term becomes simply r^2. The area element transforms like $\mathrm{d}t\,\mathrm{d}\theta = 2/(\eta^{1/3}\gamma)\,r\,\mathrm{d}r\,\mathrm{d}\varphi$ and integrating over φ from 0 to $\pi/2$, since we need integrate only over one quarter plane, (9.136) becomes finally

$$\int_{-\infty}^{\infty} \theta^2 \mathcal{A}i^2\;(z)\,\mathrm{d}\theta = \frac{1}{2\pi\eta\gamma^3}\int_0^\infty\int_0^\infty r^2 \cos\left[\tfrac{1}{12}s^3 + s\,\eta^{2/3} + r^2\right]\; r\,\mathrm{d}r\;\mathrm{d}s\;. \tag{9.137}$$

The integrand of (9.137) has now a form close to that of an Airy integral and we will try to complete that similarity. With $q = (3\xi/2)^{1/3}x$ the definition of the Airy functions AS(10.4.31)[24] are consistent with (9.129)

$$\mathcal{A}i(z) = \frac{1}{\pi}\int_0^\infty \cos\left[\tfrac{1}{3}q^3 + z\,q\right]\mathrm{d}q\,. \tag{9.138}$$

Equation (9.137) can be modified into a similar form by setting

$$w^3 = \tfrac{1}{4}s^3 \qquad \text{and} \qquad s\,(\eta^{2/3} + r^2) = y\,w\,. \tag{9.139}$$

Solving for w we get $w = s\,/\,2^{2/3}$and with $y = 2^{2/3}(\eta^{2/3} + r^2)$, $\mathrm{d}s = 2^{2/3}\mathrm{d}w$ and $\mathrm{d}y = 2^{5/3}r\,\mathrm{d}r$ equation (9.137) becomes

$$\int_{-\infty}^{\infty} \theta^2 \mathcal{A}i^2\ (z)\,\mathrm{d}\theta = \frac{1}{4\eta\gamma^3} \int_{y_0}^{\infty} \left(\frac{y}{2^{2/3}} - \eta^{2/3}\right) \mathcal{A}i\ (y)\,\mathrm{d}y\ , \tag{9.140}$$

where we have used the definition of Airy's function and where the integration starts at

$$y_0 = (2\eta)^{2/3} = \left(\tfrac{3}{2}\frac{\omega}{\omega_\mathrm{c}}\right)^{2/3} \tag{9.141}$$

corresponding to $r = 0$.

We may separate this integral into two parts and get a term $y\mathcal{A}i\ (y)$ under one of the integrals. This term is by definition of the Airy's functions AS(10.4.1) [24] equal to $\mathcal{A}i''$. Integration of this second derivative gives

$$\int_{y_0}^{\infty} \mathcal{A}i''(y)\,\mathrm{d}y = -\mathcal{A}i'(y_0) \tag{9.142}$$

and collecting all terms in (9.140) we have finally

$$\int_{-\infty}^{\infty} \theta^2 \mathcal{A}i^2\ (z)\,\mathrm{d}\theta = -\frac{1}{4\eta^{1/3}\gamma^3} \left[\frac{\mathcal{A}i'(y_0)}{y_0} + \int_{y_0}^{\infty} \mathcal{A}i\ (y)\,\mathrm{d}y\right] . \tag{9.143}$$

The derivation of the complete spectral radiation power distribution (9.132) requires also the evaluation of the integral $\int \mathcal{A}i'(z)\,\mathrm{d}\theta$. This can be done with the help of the integral $\int \mathcal{A}i(z)\,\mathrm{d}\theta$ and the integral we have just derived. We follow a similar derivation that led us just from (9.136) to (9.137) and get instead of (9.143)

$$\int_{-\infty}^{\infty} \mathcal{A}i^2\ (z)\mathrm{d}\theta = -\frac{1}{2\eta^{1/3}\gamma} \int_{y_0}^{\infty} \mathcal{A}i\ (y)\,\mathrm{d}y\,. \tag{9.144}$$

Recalling the definition of the argument $z = \eta^{2/3}\left(1 + \gamma^2\theta^2\right)$, we differentiate (9.144) twice with respect to $\eta^{2/3}$ to get

$$2\int_{-\infty}^{\infty} \left[\mathcal{A}i''(z) + \mathcal{A}i'^2(z)\right]\,\mathrm{d}\theta = -\frac{2^{1/3}}{\eta^{1/3}\gamma} \mathcal{A}i\,'(y_0)\ . \tag{9.145}$$

Using the relation $\mathcal{A}i''(z) = z\mathcal{A}i\,(z)$ and the results (9.142, 9.143) in (9.145) we get

$$\int_{-\infty}^{\infty} \mathcal{A}i'^2(z)\,\mathrm{d}\theta = -\frac{\eta^{1/3}}{4\gamma} \left[\frac{3\mathcal{A}i\,'(y_0)}{y_0} + \int_{y_0}^{\infty} \mathcal{A}i\ (y)\,\mathrm{d}y\right] . \tag{9.146}$$

At this point, all integrals have been derived that are needed to describe the spectral radiation power separately in both polarization modes and the spectral radiation power from (9.132) becomes

$$\frac{\mathrm{d}P_\gamma}{\mathrm{d}\omega} = \frac{27 P_\gamma \omega}{16\,\omega_\mathrm{c}^2}\left[\left(-\frac{3\mathcal{A}i\,'(y_0)}{y_0} - \int_{y_0}^{\infty}\mathcal{A}i\,(y)\,\mathrm{d}y\right)\right.$$
$$\left.\times\left(\frac{\mathcal{A}i\,'(y_0)}{y_0} + \int_{y_0}^{\infty}\mathcal{A}i\,(y)\,\mathrm{d}y\right)\right]\,. \qquad (9.147)$$

The first term describes the σ-mode of polarization and the second term the π-mode. Combining both polarization modes, we may derive a comparatively simple expression for the spectral radiation power. To this goal, we replace the Airy's functions by modified Bessel's functions

$$\frac{\mathcal{A}i\,'(y_0)}{y_0} = -\tfrac{1}{\sqrt{3}\pi}K_{2/3}(x_0)\,, \qquad (9.148)$$

where from (9.129, 9.130), and (9.140) $x_0 = \omega/\omega_\mathrm{c}$. With $\sqrt{y}\,\mathrm{d}y = \mathrm{d}x$, the recurrence formula $2K'_{2/3} = -K_{1/3} - K_{5/3}$ and (9.129) the Airy integral is

$$\int_{y_0}^{\infty}\mathcal{A}i\,(y)\,\mathrm{d}y = -\tfrac{2}{\sqrt{3}\pi}\int_{x_0}^{\infty}K'_{2/3}x\mathrm{d}x - \tfrac{1}{\sqrt{3}\pi}\int_{x_0}^{\infty}K_{5/3}(\xi)\,\mathrm{d}\xi$$
$$= \tfrac{2}{\sqrt{3}\pi}K_{2/3}(\xi) - \tfrac{1}{\sqrt{3}\pi}\int_{x_0}^{\infty}K_{5/3}(\xi)\,\mathrm{d}\xi\,. \qquad (9.149)$$

We use (9.148) and (9.149) in (9.147) and get the simple expression for the synchrotron radiation spectrum

$$\frac{\mathrm{d}P_\gamma}{\mathrm{d}\omega} = \frac{P_\gamma}{\omega_\mathrm{c}}\,\tfrac{9\sqrt{3}}{8\pi}\frac{\omega}{\omega_\mathrm{c}}\int_{x_0}^{\infty}K_{5/3}(x)\mathrm{d}x = \frac{P_\gamma}{\omega_\mathrm{c}}\,S\left(\frac{\omega}{\omega_\mathrm{c}}\right)\,, \qquad (9.150)$$

where we defined the universal function

$$S\left(\frac{\omega}{\omega_\mathrm{c}}\right) = \tfrac{9\sqrt{3}}{8\pi}\frac{\omega}{\omega_\mathrm{c}}\int_{\omega/\omega_\mathrm{c}}^{\infty}K_{5/3}(x)\mathrm{d}x\,. \qquad (9.151)$$

The spectral distribution depends only on the critical frequency ω_c, the total radiation power and a purely mathematical function. This result has been derived originally by Ivanenko and Sokolov [20] and independently by Schwinger [21]. Specifically, it should be noted that the synchrotron radiation spectrum, if normalized to the critical frequency, does not depend on the particle energy and is represented by the universal function shown in Fig. 9.12. The energy dependence is contained in the cubic dependence of the critical frequency acting as a scaling factor for the real spectral distribution.

The mathematical function is properly normalized as we can see by integrating over all frequencies.

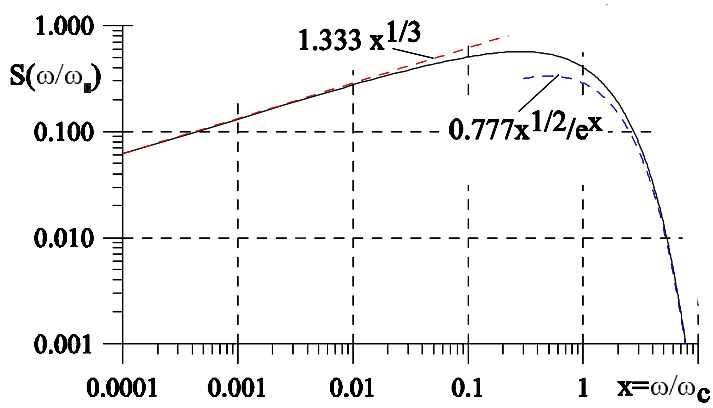

Fig. 9.12. Universal function: $S(\xi) = \frac{9\sqrt{3}}{8\pi}\xi \int_\xi^\infty K_{5/3}(x)\,\mathrm{d}x$, with $\xi = \omega/\omega_\mathrm{c}$

$$\int_0^\infty \frac{\mathrm{d}P_\gamma}{\mathrm{d}\omega}\mathrm{d}\omega = \frac{9\sqrt{3}}{8\pi}P_\gamma \int_0^\infty \int_{x_0}^\infty K_{5/3}(x)\mathrm{d}x\,\mathrm{d}x_0\,. \tag{9.152}$$

After integration by parts, the result can be derived from GR[6.561.16] [54]

$$\int_0^\infty \frac{\mathrm{d}P_\gamma}{\mathrm{d}\omega}\mathrm{d}\omega = \frac{9\sqrt{3}}{16\pi}P_\gamma \int_0^\infty x_0^2\,K_{5/3}(x_0)\mathrm{d}x_0 = \Gamma\,(4/3)\;\Gamma(2/3)\,. \tag{9.153}$$

Using the triplication formula AS(6.1.19) [24] the product of the gamma functions becomes

$$\Gamma\,(4/3)\,\Gamma(2/3) = \tfrac{4}{9}\tfrac{2\pi}{\sqrt{3}}\,. \tag{9.154}$$

With this equation the proper normalization of (9.152) is demonstrated

$$\int_0^\infty \frac{\mathrm{d}P_\gamma}{\mathrm{d}\omega}\mathrm{d}\omega = P_\gamma\,. \tag{9.155}$$

Of more practical use is the spectral photon flux per unit angle of deflection in the bending magnet. With the photon flux $\mathrm{d}\dot{N}_\mathrm{ph} = \mathrm{d}P/\hbar\omega$ we get from (9.150)

$$\frac{\mathrm{d}\dot{N}_\mathrm{ph}}{\mathrm{d}\psi} = \frac{P_\gamma}{2\pi\hbar\omega_\mathrm{c}}\frac{\Delta\omega}{\omega}\,S\left(\frac{\omega}{\omega_\mathrm{c}}\right) \tag{9.156}$$

and with (9.59) and (9.78)

$$\frac{\mathrm{d}\dot{N}_\mathrm{ph}}{\mathrm{d}\psi} = \frac{4\alpha}{9}\,\gamma\,\frac{I}{e}\frac{\Delta\omega}{\omega}\,S\left(\frac{\omega}{\omega_\mathrm{c}}\right)\,, \tag{9.157}$$

where ψ is the deflection angle in the bending magnet and α the fine structure constant. In practical units, this becomes

$$\frac{\mathrm{d}\dot{N}_{\mathrm{ph}}}{\mathrm{d}\psi} = C_\psi \, E \, I \, \frac{\Delta\omega}{\omega} \, S\left(\frac{\omega}{\omega_{\mathrm{c}}}\right) \tag{9.158}$$

with

$$C_\psi = \frac{4\alpha}{9e\,mc^2} = 3.967 \ \cdot 10^{16} \ \frac{\text{photons}}{\text{s mrad A GeV}} . \tag{9.159}$$

The synchrotron radiation spectrum in Fig. 9.12 is rather uniform up to the critical frequency beyond which the intensity falls off rapidly. Equation (9.150) is not well suited for quick calculation of the radiation intensity at a particular frequency. We may, however, express (9.150) in much simpler form for very low and very large frequencies making use of approximate expressions of Bessel's functions for large and small arguments.

For small arguments $\left(x = \frac{\omega}{\omega_{\mathrm{c}}} \ll 1\right)$ we find with AS(9.6.9) [24]

$$K_{5/3}(x \longrightarrow 0) \approx \Gamma\left(\tfrac{5}{3}\right) \frac{2^{2/3}}{x^{5/3}} , \tag{9.160}$$

which allows us to integrate (9.153) readily and get instead of (9.150)

$$\frac{\mathrm{d}P_\gamma}{\mathrm{d}\omega} \approx \tfrac{9\sqrt{3}}{8\pi} \frac{P_\gamma}{\omega_{\mathrm{c}}} 2^{2/3} \, \Gamma(2/3) \left(\frac{\omega}{\omega_{\mathrm{c}}}\right)^{1/3} \approx 1.333 \left(\frac{\omega}{\omega_{\mathrm{c}}}\right)^{1/3} \frac{P_\gamma}{\omega_{\mathrm{c}}} . \tag{9.161}$$

For high photon frequencies $\left(x = \frac{\omega}{\omega_{\mathrm{c}}} \gg 1\right)$ the modified Bessel's function becomes from AS(9.7.2) [24]

$$K_{5/3}(x \gg 1) \approx \sqrt{\frac{\pi}{2}} \frac{\mathrm{e}^{-x}}{\sqrt{x}} \tag{9.162}$$

and after integration with GR(3.361.1) and GR(3.361.2), [54] (9.150) becomes

$$\frac{\mathrm{d}P_\gamma}{\mathrm{d}\omega} \approx \tfrac{9\sqrt{3}}{\sqrt{2}\pi} \frac{P_\gamma}{\omega_{\mathrm{c}}} \sqrt{\frac{\omega}{\omega_{\mathrm{c}}}} \mathrm{e}^{\omega/\omega_{\mathrm{c}}} \approx 0.77736 \, \frac{P_\gamma}{\omega_{\mathrm{c}}} \sqrt{\frac{\omega}{\omega_{\mathrm{c}}}} \mathrm{e}^{\omega/\omega_{\mathrm{c}}} . \tag{9.163}$$

Both approximations are included in Fig. 9.12 and display actually a rather good representation of the real spectral radiation distribution. Specifically, we note the slow increase in the radiation intensity at low frequencies and the exponential drop off above the critical frequency.

9.7.1 Statistical Radiation Parameters

The emission of synchrotron radiation is a classical phenomenon. For some applications it is, however, useful to express some parameters in statistical

form. Knowing the spectral radiation distribution, we may follow Sands [14] and express some quantities in the photon picture. We have used such parameters in Chapter 7 to derive expressions for the equilibrium beam size and energy spread. Equilibrium beam parameters are determined by the statistical emission of photons and its recoil on the particle motion. For this purpose, we are mainly interested in an expression for $\varepsilon_{\mathrm{ph}}^2$ and the photon flux at energy $\varepsilon_{\mathrm{ph}}$. From these quantities, we may derive an expression for the average photon energy $\left\langle \varepsilon_{\mathrm{ph}}^2 \right\rangle_s$ emitted along the circumference of the storage ring.

With $\mathit{\Pi}\left(\varepsilon_{\mathrm{ph}}\right)$ being the probability to emit a photon with energy $\varepsilon_{\mathrm{ph}}$ we have

$$\left\langle \varepsilon_{\mathrm{ph}}^2 \right\rangle = \int_0^\infty \varepsilon_{\mathrm{ph}}^2 \mathit{\Pi}\left(\varepsilon_{\mathrm{ph}}\right) \mathrm{d}\varepsilon_{\mathrm{ph}} \,. \tag{9.164}$$

The probability $\mathit{\Pi}\left(\varepsilon_{\mathrm{ph}}\right)$ is defined by the ratio of the photon flux $\dot{n}(\varepsilon_{\mathrm{ph}})$ emitted at energy $\varepsilon_{\mathrm{ph}}$ to the total photon flux $\dot{N}_{\mathrm{ph}}$

$$\mathit{\Pi}\left(\varepsilon_{\mathrm{ph}}\right) = \frac{\dot{n}(\varepsilon_{\mathrm{ph}})}{\dot{N}_{\mathrm{ph}}} \,. \tag{9.165}$$

The photon flux at $\varepsilon_{\mathrm{ph}}$ can be derived from $\varepsilon_{\mathrm{ph}} \dot{n}(\varepsilon_{\mathrm{ph}})\, \mathrm{d}\varepsilon_{\mathrm{ph}} = P\left(\varepsilon_{\mathrm{ph}}\right) \mathrm{d}\varepsilon_{\mathrm{ph}}$. Integrating (9.156) over all angles ψ and multiplying by $\hbar\omega = \varepsilon_{\mathrm{ph}}$ we get for the spectral radiation power

$$P\left(\varepsilon_{\mathrm{ph}}\right) \mathrm{d}\varepsilon_{\mathrm{ph}} = \varepsilon_{\mathrm{ph}} \frac{\mathrm{d}\dot{N}}{\mathrm{d}\varepsilon_{\mathrm{ph}}} \mathrm{d}\varepsilon_{\mathrm{ph}} = \frac{P_\gamma}{\varepsilon_{\mathrm{c}}} S\left(\frac{\varepsilon_{\mathrm{ph}}}{\varepsilon_{\mathrm{c}}}\right) \mathrm{d}\varepsilon_{\mathrm{ph}} \,,$$

and

$$\dot{n}(\varepsilon_{\mathrm{ph}}) = \frac{P_\gamma}{\varepsilon_{\mathrm{c}}^2} \frac{S\left(x\right)}{x} \,, \qquad \text{where} \qquad x = \frac{\varepsilon_{\mathrm{ph}}}{\varepsilon_{\mathrm{c}}} \,. \tag{9.166}$$

The total number of emitted photons per unit time is just the integral

$$\dot{N}_{\mathrm{ph}} = \int_0^\infty \dot{n}(\varepsilon_{\mathrm{ph}})\, \mathrm{d}\varepsilon_{\mathrm{ph}} = \frac{P_\gamma}{\varepsilon_{\mathrm{c}}} \int_0^\infty \frac{S\left(x\right)}{x} \mathrm{d}x = \frac{15\sqrt{3}}{8} \frac{P_\gamma}{\varepsilon_{\mathrm{c}}} \,. \tag{9.167}$$

With this, the probability to emit a photon of energy $\varepsilon_{\mathrm{ph}}$ is finally

$$\mathit{\Pi}\left(\varepsilon_{\mathrm{ph}}\right) = \frac{8}{15\sqrt{3}} \frac{1}{\varepsilon_{\mathrm{c}}} \frac{S\left(x\right)}{x} \,, \tag{9.168}$$

and

$$\left\langle \varepsilon_{\mathrm{ph}}^2 \right\rangle_s = \frac{8\varepsilon_{\mathrm{c}}^2}{15\sqrt{3}} \int_0^\infty x\, S(x)\, \mathrm{d}x = \frac{11}{27} \varepsilon_{\mathrm{c}}^2 \,. \tag{9.169}$$

To calculate equilibrium beam parameters in Section 7.4.1 and thereafter, we need to know the quantity $\left\langle \dot{N}_{\rm ph} \langle \varepsilon_{\rm ph}^2 \rangle \right\rangle_s$ which is now from (9.167, 9.169)

$$\left\langle \dot{N}_{\rm ph} \langle \varepsilon^2 \rangle \right\rangle_s = \frac{55}{24\sqrt{3}} \langle \varepsilon_{\rm c} P_\gamma \rangle_s \ , \tag{9.170}$$

where the average is to be taken along the orbit and around the storage ring through all magnets. Expressing the critical photon energy by (9.78) and the radiation power by (9.59) and we get finally

$$\left\langle \dot{N}_{\rm ph} \langle \varepsilon^2 \rangle \right\rangle_s = \frac{55}{24\sqrt{3}} r_{\rm e} c\, mc^2\, \hbar c\, \gamma^7 \left\langle \frac{1}{\rho^3} \right\rangle_s \ . \tag{9.171}$$

Exercises *

Exercise 9.1 (S). Integrate the radiation power distribution (9.76) over all solid angles and prove that the total radiation power is equal to (9.59).

Exercise 9.2 (S). In the ESRF (European Synchrotron Radiation Facility) synchrotron radiation source in Grenoble (France) an electron beam of 200 mA circulates at an energy of 6 GeV. The bending magnet field is 1.0 T. Calculate and plot the spectral photon flux into a band width of 0.1% and an acceptance angle of 10 mrad as a function of photon energy.

Exercise 9.3 (S). Derive an expression identifying the angle at which the spectral intensity has dropped to p% from the maximum intensity. Derive approximate expressions for very low or very large photon energies. Find the angle at which the total radiation intensity has dropped to 10%.

Exercise 9.4. Derive the wave equations (9.3) and (9.4).

Exercise 9.5. Derive (9.17).

Exercise 9.6. Derive (9.28) from (9.27) .Show that the electrical field in the radiation regime is purely orthogonal to the direction of observation. Is the field also parallel to the acceleration?

Exercise 9.7. Design a synchrotron radiation source for a photon energy of your choice. Use a simple FODO lattice and specify the minimum beam energy, beam current, and bending radius which will produce a bending magnet photon flux of 10^{14} photons/sec/mrad at the desired photon energy and into a band width of $\Delta\omega/\omega = 1\%$. What is the minimum and maximum photon energy for which the photon flux is at least 10^{11} photons/sec/mrad? How big is your ring assuming a 30% fill factor for bending magnets?

* The argument (S) indicates an exercise for which a solution is given in Appendix A.

10. Insertion Device Radiation

Synchrotron radiation from bending magnets is characterized by a wide spectrum from microwaves up to soft or hard x-rays as determined by the critical photon energy. To optimally meet the needs of basic research with synchrotron radiation, it is desirable to provide specific radiation characteristics that cannot be obtained from ring bending magnet but require special magnets. The field strength of bending magnets and the maximum particle beam energy in circular accelerators like a storage ring is fixed leaving no adjustments to optimize the synchrotron radiation spectrum for particular experiments. To generate specific synchrotron radiation characteristics, radiation is often produced from special insertion devices installed along the particle beam path. Such insertion devices introduce no net deflection of the beam and can therefore be incorporated in a beam line without changing its geometry. Motz [56] proposed first the use of undulators or wiggler magnets to optimize characteristics of synchrotron radiation. By now, such magnets have become the most common insertion devices consisting of a series of alternating magnet poles deflecting the beam periodically in opposite directions as shown in Fig. 10.1.

In Chapter 4 the properties of wiggler radiation were discussed shortly in an introductory way. Here we concentrate on more detailed and formal derivations of radiation characteristics from relativistic electrons passing through undulator and wiggler magnets.

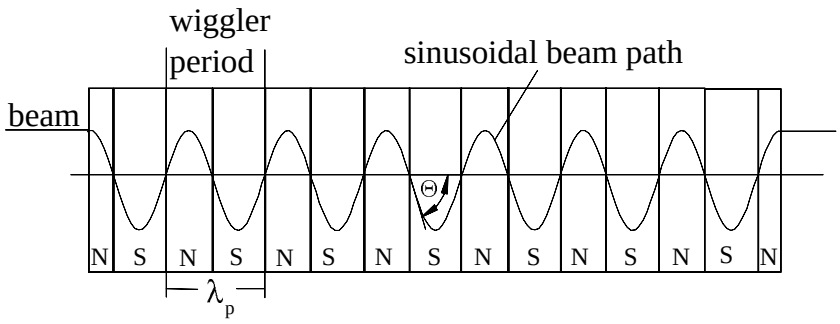

Fig. 10.1. Trajectory of a particle beam in a flat wiggler magnet

There is no fundamental difference between wiggler and undulator radiation. An undulator is basically a weak wiggler magnet. The deflection in an undulator is weak and the transverse particle momentum remains nonrelativistic. The motion is purely sinusoidal in a sinusoidal field, and the emitted radiation is monochromatic at the particle oscillation frequency which is the Lorentz-contracted periodicity of the undulator period. Since the radiation is emitted from a moving source the observer in the laboratory frame of reference then sees a Doppler shifted frequency. We call this monochromatic radiation the fundamental radiation or radiation at the fundamental frequency of the undulator.

As the undulator field is increased, the transverse motion becomes stronger and the transverse momentum starts to become relativistic. As a consequence, the so far purely sinusoidal motion becomes periodically distorted causing the appearance of harmonics of the fundamental monochromatic radiation. These harmonics increase in number and density with further increase of the magnetic field and, at higher frequencies, eventually merge into one broad spectrum characteristic for wiggler or bending magnet radiation. At very low frequencies, the theoretical spectrum is still a line spectrum showing the harmonics of the revolution frequency. Of course, there is a low frequency cut-off at wavelength comparable or longer than vacuum chamber dimensions which therefore do not show-up as radiation.

An insertion device does not introduce a net deflection of the beam and we may therefore choose any arbitrary field strength which is technically feasible to adjust the radiation spectrum to experimental needs. The radiation intensity from a wiggler magnet also can be made much higher compared to that from a single bending magnet. A wiggler magnet with say ten poles acts like a string of ten bending magnets or radiation sources aligned in a straight line along the photon beam direction. The effective photon source is therefore ten times more intense than the radiation from a single bending magnet with the same field strength.

Wiggler magnets come in a variety of types with the flat wiggler magnet being the most common. In this wiggler type only the component B_y is nonzero deflecting the beam in the horizontal plane. To generate circularly or elliptically polarized radiation, a helical wiggler magnet [36] may be used or a combination of several flat wiggler magnets deflecting the beam in orthogonal planes which will be discussed in more detail in Section 10.3.2.

10.1 Periodic Magnetic Field

Wiggler magnets are generally designed as flat wiggler magnets [56] with field components only in one plane or as helical wiggler magnets [36][57][58], where the transverse field component rotates along the magnetic axis. In this discussion, we concentrate on flat wigglers which are used widely to generate,

for example, intense beams of synchrotron radiation from electron beams, to manipulate beam parameters or to pump a free electron laser .

Whatever the application may be, the wiggler magnet deflects the electron beam transversely in an alternating fashion without introducing an overall net deflection on the beam. Wiggler magnets are generally considered to be insertion devices , meaning they are not part of the basic magnet lattice of the accelerator but are installed in a magnet free straight section of the lattice. They can be turned on or off without affecting the functioning of the accelerator.

10.1.1 Periodic Field Configuration

To eliminate an overall effect of wiggler fields on the particle beam trajectory, the integrated magnetic field along the axis of the whole magnet must be zero

$$\int_{\text{wiggler}} B_\perp \, \mathrm{d}z \; = \; 0. \tag{10.1}$$

Within this boundary condition we derive the general field configuration. Since a wiggler magnet is a straight device, we use a fixed Cartesian coordinate system (x, y, z) with the z-axis parallel to the wiggler axis to describe the wiggler field. The origin of the coordinate system is placed in the middle of one of the wiggler magnet poles. The whole magnet may be composed of N equal and symmetric pole pieces placed along the z-axis at a distance $\lambda_\mathrm{p}/2$ from pole center to pole center as depicted in Fig. 10.1. Each pair of adjacent wiggler poles forms one wiggler period with a length λ_p and the whole magnet is composed of $N_\mathrm{p} = \frac{1}{2}N$ periods. Since all periods are assumed to be equal and the beam deflection is compensated within each period no net beam deflection occurs for the complete magnet. At either end of the wiggler magnet, we must have "half poles" or "half fields" to match the external beam path.

We consider only periodic fields which can be expanded into a Fourier series along the axis including a strong fundamental component with a period length λ_p and higher harmonics expressed by the ansatz

$$B_y \; = \; B_\mathrm{o} \sum_{n=0}^{\infty} b_{2n+1}(x,y) \, \cos[(2n+1)\, k_\mathrm{p} z] \, , \tag{10.2}$$

where the wave number $k_\mathrm{p} = 2\pi/\lambda_\mathrm{p}$. The ideal configuration depends on the application. For the production of high brightness photon beams from an undulator one would choose a pure sinusoidal variation of the field with period λ_p and no higher harmonics. In applications where only flux or high photon energies are desired one would look for a magnet which exhibits some flat field profile along z in each pole. Such a configuration would include many harmonics as reflected in (10.2) .

The functions $b_{2n+1}(x,y)$ describe the variation of the field amplitude orthogonal to the beam axis for the harmonic $(2n+1)$. The content of higher harmonics is greatly influenced by the particular design of the wiggler magnet and the ratio of the period length to the pole gap aperture. For very long periods relative to the pole aperture the field profile approaches that of a hard-edge dipole field with a square field profile along the z-axis. For very short periods compared to the pole aperture, on the other hand, we find only a significant amplitude for the fundamental period and very small perturbations due to higher harmonics.

We may derive the magnetic field from Maxwell's equations based on a sinusoidal field along the axis. Each field harmonic may be determined separately due to the linear superposition of fields. To eliminate a dependence of the magnetic field on the horizontal variable x we assume a pole width which is large compared to the pole aperture in which case we may set $b_{2n+1}(x,y) = b_{2n+1}(y)$. For the same reason and from symmetry $B_x \equiv 0$. The fundamental field component $(n=0)$ can then be expressed by

$$B_y(y,z) \;=\; B_0\, b_1(y)\, \cos k_{\mathrm{p}} z\,. \tag{10.3}$$

From Maxwell's curl equation $\nabla \times \mathbf{B} = 0$ we get $\frac{\partial B_z}{\partial y} = \frac{\partial B_y}{\partial z}$ and with (10.3) we have

$$\frac{\partial B_z}{\partial y} \;=\; \frac{\partial B_y}{\partial z} \;=\; -B_0\, b_1(y)\, k_{\mathrm{p}}\, \sin k_{\mathrm{p}} z\,. \tag{10.4}$$

We have not yet determined the y-dependence of the amplitude function $b_1(y)$. From $\boldsymbol{\nabla}\mathbf{B} = 0$ and the independence of the field on the horizontal position we get with (10.3)

$$\frac{\partial B_z}{\partial z} \;=\; -\; B_0\, \frac{\partial\, b_1(y)}{\partial y}\, \cos k_{\mathrm{p}} z\,. \tag{10.5}$$

Forming the second derivatives $\partial^2 B_z/(\partial y\, \partial z)$ from (10.4) and (10.5) we get for the amplitude function the differential equation

$$\frac{\partial^2\, b_1(y)}{\partial y^2} \;=\; k_{\mathrm{p}}^2\, b_1(y)\,, \tag{10.6}$$

which can be solved by the hyperbolic functions

$$b_1(y) \;=\; a\, \cosh k_{\mathrm{p}} y + b\, \sinh k_{\mathrm{p}} y\,. \tag{10.7}$$

Since $b_1(0) = 1$ and the magnetic field is symmetric with respect to $y = 0$ the coefficients are $a = 1$ and $b = 0$. Collecting all partial results, the wiggler magnet field is finally determined by the components

$$\begin{aligned} B_x &= 0, \\ B_y &= B_0 \cosh k_{\mathrm{p}} y\, \cos k_{\mathrm{p}} z, \\ B_z &= B_0 \sinh k_{\mathrm{p}} y\, \sin k_{\mathrm{p}} z, \end{aligned} \tag{10.8}$$

where B_z is obtained by integration of (10.4) with respect to y.

The hyperbolic dependence of the field amplitude on the vertical position introduces higher-order field-errors which we determine by expanding the hyperbolic functions

$$\cosh k_\mathrm{p} y = 1 + \frac{(k_\mathrm{p} y)^2}{2!} + \frac{(k_\mathrm{p} y)^4}{4!} + \frac{(k_\mathrm{p} y)^6}{6!} + \frac{(k_\mathrm{p} y)^8}{8!} + ... \tag{10.9a}$$

$$\sinh k_\mathrm{p} y = k_\mathrm{p} y + \frac{(k_\mathrm{p} y)^3}{3!} + \frac{(k_\mathrm{p} y)^5}{5!} + \frac{(k_\mathrm{p} y)\,7}{7!} + ... \tag{10.9b}$$

Typically, the vertical gap in a wiggler magnet is smaller than the period length or $y < \lambda_\mathrm{p}$. For larger apertures the field strength reduces drastically. Due to the fast convergence of the series expansions only a few terms are required to obtain an accurate expression for the hyperbolic function within the wiggler aperture. The expansion displays the higher-order field components explicitly which, however, do not have the form of higher-order multipole fields and we cannot treat these fields just like any other multipole perturbation but must consider them separately.

To determine the path distortion due to the wiggler fields, we follow the reference trajectory through one quarter period starting at a symmetry plane in the middle of a pole. At the starting point $z = 0$ in the middle of a wiggler pole, the beam direction is parallel to the reference trajectory and the deflection angle at a downstream point z is given by

$$\begin{aligned}\vartheta(z) &= \frac{[c]\,e}{cp}\int_0^z B_y \,\mathrm{d}\bar{z} = \frac{[c]\,e}{cp} B_0 \cosh k_\mathrm{p} y \int_0^z \cos k_\mathrm{p}\bar{z}\,\mathrm{d}\bar{z} \\ &= -\frac{[c]\,e}{cp} B_0 \frac{1}{k_\mathrm{p}} \cosh k_\mathrm{p} y \,\sin k_\mathrm{p} z\,. \end{aligned} \tag{10.10}$$

The maximum deflection angle is equal to the deflection angle for a quarter period or half a wiggler pole and is from (10.10) for $y = 0$ and $k_\mathrm{p} z = \pi/2$

$$\theta \;=\; -\frac{[c]e}{cp}\, B_0\, \frac{\lambda_\mathrm{p}}{2\,\pi}\,. \tag{10.11}$$

This deflection angle is used to define the wiggler strength parameter

$$K \;=\; \beta\gamma\,\theta \;=\; \frac{[c]\,e}{2\,\pi\,m\,c^2}\, B_0\,\lambda_\mathrm{p}\,, \tag{10.12}$$

where $m\,c^2$ is the particle rest energy and γ the particle energy in units of the rest energy. In more practical units this strength parameter is

$$K = C_K\, B_0\,(\mathrm{T})\;\lambda_\mathrm{p}\,(\mathrm{cm}) \approx B_0\,(\mathrm{T})\;\lambda_\mathrm{p}\,(\mathrm{cm})\;, \tag{10.13}$$

where

$$C_K = \frac{[c]\,e}{2\,\pi\,m\,c^2} = 0.93373\;\mathrm{T}^{-1}\,\mathrm{cm}^{-1}\;. \tag{10.14}$$

10.1.2 Particle Dynamics in a Periodic Field Magnet

Particle dynamics and resulting radiation characteristics for an undulator have been derived first by Motz [56] and later in more detail by other authors [59]-[60]. A sinusoidally varying vertical field causes a periodic deflection of particles in the (x,z)-plane shown in Fig. 10.1. To describe the particle trajectory, we use the equation of motion

$$\frac{\mathbf{n}}{\rho} = [c]\frac{e}{mc^2\gamma\beta^2}[\boldsymbol{\beta}\times\boldsymbol{B}] \ , \tag{10.15}$$

where β is the particle velocity and get with (10.3) the equations of motion in component form

$$\frac{\mathrm{d}^2x}{\mathrm{d}t^2} = -\frac{eB_0}{\gamma mc}\frac{\mathrm{d}z}{\mathrm{d}t}\cos(k_\mathrm{p}z) \ , \tag{10.16a}$$

$$\frac{\mathrm{d}^2z}{\mathrm{d}t^2} = +\frac{eB_0}{\gamma mc}\frac{\mathrm{d}x}{\mathrm{d}t}\cos(k_\mathrm{p}z) \ , \tag{10.16b}$$

where we have set $k_\mathrm{p} = 2\pi/\lambda_\mathrm{p}$ and $\mathrm{d}z = \beta c\,\mathrm{d}t$ with $\beta = v/c$.

Equations (10.16) describe the coupled motion of a particle in the sinusoidal field of a flat wiggler magnet. This coupling is common to the particle motion in any magnetic field but generally in beam dynamics we set $\mathrm{d}z/\mathrm{d}t \approx v$ and $\mathrm{d}x/\mathrm{d}t \approx 0$ because $\mathrm{d}x/\mathrm{d}t \ll \mathrm{d}z/\mathrm{d}t$. This approximation is justified in most beam transport applications for relativistic particles, but here we have to be cautious not to neglect effects that might be of relevance on a very short time or small geometric scale comparable to the oscillation period and wavelength of synchrotron radiation.

We will keep the $\mathrm{d}x/\mathrm{d}t$-term and get from (10.16a) with $\mathrm{d}z/\mathrm{d}t \approx v$ and after integrating twice that the particle trajectory follows the magnetic field in the sense that the oscillatory motion reaches a maximum where the magnetic field reaches a maximum and crosses the beam axis where the field is zero. We start at the time $t = 0$ in the middle of a magnet pole where the transverse velocity $\dot{x}_0 = 0$ while the longitudinal velocity $\dot{z}_0 = \beta c$ and integrate both equations (10.16) utilizing the integral of the first equation in the second to get

$$\frac{\mathrm{d}x}{\mathrm{d}t} = -\beta c\frac{K}{\gamma}\sin(k_\mathrm{p}\,z) \ , \tag{10.17a}$$

$$\frac{\mathrm{d}z}{\mathrm{d}t} = \beta c\left[1 - \frac{K^2}{2\gamma^2}\sin^2(k_\mathrm{p}\,z)\right] . \tag{10.17b}$$

The transverse motion describes the expected oscillatory motion and the longitudinal velocity v exhibits a periodic modulation reflecting the varying projection of the velocity vector to the z-axis. Closer inspection of this velocity modulation shows that its frequency is twice that of the periodic motion.

It is convenient to describe the longitudinal particle motion with respect to a Cartesian reference frame moving uniformly along the z-axis with the average longitudinal particle velocity $\bar{\beta}c = \langle \dot{z} \rangle$ which can be derived from (10.17b)

$$\bar{\beta} \;=\; \beta \left(1 - \tfrac{K^2}{4\gamma^2}\right) . \tag{10.18}$$

In this reference frame the particle follows a figure-of-eight trajectory composed of the transverse oscillation and a longitudinal oscillation with twice the frequency. We will come back to this point since both oscillations contribute to the radiation spectrum. A second integration of (10.17b) results finally in the equation of motion in component representation

$$x(t) = \frac{K}{\gamma k_\mathrm{p}} \cos\left(k_\mathrm{p}\, \bar{\beta}\, ct\right) , \tag{10.19a}$$

$$z(t) = \bar{\beta} ct + \frac{K^2}{8\gamma^2 k_\mathrm{p}} \sin^2\left(2k_\mathrm{p}\, \bar{\beta}\, ct\right) , \tag{10.19b}$$

where we set $z = \bar{\beta}\, c\, t$. The maximum amplitude a of the transverse particle oscillation is finally from

$$a = \frac{K}{\gamma k_\mathrm{p}} = \frac{\lambda_\mathrm{p} K}{2\pi\gamma} . \tag{10.20}$$

This last expression gives another simple relationship between the wiggler strength parameter and the transverse displacement of the beam trajectory

$$a\,(\mu\mathrm{m}) = 0.8133\, \frac{\lambda_\mathrm{p}\,(\mathrm{cm})\;K}{E\,(\mathrm{GeV})} . \tag{10.21}$$

For general cases, this beam displacement is very small.

10.1.3 Focusing in a Wiggler Magnet

As mentioned earlier, a wiggler magnet should be transparent to the electron beam which can be achieved only approximately. Every pole end generates some fringe fields which cause a focusing effect on the particle beam. In low energy storage rings with strong superconducting wavelength shifters this effect can be a major perturbation which requires significant compensation in the ring lattice proper. A detailed derivation of such fringe fields and their effect on the beam can be found in [45][46]. Here, we will only repeat some of the more salient features and results.

The beam path in a wiggler magnet is generally not parallel to the reference trajectory z because of the transverse deflection in the wiggler field following a periodic sinusoidal form along the reference path. For this reason, the fringe field component B_z appears to the particle partially as a transverse field which varies linearly with y. Such a field term constitutes focusing similar to that in a quadrupole with a strength for each wiggler pole end of

$$k_y \ell = -\frac{1}{f_y} = -\frac{\lambda_\mathrm{p}}{8\rho_0^2}\,. \tag{10.22}$$

The focusing occurs in the vertical plane only assuming that the wiggler magnet deflects the beam in the horizontal plane, and is positive and independent of the sign of the deflection. For N wiggler poles, we have $2N$ times the focusing strength of each individual pole end and the focal length of the total wiggler magnet of length $L_\mathrm{w} = \frac{1}{2} N \lambda_\mathrm{p}$ expressed in units of the wiggler strength parameter K becomes

$$\frac{1}{f_y} = \frac{K^2}{2\gamma^2} k_\mathrm{p}^2 L_\mathrm{w}\,. \tag{10.23}$$

Tacitly, a rectangular form of the wiggler poles has been assumed (Fig. 10.2) and consistent with our sign convention we find that wiggler fringe fields cause focusing in the nondeflecting plane. Within the approximation used, there is no corresponding focusing effect in the deflecting plane. This is the situation for most wiggler magnet poles except for the first and last half pole where the beam enters the magnetic field normal to the pole face and no focusing occurs.

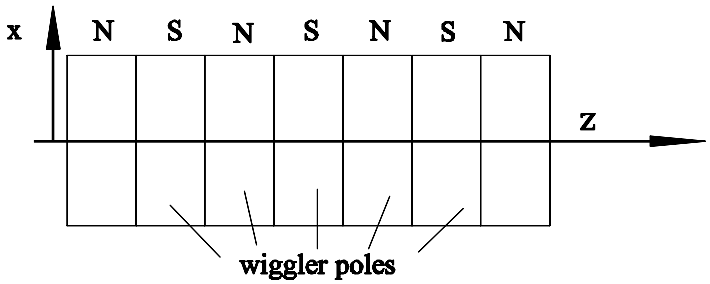

Fig. 10.2. Wiggler magnet with parallel pole end-faces

A reason to possibly use wiggler magnets with rotated pole faces like wedge magnets originates from the fact that the wiggler focusing is asymmetric, not part of the lattice focusing and may therefore need to be compensated. For moderately strong wiggler fields the asymmetric focusing in both planes can be compensated by small adjustments of lattice quadrupoles. The focusing effect of strong wiggler magnets, however, may generate a significant perturbation of the lattice focusing structure or create a situation where no stable solution for betatron functions exist. The severity of this problem can be reduced by designing the wiggler poles as wedge magnets in such a way as to split the focusing equally between both the horizontal and vertical plane (Fig. 10.3). In this case, local correction can be applied efficiently in nearby lattice or separate quadrupoles.

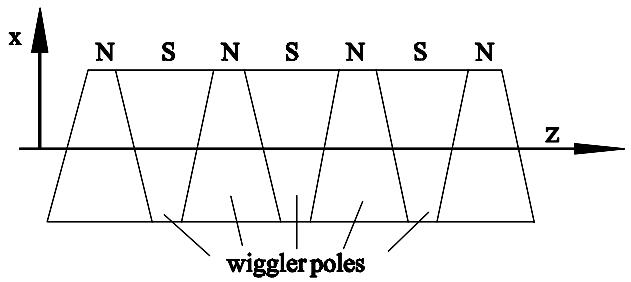

Fig. 10.3. Wiggler magnet with wedge shaped poles

The focal length of one half pole in the horizontal deflecting plane is from [45], Sect. 5.3.2

$$\frac{1}{f_x} = \frac{\eta + \theta}{\rho_x}\,, \tag{10.24}$$

where the pole face rotation angle η has been assumed to be small and of the order of the wiggler deflection angle per pole and $\theta = K/\gamma$ is the deflection angle of a half pole. In the case of a rectangular wiggler pole $\eta = -\theta$ and the focusing in the deflecting plane vanishes as we would expect.
In the nondeflecting plane, equation (5.66) in [45] applies and the focal length for small angles η and θ is

$$\frac{1}{f_y} = -\frac{\eta + \theta}{\rho_x} - \frac{\pi\theta}{4\rho_x}\,. \tag{10.25}$$

The focusing in each single wiggler pole is rather weak and we may apply thin lens approximation to derive the transformation matrices. For this we consider the focusing to occur in the middle of each wiggler pole with drift spaces of length $\lambda_\mathrm{p}/4$ on each side. With $2/f$ being the focal length of a full pole in either the horizontal plane (10.24) or the vertical plane (10.25) the transformation matrix for each wiggler pole is finally

$$\begin{aligned}\mathcal{M}_\mathrm{pole} &= \begin{pmatrix} 1 & \lambda_\mathrm{p}/4 \\ 0 & 1 \end{pmatrix} \begin{pmatrix} 1 & 0 \\ -2/f & 1 \end{pmatrix} \begin{pmatrix} 1 & \lambda_\mathrm{p}/4 \\ 0 & 1 \end{pmatrix} \\ &= \begin{pmatrix} 1 - \frac{\lambda_\mathrm{p}}{2f} & \frac{\lambda_\mathrm{p}}{2}\left(1 - \frac{\lambda_\mathrm{p}}{4f}\right) \\ -\frac{2}{f} & 1 - \frac{\lambda_\mathrm{p}}{2f} \end{pmatrix} \approx \begin{pmatrix} 1 & \frac{1}{2}\lambda_\mathrm{p} \\ -2/f & 1 \end{pmatrix}\,,\end{aligned} \tag{10.26}$$

where the approximation $\lambda_\mathrm{p} \ll f$ was used. For a wiggler magnet of length $L_\mathrm{w} = \frac{1}{2} N \lambda_\mathrm{p}$ we have N poles and the total transformation matrix is

$$\mathcal{M}_\mathrm{wiggler} = \mathcal{M}_\mathrm{pole}^N\,. \tag{10.27}$$

This transformation matrix can be applied to each plane and any pole rotation angle η. Specifically, we set $\eta = -K/\gamma$ for a rectangular pole cross section and $\eta = 0$ for pole rotations orthogonal to the path like in sector magnets.

10.1.4 Hard Edge Wiggler Model

Although the magnetic properties of wiggler magnets are well understood and easy to apply it is nonetheless often desirable to derive the focusing effects from hard-edge wiggler magnets. This is particularly true when special numerical programs are to be used which are not designed to properly model a sinusoidal wiggler field. We would like therefore to represent a sinusoidal wiggler magnet by a constant field magnet, called a hard-edge model. On the other hand, accurate field representation is important since frequently strong wiggler magnets are to be inserted into a beam transport lattice.

For the proper representation of linear focusing properties of wiggler magnets by a hard-edge model we require three conditions to be fulfilled. First, the deflection angle for each hard-edge pole should be the same as that for the real wiggler magnet. Second, the edge focusing must be the same. Third, like any other bending magnet in an electron circular accelerator, a wiggler magnet also contributes to quantum excitation and damping of beam emittance and energy spread. The quantum excitation is in first approximation proportional to the third power of the curvature while the damping scales like the square of the curvature similar to focusing.

We consider now a wiggler field

$$B(z) \;=\; B_0 \,\cos k_{\mathrm{p}} z \tag{10.28}$$

and try to model the field for a half pole with parallel endpoles by a hard-edge magnet. The deflection angle of the hard-edge model of length ℓ and field B must be the same as that for a wiggler half pole, or

$$\theta \;=\; \frac{\ell_{\mathrm{h}}}{\rho_{\mathrm{h}}} \;=\; \frac{[c]e}{cp_0}\int_{\mathrm{halfpole}} B_y(z)\,\mathrm{d}z \;=\; \frac{\lambda_{\mathrm{p}}}{2\pi\,\rho_0}\,. \tag{10.29}$$

Here we use ρ_{h} for the bending radius of the hard-edge model and ρ_0 for the bending radius at the peak wiggler field B_{o}. The edge focusing condition can be expressed by

$$\frac{1}{f} = \frac{\ell_{\mathrm{h}}}{\rho_{\mathrm{h}}^2} \;=\; \frac{1}{\rho_0^2}\int_{\mathrm{halfpole}} \cos^2 k_{\mathrm{p}} z\,\mathrm{d}z \;=\; \frac{\lambda_{\mathrm{p}}}{8\rho_0^2}\,. \tag{10.30}$$

Modeling a wiggler field by a single hard-edge magnet requires in linear beam optics only two conditions to be met which can be done with the two available parameters $B(z)$ and ℓ. From (10.29,10.30) we get therefore the hard-edge magnet parameters (Fig. 10.4)

$$\rho_{\rm h} = \frac{4}{\pi}\,\rho_0 \qquad \text{and} \qquad \ell_{\rm h} = \frac{2}{\pi^2}\,\lambda_{\rm p}\,. \tag{10.31}$$

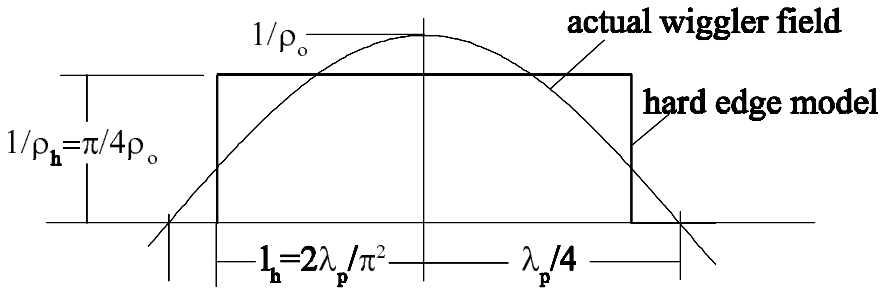

Fig. 10.4. Hard edge model for a wiggler magnet pole

For a perfect modeling of the equilibrium energy spread and emittance due to quantum excitation in electron storage rings we would also like the cubic term to be the same

$$\frac{\ell_{\rm h}}{\rho_{\rm h}^3} \stackrel{?}{=} \frac{1}{\rho_0^3}\int_{\rm halfpole} \cos^3 k_{\rm p} z\,{\rm d}z \;=\; \frac{\lambda_{\rm p}}{3\pi\,\rho_0^3}\,. \tag{10.32}$$

Since we have no more free parameters available, we can at this point only estimate the mismatch. With (10.30,10.31) we get from (10.32) the inequality

$$\frac{1}{3\pi} \;\neq\; \frac{\pi}{32}\,,$$

which indicates that the quantum excitation from wiggler magnets is not correctly treated although the error is only about 8%. Alternatively to the choice of modeling conditions just made, one could decide that the quadratic and cubic terms must be equal while the deflection angle is not constrained. This would be a reasonable assumption since the total deflection angle of a wiggler is compensated anyway. In this case the deflection angle would be underestimated by about 8%. Where these mismatches are not significant, the simple hard-edge model (10.32) can be applied. For more accuracy the sinusoidal wiggler field must can be represented more accurately by splitting each half-pole into a series of hard-edge magnets with.

10.2 Undulator Radiation

The physical process of undulator radiation is not different from the radiation produced from a single bending magnet. However, the radiation received

at great distances from the undulator exhibits special features which we will discus in more detail. Basically, we observe an electron performing N_p oscillations while passing through an undulator, where N_p is the number of undulator periods. The observed radiation spectrum is the Fourier transform of the electron motion and therefore quasi-monochromatic with a finite line width inversely proportional to the number of oscillations performed.

10.2.1 Fundamental Wavelength

Undulator radiation can also be viewed as a superposition of radiation fields from N_p sources yielding quasi-monochromatic radiation as a consequence of interference. To see that, we observe the radiation at an angle ϑ with respect to the path of the electron as shown in Fig. 10.5.

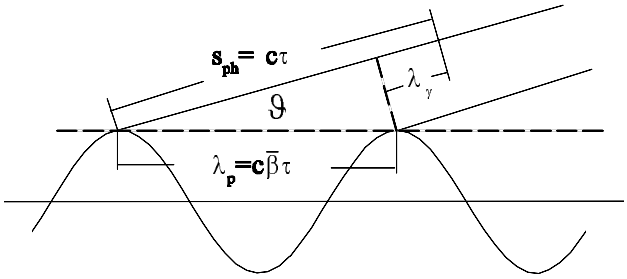

Fig. 10.5. Interference of undulator radiation

The electron travels on its path at an average velocity given by (10.18) and it takes the time

$$\tau \;=\; \frac{\lambda_\mathrm{p}}{c\bar{\beta}} \;=\; \frac{\lambda_\mathrm{p}}{c\beta\,[1 - K^2/(4\gamma^2)]} \tag{10.33}$$

to move along one undulator period. During that same time, the radiation front proceeds a distance

$$s_\mathrm{ph} \;=\; \tau\, c \;=\; \frac{\lambda_\mathrm{p}}{\beta\,[1 - K^2/(4\gamma^2)]} \tag{10.34}$$

moving ahead of the particle since $s_\mathrm{ph} > \tau c\bar{\beta}$. For constructive superposition of radiation from all undulator periods, we require that the difference $s_\mathrm{ph} - \lambda_\mathrm{p} \cos\vartheta$ be equal to an integer multiple of the wavelength λ_k or for small observation angles $\vartheta \ll 1$

$$k\,\lambda_k \;=\; \frac{\lambda_\mathrm{p}}{\beta\,[1 - K^2/(4\gamma^2)]} - \lambda_\mathrm{p}\,(1 - \tfrac{1}{2}\,\vartheta^2)\,. \tag{10.35}$$

After some manipulations, we get with $K^2/\gamma^2 \ll 1$ and $\beta \approx 1$ for the k^{th} harmonic of the fundamental wavelength of radiation into and angle ϑ

$$\lambda_k = \frac{\lambda_\text{p}}{2\gamma^2\, k}\left(1 + \tfrac{1}{2}K^2 + \gamma^2\vartheta^2\right) . \tag{10.36}$$

From an infinitely long undulator, the radiation spectrum consists of spectral lines at a wavelength determined by (10.36). In particular, we note that the shortest wavelength is emitted into the forward direction while the radiation at a finite angle ϑ appears red shifted by the Doppler effect. For an undulator with a finite number of periods, the spectral lines are widened to a width of about $1/N_\text{p}$ or less as we will discuss in the next section.

10.2.2 Radiation Power

The radiation power is from (9.41)

$$P \;=\; \tfrac{2}{3}\, r_\text{c}\, mc\, |\, \dot{\beta}^*\, |^2_\text{r}\, , \tag{10.37}$$

where * indicates quantities to be evaluated in the particle reference system. We may use this expression in the particle system to calculate the total radiated energy from an electron passing through an undulator. The transverse particle acceleration is expressed by $m\dot{\mathbf{v}}^* = \mathrm{d}\mathbf{p}_\perp/\mathrm{d}t^* = \gamma \mathrm{d}\mathbf{p}_\perp/\mathrm{d}t$ where we used $t^* = t/\gamma$ and inserting into (10.37) we get

$$P \;=\; \tfrac{2}{3}\,\frac{r_\text{c}\,\gamma^2}{mc}\left(\frac{\mathrm{d}\mathbf{p}_\perp}{\mathrm{d}t}\right)^2 . \tag{10.38}$$

The transverse momentum is determined by the particle deflection in the undulator with a period length λ_p and is for a particle of momentum cp_0

$$p_\perp \;=\; \hat{p}\, \sin\omega_\text{p} t\, , \tag{10.39}$$

where $\hat{p} = p_0\theta$ and $\omega_\text{p} = ck_\text{p} = 2\pi c/\lambda_\text{p}$. The angle $\theta = K/\gamma$ is the maximum deflection angle defined in (10.12). With these expressions and averaging over one period, we get from (10.38) for the instantaneous radiation power from a charge e traveling through an undulator

$$P_\text{inst} = \tfrac{1}{3}\, cr_\text{c} mc^2\gamma^2 K^2 k_\text{p}^2\, , \tag{10.40}$$

where r_c is the classical electron radius. The duration of the radiation pulse is equal to the travel time through an undulator of length $L_\text{u} = \lambda_\text{p} N_\text{p}$ and the total radiated energy per electron is therefore

$$\Delta E \;=\; \tfrac{1}{3}\, r_\text{c}\, mc^2\, \gamma^2\, K^2\, k_\text{p}^2\, L_\text{u}\, . \tag{10.41}$$

In more practical units

$$\Delta E(\mathrm{eV}) \;=\; C_{\mathrm{u}} \frac{E^2\,K^2}{\lambda_{\mathrm{p}}^2}\,L_{\mathrm{u}} \;=\; 725.69 \frac{E^2(\mathrm{GeV})\,K^2}{\lambda_{\mathrm{p}}^2(\mathrm{cm})}\,L_{\mathrm{u}}(\mathrm{m}) \tag{10.42}$$

with

$$C_{\mathrm{u}} \;=\; \frac{4\pi^2\,r_{\mathrm{c}}}{3\,mc^2} \;=\; 7.2569 \times 10^{-20}\,\frac{\mathrm{m}}{\mathrm{eV}}\,. \tag{10.43}$$

The average total undulator radiation power for an electron beam circulating in a storage ring is then just the radiated energy (10.41) multiplied by the number of particles N_{b} in the beam and the revolution frequency or

$$P_{\mathrm{avg}} \;=\; \tfrac{1}{3}\,r_{\mathrm{c}}\,c\,mc^2\,\gamma^2\,K^2\,k_{\mathrm{p}}^2\,N_{\mathrm{b}}\,\frac{L_{\mathrm{u}}}{2\pi\,\bar{R}} \tag{10.44}$$

or

$$P_{\mathrm{avg}}(\mathrm{W}) \;=\; 6.336\,E^2(\mathrm{GeV})\,B_0^2(\mathrm{kG})\;I(\mathrm{A})\;L_{\mathrm{u}}(\mathrm{m})\,, \tag{10.45}$$

where I is the circulating electron beam current. The total angle integrated radiation power from an undulator in a storage ring is proportional to the square of the beam energy and maximum undulator field B_0 and proportional to the beam current and undulator length.

10.2.3 Spatial and Spectral Distribution

For bending magnet radiation, the particle dynamics is relatively simple being determined only by the particle velocity and the bending radius of the magnet. In a wiggler magnet, the magnetic field parameters are different from those in a constant field magnet and we will therefore derive again the synchrotron radiation spectrum for the beam dynamics in a general wiggler magnet. No special assumptions on magnetic field configurations have been made to derive the radiation spectrum (9.89) and we can therefore use this expression together with the appropriate beam dynamics to derive the radiation spectrum from a wiggler magnet

$$\frac{\mathrm{d}^2W}{\mathrm{d}\omega\,\mathrm{d}\Omega} \;=\; \frac{r_{\mathrm{c}}\,mc\,\omega^2}{4\pi^2} \left| \int_{-\infty}^{\infty} \boldsymbol{n} \times [\boldsymbol{n} \times \boldsymbol{\beta}]\,\mathrm{e}^{-\mathrm{i}\omega\left(t_{\mathrm{r}}+\frac{R}{c}\right)}\,\mathrm{d}\,t_{\mathrm{r}} \right|^2 . \tag{10.46}$$

The integrand in (10.46) can be evaluated from known particle dynamics in a wiggler magnet noting that all quantities are to be taken at the retarded time t_{r}. The unit vector from the observer to the radiating particle is from Fig. 10.6

$$\boldsymbol{n} \;=\; -\boldsymbol{x}\,\cos\varphi\,\sin\vartheta - \boldsymbol{y}\,\sin\varphi\,\sin\vartheta - \boldsymbol{z}\,\cos\vartheta\,. \tag{10.47}$$

The exponent in (10.46) includes the term $R/c = \boldsymbol{n}\boldsymbol{R}/c$. We express again the vector $\boldsymbol{R}$ from the observer to the particle by the constant vector $\boldsymbol{r}$ from

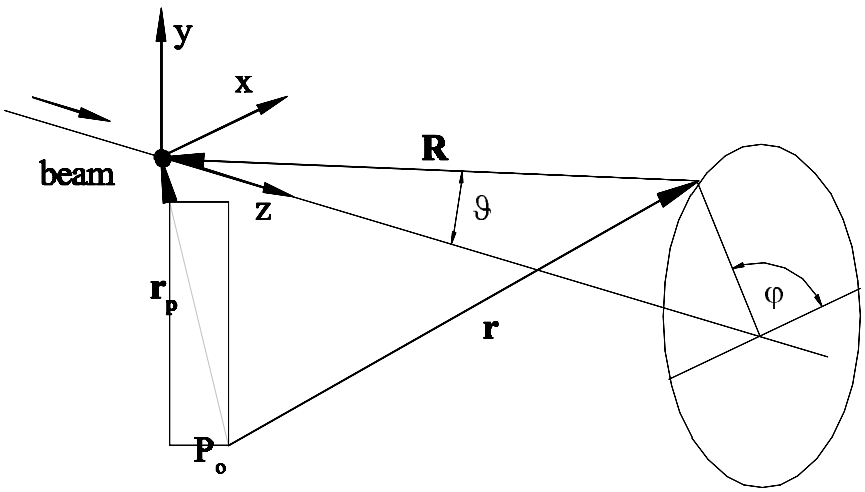

Fig. 10.6. Particle trajectory and radiation geometry in a wiggler magnet

the origin of the coordinate system to the observer and the vector $\boldsymbol{r}_\mathrm{p}$ from the coordinate origin to the particle for $\boldsymbol{R} = -\boldsymbol{r} + \boldsymbol{r}_\mathrm{p}$ as shown in Fig. 10.6.

The $\boldsymbol{r}$-term gives only a constant phase shift and can therefore be ignored. The location vector $\boldsymbol{r}_\mathrm{p}$ of the particle with respect to the origin of the coordinate system is

$$\boldsymbol{r}_\mathrm{p}(t_\mathrm{r}) \;=\; x(t_\mathrm{r})\;\boldsymbol{x} + z(t_\mathrm{r})\;\boldsymbol{z}$$

and with the solutions (10.19) we have

$$\boldsymbol{r}_\mathrm{p}(t_\mathrm{r}) \;=\; \frac{K}{k_\mathrm{p}\,\gamma}\,\cos(\omega_\mathrm{p} t_\mathrm{r})\;\boldsymbol{x} + \left[\bar{\beta}\,c\,t_\mathrm{r} + \frac{K^2}{8\pi\,k_\mathrm{p}}\,\sin(2\omega_\mathrm{p}\,t_\mathrm{r})\right]\;\boldsymbol{z}\;, \qquad (10.48)$$

where

$$\omega_\mathrm{p} \;=\; k_\mathrm{p}\,\bar{\beta} c\,. \qquad (10.49)$$

The velocity vector finally is just the time derivative of (10.48)

$$\beta(t_\mathrm{r}) \;=\; -\frac{K}{\gamma}\,\bar{\beta}\,\sin(\omega_\mathrm{p} t_\mathrm{r})\,\boldsymbol{x} + \bar{\beta}\,\left[1 + \frac{K^2}{4\gamma^2}\,\cos(2\omega_\mathrm{p} t_\mathrm{r})\right]\boldsymbol{z}\,. \qquad (10.50)$$

We use these vector relations to evaluate the integrand in (10.46). First, we express the triple vector product $\boldsymbol{n}\times[\boldsymbol{n}\times\boldsymbol{\beta}]$ by its components and get with (10.47, 10.50)

$$\begin{aligned}\boldsymbol{n}\times[\,\boldsymbol{n}\times\boldsymbol{\beta}] = +\boldsymbol{x}\Bigg[&-\frac{K}{\gamma}\bar{\beta}\,\sin^2\vartheta\,\cos^2\varphi\,\cos\omega_{\rm p}t_{\rm r}+\frac{K}{\gamma}\,\bar{\beta}\,\sin\omega_{\rm p}t_{\rm r}\\&+\bar{\beta}\left(1+\frac{K^2}{4\gamma^2}\,\cos 2\omega_{\rm p}t_{\rm r}\right)\sin\vartheta\,\cos\vartheta\,\cos\varphi\Bigg]\\+\boldsymbol{y}\Bigg[&-\frac{K}{\gamma}\bar{\beta}\,\sin^2\vartheta\,\sin\varphi\cos\varphi\,\sin\omega_{\rm p}t_{\rm r}\\&+\bar{\beta}\left(1+\frac{K^2}{4\gamma^2}\,\cos 2\omega_{\rm p}t_{\rm r}\right)\sin\vartheta\,\cos\vartheta\,\sin\varphi\Bigg]\\+\boldsymbol{z}\Bigg[&-\frac{K}{\gamma}\bar{\beta}\,\sin\vartheta\,\cos\vartheta\cos\varphi\,\cos\omega_{\rm p}t_{\rm r}\\&+\bar{\beta}\left(1+\frac{K^2}{4\gamma^2}\,\cos 2\omega_{\rm p}t_{\rm r}\right)\left(\cos^2\vartheta-1\right)\Bigg]\,.\end{aligned}\tag{10.51}$$

This expression can be greatly simplified considering that the radiation is emitted into only a very small angle $\vartheta \ll 1$. Furthermore, we note that the deflection due to the wiggler field is in most practical cases very small and therefore $K \ll \gamma$ and $\bar{\beta} = \beta\left(1-\frac{K^2}{4\gamma^2}\right) \approx \beta$. Finally, we carefully set $\beta \approx 1$ where this term does not appear as a difference to unity. With this and ignoring second order terms in ϑ and K/γ we get from (10.51)

$$\boldsymbol{n}\times[\,\boldsymbol{n}\times\boldsymbol{\beta}\,] \;=\; \left(\bar{\beta}\,\vartheta\,\cos\varphi+\bar{\beta}\,\frac{K}{\gamma}\,\sin\omega_{\rm p}t_{\rm r}\right)\boldsymbol{x}+\bar{\beta}\,\vartheta\,\sin\varphi\;\;\boldsymbol{y}\,.\tag{10.52}$$

The vector product in the exponent of the exponential function is just the product of (10.47) and (10.48)

$$\frac{1}{c}\boldsymbol{n}\boldsymbol{r}_{\rm p}(t_{\rm r}) \;=\; -\frac{K\bar{\beta}}{\gamma\omega_{\rm p}}\,\sin\vartheta\,\cos\varphi\,\cos\omega_{\rm p}t_{\rm r}-\left(\bar{\beta}\;t_{\rm r}+\frac{K^2\bar{\beta}}{8\gamma^2\omega_{\rm p}}\,\sin 2\omega_{\rm p}\,t_{\rm r}\right)\cos\vartheta\,.\tag{10.53}$$

Employing again the approximation $\vartheta \ll 1$ and keeping only linear terms we get from (10.53)

$$t_{\rm r}+\frac{1}{c}\boldsymbol{n}\boldsymbol{r}_{\rm p}(t_{\rm r}) \;=\; t_{\rm r}(1-\bar{\beta}\,\cos\vartheta)-\frac{K\,\bar{\beta}\vartheta}{\gamma\omega_{\rm p}}\,\cos\varphi\,\cos\omega_{\rm p}t_{\rm r}-\frac{K^2\,\bar{\beta}}{8\gamma^2\omega_{\rm p}}\,\sin 2\omega_{\rm p}\,t_{\rm r}\,.\tag{10.54}$$

With (10.18) and $\cos\vartheta \approx 1-\frac{1}{2}\,\vartheta^2$, the first term becomes

$$1-\bar{\beta}\cos\vartheta \;=\; \frac{1}{2\gamma^2}\,\left(1+\tfrac{1}{2}K^2+\gamma^2\vartheta^2\right) \;=\; \frac{\omega_{\rm p}}{\omega_1}\,,\tag{10.55}$$

where we have defined the fundamental wiggler frequency $\omega_1$by

$$\omega_1 \;=\; \omega_\mathrm{p}\,\frac{2\gamma^2}{1+\frac{1}{2}K^2+\gamma^2\vartheta^2} \tag{10.56}$$

or the fundamental wavelength of the radiation

$$\lambda_1 \;=\; \frac{\lambda_\mathrm{p}}{2\gamma^2}\,\left(1+\tfrac{1}{2}\,K^2+\gamma^2\vartheta^2\right) \tag{10.57}$$

in full agreement with (10.36) . At this point, it is worth to remember that the term $\frac{1}{2}\,K^2$ becomes K^2 for a helical wiggler [36]. With (10.55), the complete exponential term in (10.46) can be evaluated

$$-\,\mathrm{i}\,\omega\left[t_\mathrm{r}+\tfrac{1}{c}\boldsymbol{n}\boldsymbol{r}_\mathrm{p}(t_\mathrm{r})\,\right] = \\ -\,\mathrm{i}\,\frac{\omega}{\omega_1}\left(\omega_\mathrm{p}t_\mathrm{r}-\frac{K\bar{\beta}\vartheta}{\gamma}\,\frac{\omega_1}{\omega_\mathrm{p}}\cos\varphi\,\cos\omega_\mathrm{p}t_\mathrm{r}-\frac{K^2\bar{\beta}}{8\gamma^2}\,\frac{\omega_1}{\omega_\mathrm{p}}\sin 2\omega_\mathrm{p}t_\mathrm{r}\right)\,.$$

Equation (10.46) can be modified with these expressions into a form suitable for integration by inserting (10.52) and (10.55) into (10.46) for

$$\frac{\mathrm{d}^2W}{\mathrm{d}\omega\,\mathrm{d}\Omega} \;=\; \frac{r_\mathrm{c}\,mc\,\omega^2}{4\pi^2}\,\bar{\beta}^2 \tag{10.58}$$
$$\times\left|\int_{-\infty}^{\infty}\left[\left(\,\vartheta\,\cos\varphi+\frac{K}{\gamma}\,\sin\omega_\mathrm{p}t_\mathrm{r}\,\right)\,\boldsymbol{x}+\,\vartheta\,\sin\varphi\,\boldsymbol{y}\right]\,\mathrm{e}^X\,\mathrm{d}t_\mathrm{r}\right|^2\,,$$

where

$$X=\left[-\mathrm{i}\,\frac{\omega}{\omega_1}\left(\omega_\mathrm{p}t_\mathrm{r}-\frac{K\vartheta}{\gamma}\,\frac{\omega_1}{\omega_\mathrm{p}}\cos\varphi\,\cos\omega_\mathrm{p}t_\mathrm{r}-\frac{K^2}{8\gamma^2}\,\frac{\omega_1}{\omega_\mathrm{p}}\sin 2\omega_\mathrm{p}\,t_\mathrm{r}\right)\right]\,.$$

We are now ready to perform the integration of (10.58) noticing that the integration over all times can be simplified by separation into an integral along the wiggler magnet alone and an integration over the rest of the time while the particle is traveling in a field free space. We write symbolically

$$\int_{-\infty}^{\infty} \;=\; \int_{-\pi N_\mathrm{p}/\omega_\mathrm{p}}^{\pi N_\mathrm{p}/\omega_\mathrm{p}}(K\neq 0)+\int_{-\infty}^{\infty}(K=0)-\int_{-\pi N_\mathrm{p}/\omega_\mathrm{p}}^{\pi N_\mathrm{p}/\omega_\mathrm{p}}(K=0)\,. \tag{10.59}$$

First we evaluate the second integral for $K=0$ which is of the form

$$\int_{-\infty}^{\infty}\mathrm{e}^{\mathrm{i}\kappa\omega t}\,\mathrm{d}t \;=\; \frac{2\pi}{|\kappa|}\,\delta(\omega)\,,$$

where $\delta(\omega)$ is the Dirac δ-function. The value of the integral is nonzero only for $\omega=0$ in which case the factor ω^2 in (10.58) causes the whole expression to vanish. The second integral is therefore zero.

The third integral has the same form as the second integral, but since the integration is conducted only over the length of the wiggler magnet we get

$$\int\limits_{-\pi N_\mathrm{p}/\omega_\mathrm{p}}^{\pi N_\mathrm{p}/\omega_\mathrm{p}} \mathrm{e}^{-\mathrm{i}\,\frac{\omega}{2\gamma^2}\,t_\mathrm{r}}\;\mathrm{d}t_\mathrm{r} \;=\; \frac{2\pi N_\mathrm{p}}{\omega_\mathrm{p}}\,\frac{\sin\frac{\pi N_\mathrm{p}}{2\gamma^2}\,\frac{\omega}{\omega_\mathrm{p}}}{\frac{\pi N_\mathrm{p}}{2\gamma^2}\,\frac{\omega}{\omega_\mathrm{p}}}\,. \tag{10.60}$$

The value of this integral reaches a maximum of $2\pi\frac{N_\mathrm{p}}{\omega_\mathrm{p}}$ for $\omega \to 0$. From (10.58) we note the coefficient of this integral to include the angle $\vartheta \gtrsim 1/\gamma$ and the whole integral is therefore of the order or less than $L_\mathrm{u}/(c\gamma)$, where $L_\mathrm{u} = N_\mathrm{p}\lambda_\mathrm{p}$ is the total length of the wiggler magnet. This value is in general very small compared to the first integral and can therefore be neglected. Actually, this statement is only partially true since the first integral, as we will see, is a fast varying function of the radiation frequency with a distinct line spectrum. Being, however, primarily interested in the peak intensities of the spectrum we may indeed neglect the third integral. Only between the spectral lines does the radiation intensity from the first integral become so small that the third integral would be a relatively significant although absolutely a small contribution.

To evaluate the first integral in (10.59) with $K \neq 0$ we follow Alferov [59] and introduce with (10.56) the abbreviations

$$C = \frac{2K\;\bar{\beta}\,\gamma\vartheta\cos\varphi}{1+\frac{1}{2}K^2+\gamma^2\vartheta^2}\,, \tag{10.61a}$$

$$S = \frac{K^2\;\bar{\beta}}{4\left(1+\frac{1}{2}K^2+\gamma^2\vartheta^2\right)} \tag{10.61b}$$

and get from (10.58) the exponential functions in the form

$$\mathrm{e}^{-\mathrm{i}\,\frac{\omega}{\omega_1}\,\omega_\mathrm{p}t_\mathrm{r}}\,\mathrm{e}^{\mathrm{i}\,\frac{\omega}{\omega_1}\,C\,\cos\omega_\mathrm{p}t_\mathrm{r}}\,\mathrm{e}^{\mathrm{i}\,\frac{\omega}{\omega_1}\,S\,\sin 2\omega_\mathrm{p}t_\mathrm{r}}\,. \tag{10.62}$$

The integral in the radiation power spectrum (10.58) has two distinct forms, one where the integrand is just the exponential function multiplied by a time independent factor while the other includes the sine function $\sin\omega_\mathrm{p}t_\mathrm{r}$ as a factor of the exponential function. To proceed further we replace the exponential functions by an infinite sum of Bessel's functions

$$\mathrm{e}^{\mathrm{i}\kappa\sin\psi} \;=\; \sum_{p=-\infty}^{p=\infty} J_p(\kappa)\,\mathrm{e}^{\mathrm{i}p\psi} \tag{10.63}$$

and apply this identity to the first integral type in (10.58). Applying the identity (10.63) also to the second and third exponential factors in (10.62), we get with $\mathrm{e}^{a\cos x} = \mathrm{e}^{a\sin(x+\pi/2)}$ the product of the exponential functions

$$\mathrm{e}^{-\mathrm{i}\left(\frac{\omega}{\omega_1}\,\omega_\mathrm{p} t_\mathrm{r} - \frac{\omega}{\omega_1}\,C\,\cos\omega_\mathrm{p} t_\mathrm{r} - \frac{\omega}{\omega_1}\,S\,\sin 2\omega_\mathrm{p} t_\mathrm{r}\right)} = \sum_{\substack{m=\\-\infty}}^{\infty}\sum_{\substack{n=\\-\infty}}^{\infty} J_m(u)\,J_n(v)\,\mathrm{e}^{\mathrm{i}\frac{1}{2}\pi n}\mathrm{e}^{-\mathrm{i}\,R_\omega\,\omega_\mathrm{p} t_\mathrm{r}}\,, \tag{10.64}$$

where

$$\begin{aligned} R_\omega &= \frac{\omega}{\omega_1} - n - 2m\,, \\ u &= \frac{\omega}{\omega_1}\,S, \qquad\qquad \text{and} \\ v &= \frac{\omega}{\omega_1}\,C\,. \end{aligned} \tag{10.65}$$

The time integration along the length of the wiggler magnet is straight forward for this term since no other time dependent factors are involved and we get

$$\int\limits_{-\pi N_\mathrm{p}/\omega_\mathrm{p}}^{\pi N_\mathrm{p}/\omega_\mathrm{p}} \mathrm{e}^{-\mathrm{i}\left(\frac{\omega}{\omega_1}-n-2m\right)\omega_\mathrm{p} t_\mathrm{r}}\,\mathrm{d}\,t_\mathrm{r} = \frac{2\pi N_\mathrm{p}}{\omega_\mathrm{p}}\,\frac{\sin\pi N_\mathrm{p}\,R_\omega}{\pi N_\mathrm{p}\,R_\omega}\,. \tag{10.66}$$

In the second form of the integrand, we replace the trigonometric factor, $\sin\omega_\mathrm{p} t_\mathrm{r}$, by exponential functions and get with (10.66) integrals of the form

$$\begin{aligned} &\int\limits_{-\pi N_\mathrm{p}/\omega_\mathrm{p}}^{\pi N_\mathrm{p}/\omega_\mathrm{p}} \sin\omega_\mathrm{p} t_\mathrm{r}\,\mathrm{e}^{-\mathrm{i}R_\omega\,\omega_\mathrm{p} t_\mathrm{r}}\,\mathrm{d}\,t_\mathrm{r} \\ &= -\mathrm{i}\frac{1}{2}\int\limits_{-\pi N_\mathrm{p}/\omega_\mathrm{p}}^{\pi N_\mathrm{p}/\omega_\mathrm{p}} \left(\mathrm{e}^{\mathrm{i}\,\omega_\mathrm{p} t_\mathrm{r}} - \mathrm{e}^{-\mathrm{i}\,\omega_\mathrm{p} t_\mathrm{r}}\right)\mathrm{e}^{-\mathrm{i}R_\omega\,\omega_\mathrm{p} t_\mathrm{r}}\mathrm{d}\,t_\mathrm{r} \\ &= \mathrm{i}\,\frac{\pi N_\mathrm{p}}{\omega_\mathrm{p}}\,\frac{\sin\pi N_\mathrm{p}\,(R_\omega+1)}{\pi N_\mathrm{p}(\,R_\omega+1)} - \mathrm{i}\,\frac{\pi N_\mathrm{p}}{\omega_\mathrm{p}}\,\frac{\sin\pi N_\mathrm{p}\,(R_\omega-1)}{\pi N_\mathrm{p}\,(R_\omega-1)}\,. \end{aligned} \tag{10.67}$$

Both integrals (10.66) and (10.67) exhibit the character of multibeam interference spectra well known from optical interference theory. The physical interpretation here is that the radiation from the N_p wiggler periods consists of N_p photon beamlets which have a specific phase relationship such that the intensities are strongly reduced for all frequencies but a few specific frequencies as determined by the $\frac{\sin x}{x}$-factors. The resulting line spectrum, characteristic for undulator radiation, is the more pronounced the more periods or beamlets are available for interference. To get a more complete picture of the interference pattern, we collect now all terms derived separately so far and use them in (10.58) which becomes with (10.62)

$$\frac{\mathrm{d}^2W}{\mathrm{d}\omega\,\mathrm{d}\Omega} = a\left|\int_{-\pi N_\mathrm{p}/\omega_\mathrm{p}}^{\pi N_\mathrm{p}/\omega_\mathrm{p}} [(A_0 + A_1\sin\omega_\mathrm{p}t_\mathrm{r})\,\boldsymbol{x} + B_0\;\boldsymbol{y}] \times \mathrm{e}^{-\mathrm{i}\frac{\omega}{\omega_1}\omega_\mathrm{p}t_\mathrm{r}}\,\mathrm{e}^{\mathrm{i}\,v\,\cos\omega_\mathrm{p}t_\mathrm{r}}\,\mathrm{e}^{\mathrm{i}\,u\,\sin 2\omega_\mathrm{p}t_\mathrm{r}}\,\mathrm{d}\,t_\mathrm{r}\right|^2 ,$$

where $a = \frac{r_\mathrm{e}\,mc\bar{\beta}^2}{4\pi^2}\omega^2$, $A_0 = \vartheta\cos\varphi$, $A_1 = \frac{K}{\gamma}$, and $B_0 = \vartheta\sin\varphi$. Introducing the identity (10.62), the photon energy spectrum becomes

$$\frac{\mathrm{d}^2W}{\mathrm{d}\omega\,\mathrm{d}\Omega} = a\left|\int_{-\pi N_\mathrm{p}/\omega_\mathrm{p}}^{\pi N_\mathrm{p}/\omega_\mathrm{p}} [(A_0 + A_1\sin\omega_\mathrm{p}t_\mathrm{r})\,\boldsymbol{x} + B_0\;\boldsymbol{y}] \times \sum_{m=-\infty}^{\infty}\sum_{n=-\infty}^{\infty} J_m(u)\,J_n(v)\,\mathrm{e}^{\mathrm{i}\frac{1}{2}\pi n}\mathrm{e}^{-\mathrm{i}R_\omega\omega_\mathrm{p}t_\mathrm{r}}\,\mathrm{d}\,t_\mathrm{r}\right|^2$$

and after integration with (10.66) and (10.67)

$$\begin{aligned}\frac{\mathrm{d}^2W}{\mathrm{d}\omega\,\mathrm{d}\Omega} = a\Bigg|\;& \boldsymbol{x}\;A_0\sum_{\substack{m=\\-\infty}}^{\infty}\sum_{\substack{n=\\-\infty}}^{\infty} J_m(u)\,J_n(v)\,\mathrm{e}^{\mathrm{i}\frac{1}{2}\pi n}\frac{2\pi N_\mathrm{p}}{\omega_\mathrm{p}}\,\frac{\sin\pi N_\mathrm{p}\,R_\omega}{\pi N_\mathrm{p}R_\omega} \\ &+\boldsymbol{x}\;A_1\sum_{\substack{m=\\-\infty}}^{\infty}\sum_{\substack{n=\\-\infty}}^{\infty} J_m(u)\,J_n(v)\,\mathrm{e}^{\mathrm{i}\frac{1}{2}\pi n} \\ &\times\;\mathrm{i}\,\frac{\pi N_\mathrm{p}}{2\omega_\mathrm{p}}\left[\frac{\sin\pi N_\mathrm{p}\,(R_\omega+1)}{\pi N_\mathrm{p}\,(R_\omega+1)} - \mathrm{i}\;\frac{\pi N_\mathrm{p}}{\omega_\mathrm{p}}\,\frac{\sin\pi N_\mathrm{p}\,(R_\omega-1)}{\pi N_\mathrm{p}\,(R_\omega-1)}\right] \\ &+\boldsymbol{y}\,B_0\sum_{\substack{m=\\-\infty}}^{\infty}\sum_{\substack{n=\\-\infty}}^{\infty} J_m(u)\,J_n(v)\,\mathrm{e}^{\mathrm{i}\frac{1}{2}\pi n}\,\frac{2\pi N_\mathrm{p}}{\omega_\mathrm{p}}\,\frac{\sin\pi N_\mathrm{p}R_\omega}{\pi N_\mathrm{p}R_\omega}\Bigg|^2 .\end{aligned} \tag{10.68}$$

To determine the frequency and radiation intensity of the line maxima, we simplify the double sum of Bessel's functions by selecting only the most dominant terms. The first and third sums in (10.68) show an intensity maximum for $R_\omega = 0$ at frequencies

$$\omega = (n+2m)\,\omega_1 , \tag{10.69}$$

and intensity maxima appear therefore at the frequency ω_1 and harmonics thereof. The transformation of a lower frequency to very high values has two physical components. In the system of relativistic particles, the static magnetic field of the wiggler magnet appears Lorentz contracted by the factor γ, and particles passing through the wiggler magnet oscillate with the frequency $\gamma\omega_\mathrm{p}$ in its own system emitting radiation at that frequency. The observer in

the laboratory system receives this radiation from a source moving with relativistic velocity and experiences therefore a Doppler shift by the factor 2γ. The wavelength of the radiation emitted in the forward direction, $\vartheta = 0$, from a weak wiggler magnet, $K \ll 1$, with the period length λ_p is therefore reduced by the factor $2\gamma^2$. In cases of a stronger wiggler magnet or when observing at a finite angle ϑ, the wavelength is somewhat longer as one would expect from higher order terms of the Doppler effect.

From (10.68) we determine two more dominant terms originating from the second term for $R_\omega \pm 1 = 0$ at frequencies

$$\omega = (n + 2m - 1)\ \omega_1 \tag{10.70a}$$

$$\omega = (n + 2m + 1)\ \omega_1\,, \tag{10.70b}$$

respectively. The summation indices n and m are arbitrary integers between $-\infty$ and ∞. Among all possible resonant terms we collect such terms which contribute to the same harmonic k of the fundamental frequency ω_1. To collect these dominant terms for the same harmonic we set $\omega = \omega_k = k\,\omega_1$ where k is the harmonic number of the fundamental and express the index n by k and m to get

$$\begin{aligned} &\text{from (10.69):} && n = k - 2m, \\ &\text{and from (10.70a):} && n = k - 2m + 1 \\ &\text{and(10.70b):} && n = k - 2m - 1\,. \end{aligned} \tag{10.71}$$

Introducing these conditions into (10.68) all trigonometric factors assume the form $\frac{\sin(\pi N_\mathrm{p}\ \Delta\omega_k/\omega_1)}{\pi N_\mathrm{p}\ \Delta\omega_k/\omega_1}$, where

$$\frac{\Delta\omega_k}{\omega_1} \;=\; \frac{\omega}{\omega_1} - k \tag{10.72}$$

and we get the photon energy spectrum of the $k-$th harmonic

$$\begin{aligned} \frac{\mathrm{d}^2 W_k(\omega)}{\mathrm{d}\omega\,\mathrm{d}\Omega} = \frac{r_\mathrm{c}\, mc\,\bar{\beta}^2 N_\mathrm{p}^2}{\gamma^2}\frac{\omega^2}{\omega_\mathrm{p}^2}\left(\frac{\sin\pi N_\mathrm{p}\ \Delta\omega_k/\omega_1}{\pi N_\mathrm{p}\ \Delta\omega_k/\omega_1}\right)^2 \\ \times\Bigg| +\boldsymbol{x}\ A_0 \sum_{m=-\infty}^{\infty} J_m(u)\, J_{k-2m}(v)\, \mathrm{e}^{\mathrm{i}\frac{1}{2}\pi(k-2m)} \\ +\boldsymbol{y}\ B_0 \sum_{m=-\infty}^{\infty} J_m(u)\, J_{k-2m}(v)\, \mathrm{e}^{\mathrm{i}\frac{1}{2}\pi(k-2m)} \\ +\mathrm{i}\,\tfrac{1}{2}\,\boldsymbol{x}\ A_1 \sum_{m=-\infty}^{\infty} J_m(u)\, J_{k-2m+1}(v)\, \mathrm{e}^{\mathrm{i}\frac{1}{2}\pi(k-2m+1)} \\ -\mathrm{i}\,\tfrac{1}{2}\,\boldsymbol{x}\ A_1 \sum_{m=-\infty}^{\infty} J_m(u)\, J_{k-2m-1}(v)\, \mathrm{e}^{\mathrm{i}\frac{1}{2}\pi(k-2m-1)}\Bigg|^2\,. \end{aligned} \tag{10.73}$$

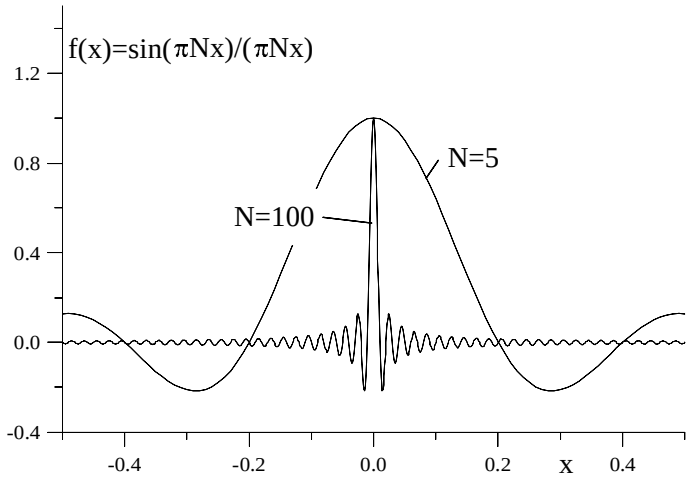

Fig. 10.7. $\frac{\sin \pi N_\mathrm{p}\, x}{\pi N_\mathrm{p}\, x}$ distribution for $N_\mathrm{p} = 5$ and $N_\mathrm{p} = 100$

All integrals exhibit the resonance character defining the locations of the spectral lines. The $(\sin x/x)$-terms are known from interference theory and represents the line spectrum of the radiation. Specifically, the number N_p of beamlets, here source points, determines the spectral purity of the radiation. In Fig. 10.7 the $(\sin x/x)$-function is shown for $N_\mathrm{p} = 5$ and $N_\mathrm{p} = 100$. It is clear that the spectral purity improves greatly as the number of undulator periods is increased. This is one of the key features of undulator magnets to gain spectral purity by maximizing the number of undulator periods.

The spectral purity or line width is determined by the shape of the $(\sin x/x)$-function. We define the line width by the frequency at which $\sin x/x = 0$ or where $\pi N_\mathrm{p}\, \Delta\omega_k / \omega_1 = \pi$ defining the line width for the k^{th} harmonic

$$\frac{\Delta\omega_k}{\omega_k} = \pm \frac{1}{k\, N_\mathrm{p}}\,. \tag{10.74}$$

The spectral width of the undulator radiation is reduced proportional to the number of undulator periods, but reduces also proportional to the harmonic number.

The Bessel functions $J_m(u)$ etc. determine mainly the intensity of the line spectrum. For an undulator with $K \ll 1$, the argument $u \propto K^2 \ll 1$ and the contributions of higher order Bessel's functions are very small. The radiation spectrum consists therefore only of the fundamental line. For stronger undulators with $K > 1$, higher order Bessel's functions grow and higher harmonic radiation appears in the line spectrum of the radiation.

Summing over all harmonics of interest, one gets the total power spectrum. In the third and fourth terms of (10.73) we use the identities $\mathrm{i}\, \mathrm{e}^{\pm \mathrm{i}\pi/2} = \mp 1$,

$J_m(u)\,\mathrm{e}^{\mathrm{i}\pi m} = J_{-m}(u)$ and abbreviate the sums of Bessel's functions by the symbols

$$\sum\nolimits_1 = \sum_{m=-\infty}^{\infty} J_{-m}(u)\, J_{k-2m}(v) \tag{10.75a}$$

$$\sum\nolimits_2 = \sum_{m=-\infty}^{\infty} J_{-m}(u)\, \left[J_{k-2m-1}(v) + J_{k-2m+1}(v)\right] . \tag{10.75b}$$

The total number of photons N_{ph} emitted into a spectral band width $\Delta\omega/\omega$ by a single electron moving through a wiggler magnet is finally with $N_{\mathrm{ph}}(\omega) = W(\omega)/(\hbar\omega)$

$$\frac{\mathrm{d}N_{\mathrm{ph}}\,(\omega)}{\mathrm{d}\Omega} = \alpha\gamma^2\bar{\beta}^2 N_{\mathrm{p}}^2 \frac{\Delta\omega}{\omega} \sum_{k=1}^{\infty} k^2 \left(\frac{\sin\pi N_{\mathrm{p}}\,\Delta\omega_k/\omega_1}{\pi N_{\mathrm{p}}\,\Delta\omega_k/\omega_1}\right)^2 \tag{10.76}$$
$$\times\, \frac{\left(2\gamma\vartheta\sum\nolimits_1\cos\varphi - K\sum\nolimits_2\right)^2 \boldsymbol{x}^2 + \left(2\gamma\vartheta\sum\nolimits_1\sin\varphi\right)^2 \boldsymbol{y}^2}{\left(1+\frac{1}{2}K^2+\gamma^2\vartheta^2\right)^2} ,$$

where α is the fine structure constant and where we have kept the coordinate unit vectors to keep track of the polarization modes. The vectors $\mathbf{x}$ and $\mathbf{y}$ are orthogonal unit vectors indicating the directions of the electric field or the polarization of the radiation. Performing the squares does therefore not produce cross terms and the two terms in (10.76) with the expressions (10.75) represent the amplitude factors for both polarization directions, the σ-mode and π-mode respectively.

We also made use of (10.72) and the resonance condition

$$\frac{\omega}{\omega_{\mathrm{p}}} = \frac{k\,\omega_1 + \Delta\omega_k}{\omega_{\mathrm{p}}} \approx k\,\frac{\omega_1}{\omega_{\mathrm{p}}} = \frac{2\gamma^2 k}{1+\frac{1}{2}K^2+\gamma^2\vartheta^2} , \tag{10.77}$$

realizing that the photon spectrum is determined by the $(\sin x/x)^2$-function. For not too few periods, this function is very small for frequencies away from the resonance conditions.

Storage rings optimized for very small beam emittance are being used as modern synchrotron radiation sources to reduce the line width of undulator radiation and concentrate all radiation to the frequency desired. The progress in this direction is demonstrated in the spectrum of Fig. 10.8 derived from the first electron storage ring operated at a beam emittance below 10 nm at 7.1 GeV [61]. In Fig. 10.8 a measured undulator spectrum is shown as a function of the undulator strength K [37]. For a strength parameter $K \ll 1$ there is only one line at the fundamental frequency. As the strength parameter increases, additional lines appear in addition to being shifted to lower frequencies. The spectral lines from a real synchrotron radiation source are not infinitely narrow as (10.88) would suggest. Because of the finite size of the pinhole opening, some light at small angles with respect to the axis

passes through, and we observe therefore also some signal of the even order harmonic radiation.

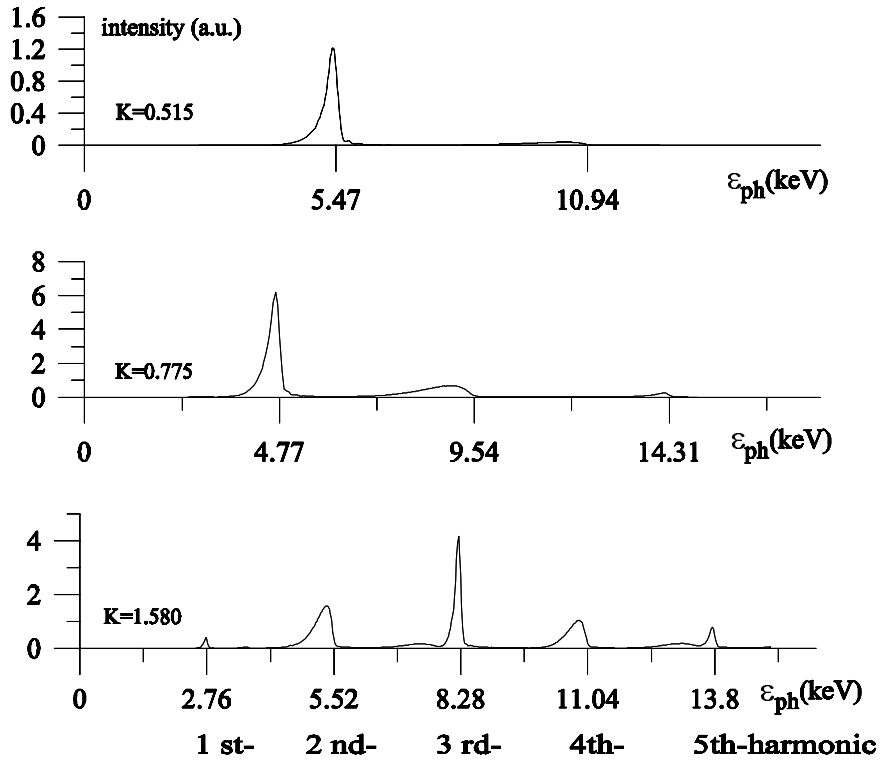

Fig. 10.8. Measured frequency spectrum from an undulator for different strength parameters K [37]

Even for an extremely small pin hole, we would observe a similar spectrum as shown in Fig. 10.8 because of the finite beam divergence of the electron beam. The electrons follow oscillatory trajectories due not only to the undulator field but also due to betatron oscillations. We observe therefore always some radiation at a finite angle given by the particle trajectory with respect to the undulator axis. Fig. 10.8 also demonstrates the fact that all experimental circumstances must be included to meet theoretical expectations. The amplitudes of the measured low energy spectrum is significantly suppressed compared to theoretical expectations which is due to a Be-window being used to extract the radiation from the ultra high vacuum chamber of the accelerator. This material absorbs radiation significantly below a photon energy of about 3 keV.

While we observe a line spectrum expressed by the $(\sin x/x)^2$-function, we also notice that this line spectrum is red shifted as we increase the observation angle ϑ. Only, when we observe the radiation though a very small aperture, pin hole, do we actually see this line spectrum. Viewing the undulator radiation through a large aperture integrates the linespectra over a finite range of angles ϑ producing an almost continuous spectrum with small spikes at the locations of the harmonic lines.

The difference between a pin hole undulator spectrum and an angle-integrated spectrum becomes apparent from the experimental spectra shown in Fig. 10.9 [61]. While the pin hole spectrum demonstrates well the line character of undulator radiation, much radiation appears between these spectral lines as the pin hole is removed and radiation over a large solid angle is collected by the detector. The pin hole undulator line spectrum shows up as mere spikes on top of a broad continuous spectrum.

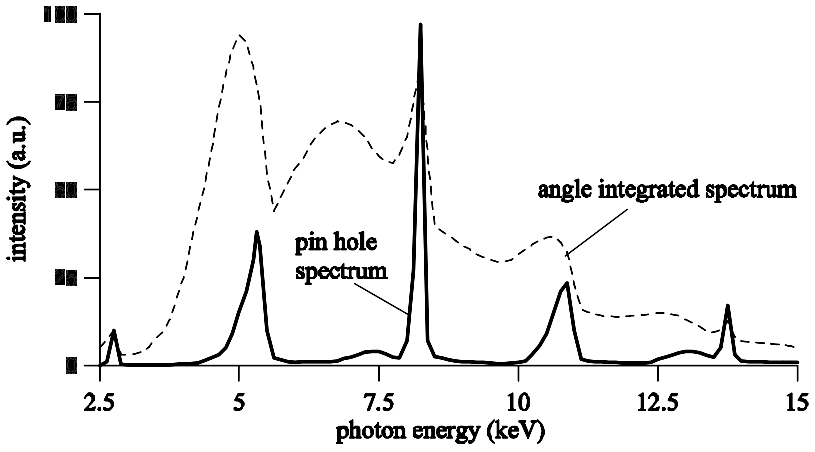

Fig. 10.9. Actual radiation spectra from an undulator with a maximum field of 0.2 T and a beam energy of 7.1 GeV through a pin hole and angle-integrated after removal of the pin hole [61]

The overall spatial intensity distribution includes a complex set of different radiation lobes depending on frequency, emission angle and polarization. In Fig. 10.10 the radiation intensity distributions described by the last factor in (10.76)

$$I_{\sigma,k} = \frac{(2\gamma\vartheta\,\Sigma_1\cos\varphi - K\,\Sigma_2)^2}{(1+\frac{1}{2}K^2+\gamma^2\vartheta^2)^2}$$

for the σ-mode polarization and

$$I_{\pi,k} = \frac{(2\gamma\vartheta\,\Sigma_1\,\sin\varphi)^2}{(1+\frac{1}{2}\,K^2+\gamma^2\vartheta^2)^2}$$

for the π-mode polarization are shown for the lowest order harmonics.

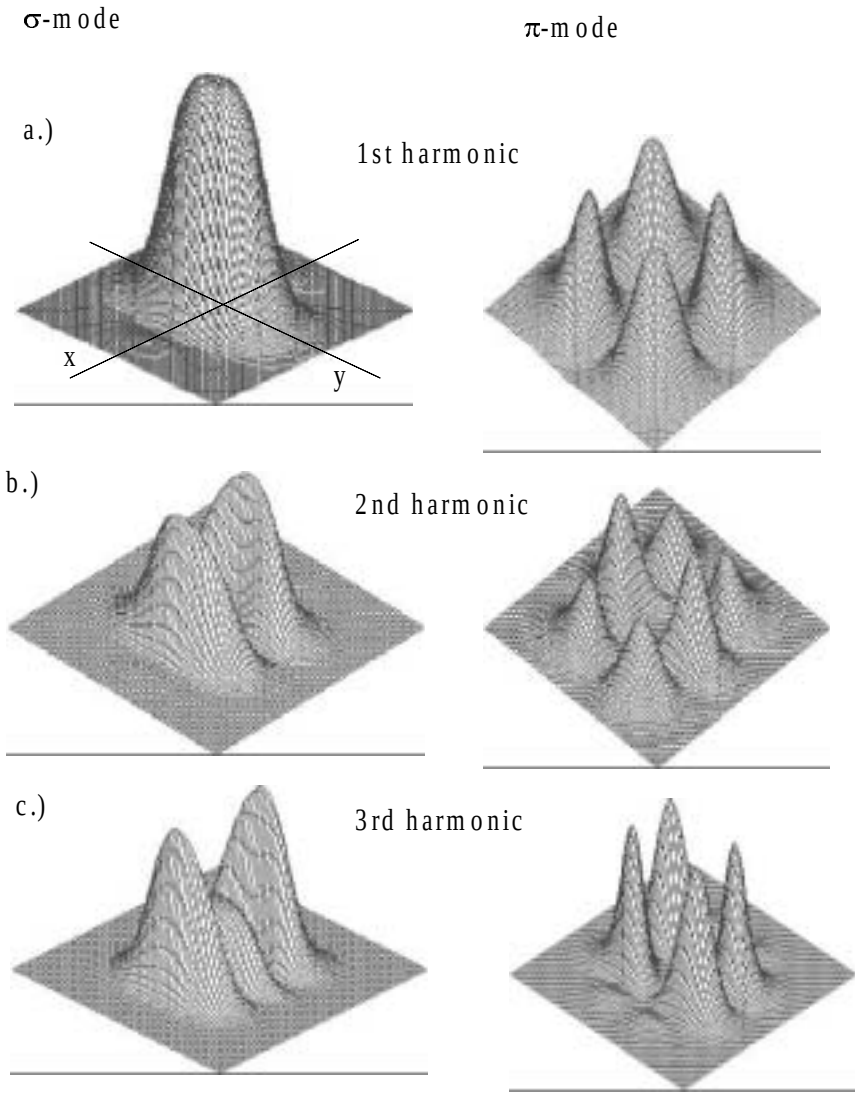

Fig. 10.10. Undulator radiation distribution in σ- and π-mode for the lowest order harmonics

We note clearly the strong forward lobe at the fundamental frequency in σ-mode while there is no emission in π-mode along the path of the particle. The second harmonic radiation vanishes in the forward direction, an observation that is true for all even harmonics. By inspection of (10.76), we note that $v = 0$ for $\vartheta = 0$ and the square bracket in (10.75b) vanishes for all odd indices or for all even harmonics k. There is therefore no forward radiation for even harmonics of the fundamental undulator frequency.

A contour plot of the first harmonic σ-and π-mode radiation is shown in Fig. 10.11. There is an slight asymmetry in the radiation distribution between the deflecting and nondeflecting plane as one might expect. It is obvious that the pin hole radiation is surrounded by many radiation lobes not only from the first harmonics but also from higher harmonics compromising the pure line spectrum for large apertures.

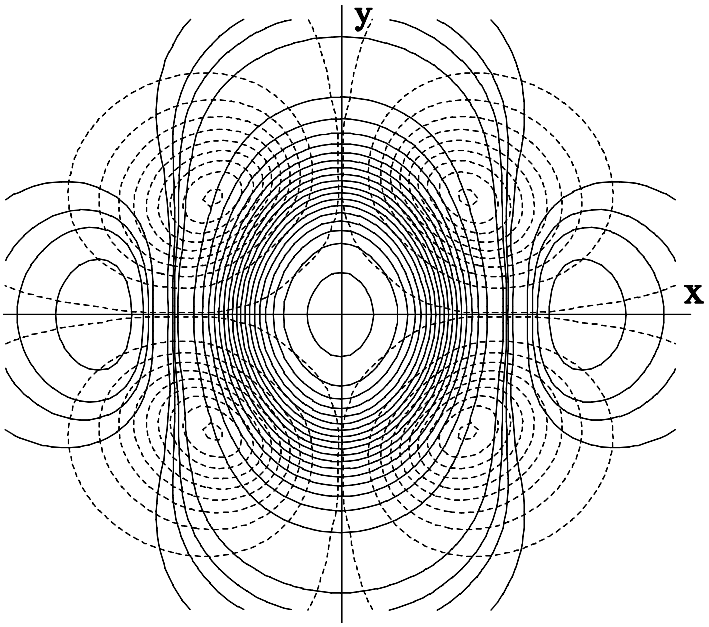

Fig. 10.11. Contour plot of the first harmonic σ-mode (*solid*) and π-mode (*dashed*) undulator radiation distribution

10.2.4 Line Spectrum

To exhibit other important and desirable features of the radiation spectrum (10.76), we ignore the actual frequency distribution in the vicinity of the harmonics and set $\Delta\omega_k = 0$ because the spectral lines are narrow for large numbers of wiggler periods N_p. Further, we are interested for now only in the

forward radiation where $\vartheta = 0$, keeping in mind that the radiation is mostly emitted into a small angle $\langle\vartheta\rangle = 1/\gamma$.

There is no radiation for the π-mode in the forward direction and the only contribution to the forward radiation comes from the second term in (10.76) of the σ-mode. From (10.65), we get for this case with $\omega/\omega_1 = k$

$$u_0 \;=\; \frac{k\,K^2}{4+2K^2} \qquad \text{and} \qquad v_0 \;=\; 0\,. \tag{10.78}$$

The sums of Bessel's functions simplify in this case greatly because only the lowest order Bessel's function has a nonvanishing value for $v_0 = 0$. In the expression for Σ_2, all summation terms vanish except for the two terms for which the index is zero or for which

$$k - 2m - 1 = 0, \qquad \text{or} \qquad k - 2m + 1 = 0 \tag{10.79}$$

and

$$\begin{aligned}\sum\nolimits_2 &= \sum_{m=-\infty}^{\infty} J_{-m}(u)\;[J_{k-2m-1}(0) + J_{k-2m+1}(0)] \\ &= J_{-\frac{1}{2}(k-1)}(u_0) + J_{-\frac{1}{2}(k+1)}(u_0)\,.\end{aligned} \tag{10.80}$$

The harmonic condition (10.79) implies that k is an odd integer. For even integers, the condition cannot be met as we would expect from earlier discussions on harmonic radiation in the forward direction. Using the identity $J_{-n} = (-1)^n J_n$ and (10.78), we get finally with $N_{\mathrm{ph}} = W\,/\,\hbar\omega$ the photon flux per unit solid angle from a highly relativistic particle passing through an undulator

$$\left.\frac{\mathrm{d}N_{\mathrm{ph}}(\omega)}{\mathrm{d}\Omega}\right|_{\theta=0} = \alpha\gamma^2 N_{\mathrm{p}}^2 \frac{\Delta\omega}{\omega} \frac{K^2}{\left(1+\frac{1}{2}K^2\right)^2} \sum_{k=1}^{\infty} k^2 \left(\frac{\sin\pi N_{\mathrm{p}}\,\Delta\omega_k/\omega_1}{\pi N_{\mathrm{p}}\,\Delta\omega_k/\omega_1}\right)^2 \times JJ^2\,, \tag{10.81}$$

where the JJ–function is defined by

$$JJ = \left[J_{\frac{1}{2}(k-1)}\left(\frac{kK^2}{4+2K^2}\right) + J_{\frac{1}{2}(k+1)}\left(\frac{kK^2}{4+2K^2}\right)\right]\,. \tag{10.82}$$

The amplitudes of the harmonics are given by

$$A_k(K) \;=\; \frac{k^2\,K^2}{(1+\frac{1}{2}K^2)^2}\,JJ^2\,. \tag{10.83}$$

The strength parameter greatly determines the radiation intensity as shown in Fig. 10.12 for the lowest order harmonics. For the convenience of numerical calculations, $A_k(K)$ is tabulated for odd harmonics in Table 10.1.

For weak magnets, $K \ll 1$, the intensity increases with the square of the magnet field or undulator strength parameter There is an optimum value for the strength parameter for maximum photon flux depending on the harmonic under consideration. In particular, radiation in the forward direction at the fundamental frequency reaches a maximum photon flux for strength parameters $K \approx 1.3$. The photon flux per unit solid angle increases like the square of the number of wiggler periods N_p, which is a result of the interference effect of many beams concentrating the radiation more and more into one frequency and its harmonics as the number of interfering beams is increased.

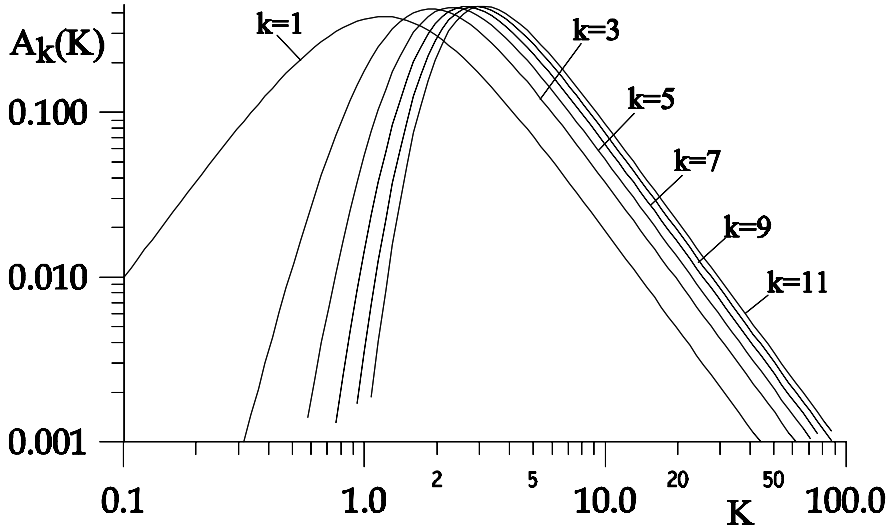

Fig. 10.12. Undulator radiation intensity $A_k(K)$ in the forward direction as a function of the strength parameter K for the six lowest order odd harmonics

The radiation opening angle is primarily determined by the $(\sin x/x)^2$-term. We define the rms opening angle for the k^{th} harmonic radiation by ϑ_k being the angle for which $\sin x/x = 0$ for the first time. In this case, $x = \pi$ or $N_\mathrm{p}\, \Delta\omega_k/\omega_1 = 1$. With $\omega_1 = \omega_\mathrm{p} \frac{2\gamma^2}{1+\frac{1}{2}K^2}$, $\omega_k = k\,\omega_\mathrm{p} \frac{2\gamma^2}{1+\frac{1}{2}K^2+\gamma^2\vartheta_k^2}$ and $\frac{\Delta\omega_k}{\omega_1} = \left|\frac{\omega_k}{\omega_1} - k\right|$, we get $\frac{N_\mathrm{p}\, k\, \gamma^2\, \vartheta_k^2}{1+\frac{1}{2}K^2+\gamma^2\vartheta_k^2} = 1$ or after solving for ϑ_k

$$\vartheta_k^2 \;=\; \frac{1+\frac{1}{2}K^2}{\gamma^2\,(kN_\mathrm{p}-1)}\;. \tag{10.84}$$

Assuming an undulator with many periods $k\,N_\mathrm{p} \gg 1$, the rms opening angle of undulator radiation is finally

Table 10.1. Amplitudes $A_k(K)$ for $k = 1, 3, 5, 7, 9, 11$

K	A_1	A_3	A_5	A_7	A_9	A_{11}
0.1	0.010	0	0	0	0	0
0.2	0.038	0	0	0	0	0
0.4	0.132	0.004	0	0	0	0
0.6	0.238	0.027	0.002	0	0	0
0.8	0.322	0.087	0.015	0.002	0	0
1.0	0.368	0.179	0.055	0.015	0.004	0.001
1.2	0.381	0.276	0.128	0.051	0.019	0.007
1.4	0.371	0.354	0.219	0.118	0.059	0.028
1.8	0.320	0.423	0.371	0.286	0.206	0.142
2.0	0.290	0.423	0.413	0.354	0.285	0.220
5.0	0.071	0.071	0.139	0.188	0.228	0.290
10.0	0.019	0.037	0.051	0.064	0.075	0.085
20.0	0.005	0.010	0.013	0.016	0.019	0.022

$$\sigma_{r'} = \tfrac{1}{\sqrt{2}}\vartheta_k \approx \frac{1}{\gamma}\sqrt{\frac{1+\frac{1}{2}K^2}{2\,k\,N_\mathrm{p}}}\,. \tag{10.85}$$

Radiation emitted into a solid angle defined by this opening angle

$$\mathrm{d}\Omega = 2\pi\,\sigma_{\mathrm{r}'}^2 \tag{10.86}$$

is referred to as the forward radiation cone. The opening angle of undulator radiation becomes more collimated as the number of periods and the order of the harmonic increases. On the other hand, the radiation cone opens up as the undulator strength K is increased. We may use this opening angle to calculate the total photon intensity of the k^{th} harmonic within a bandwidth $\frac{\Delta\omega}{\omega}$ into the forward cone

$$N_{\mathrm{ph}}(\omega_k)|_{\vartheta=0} = \pi\,\alpha\,N_\mathrm{p}\,\frac{\Delta\omega}{\omega_k}\,k\,\frac{K^2}{1+\frac{1}{2}K^2}\,JJ^2\,, \tag{10.87}$$

where $\omega_k = k\,\omega_1$. The radiation spectrum from an undulator magnet into the forward direction has been reduced to a simple form exhibiting the most important characteristic parameters. Utilizing (10.83), the number of photons emitted into a band width $\frac{\Delta\omega}{\omega_k}$ from a single electron passing through an undulator in the $k-$th harmonic is

$$N_{\mathrm{ph}}(\omega_k)|_{\vartheta=0} \;=\; \pi\,\alpha\,N_\mathrm{p}\,\frac{\Delta\omega}{\omega_k}\,\frac{1+\frac{1}{2}K^2}{k}\,A(K)\,. \tag{10.88}$$

Equation (10.88) is to be multiplied by the number of particles in the electron beam to get the total photon intensity. In case of a storage ring, particles circulate with a high revolution frequency and we get from (10.88) by multiplication with $I\,/\,e$, where I is the circulating beam current, the photon flux

$$\left.\frac{\mathrm{d}\,N_{\mathrm{ph}}(\omega_k)}{\mathrm{d}\,t}\right|_{\vartheta=0} = \pi\,\alpha\,N_{\mathrm{p}}\,\frac{I}{e}\frac{\Delta\omega}{\omega_k}\,\frac{1+\frac{1}{2}\,K^2}{k}A(K)\,. \tag{10.89}$$

The spectrum includes only odd harmonic since all even harmonics are suppressed through the cancellation of Bessel's functions.

10.2.5 Spectral Undulator Brightness

The spectral brightness of undulator radiation is defined as the photon density in six-dimensional phase space

$$\mathcal{B}\,(\omega) = \frac{\dot{N}_{\mathrm{ph}}(\omega)}{4\pi^2\,\sigma_x\sigma_{x'}\sigma_y\sigma_{y'}(\mathrm{d}\omega/\omega)}\,. \tag{10.90}$$

In the laser community, this quantity is called the radiance while the term spectral brightness is common in the synchrotron radiation community. The maximum value of the brightness is limited by diffraction to

$$\mathcal{B}_{\mathrm{max}} = \dot{N}_{\mathrm{ph}}\,\frac{(4/\lambda^2)}{\mathrm{d}\omega/\omega}\,. \tag{10.91}$$

The actual photon brightness is reduced from the diffraction limit due to betatron motion of the particles, transverse beam oscillation in the undulator, apparent source size on axis and under an oblique angle. All of these effects tend to increase the source size and reduce brightness.

The particle beam cross section varies in general along the undulator. We assume here for simplicity that the beam size varies symmetrically along the undulator with a waist in its center. From beam dynamics it is then known that, for example, the horizontal beam size varies like $\sigma_{\mathrm{b}}^2 = \sigma_{\mathrm{b0}}^2 + \sigma_{\mathrm{b0}}'^2\,s^2$, where σ_{b0} is the beam size at the waist, σ_{b0}' the divergence of the beam at the waist and $-\frac{1}{2}L \leqq s \leqq \frac{1}{2}L$ the distance from the waist. The average beam size along the undulator length L is then

$$\langle\sigma_{\mathrm{b}}^2\rangle = \sigma_{\mathrm{b0}}^2 + \tfrac{1}{12}\sigma_{\mathrm{b0}}'^2\,L^2\,. \tag{10.92}$$

Similarly, due to an oblique observation angle ϑ with respect to the (y,z)-plane or ψ with respect to the (x,z)-plane we get a further additive contribution $\frac{1}{6}\,\vartheta\,L$ to the apparent beam size. Finally, the apparent source size is widened by the transverse beam wiggle in the periodic undulator field. This oscillation amplitude is from (10.20) $a = \lambda_{\mathrm{p}}K\,/\,(2\pi\gamma)$.

Collecting all contributions and adding them in quadrature, the total effective beam-size parameters are given by

$$\sigma_{t,x}^2 = \tfrac{1}{2}\,\sigma_r^2 + \sigma_{\mathrm{b}0,x}^2 + \left(\frac{\lambda_\mathrm{p} K}{2\pi\gamma}\right)^2 + \tfrac{1}{12}\sigma_{\mathrm{b}0,x'}^2 L^2 + \tfrac{1}{36}\vartheta^2 L^2\,, \tag{10.93a}$$

$$\sigma_{t,x'}^2 = \tfrac{1}{2}\,\sigma_{r'}^2 + \sigma_{\mathrm{b}0,x'}^2\,, \tag{10.93b}$$

$$\sigma_{t,y}^2 = \tfrac{1}{2}\,\sigma_r^2 + \sigma_{\mathrm{b}0,y}^2 + \left(\frac{\lambda_\mathrm{p} K}{2\pi\gamma}\right)^2 + \tfrac{1}{12}\sigma_{\mathrm{b}0,y'}^2 L^2 + \tfrac{1}{36}\psi^2 L^2\,, \tag{10.93c}$$

$$\sigma_{t,y'}^2 = \tfrac{1}{2}\,\sigma_{r'}^2 + \sigma_{\mathrm{b}0,y'}^2\,, \tag{10.93d}$$

where the particle beam sizes can be expressed by the beam emittance and betatron function as $\sigma_\mathrm{b}^2 = \epsilon\,\beta$, $\sigma_\mathrm{b}'^{\,2} = \epsilon/\beta$, and the diffraction limited beam parameters are $\sigma_r = \sqrt{\lambda/L}$, and $\sigma_{r'} = \sqrt{\lambda\,L}/(2\pi)$.

10.3 Elliptical Polarization

During the discussion of bending magnet radiation in Chap. 9 and insertion radiation in this chapter we noticed the appearance of two orthogonal components of the radiation field which we identified with the σ-mode and π-mode polarization. The π-mode radiation is observable only at a finite angle with the plane defined by the particle trajectory and the acceleration force vector, which is in general the horizontal plane. As we will see, both polarization modes can, under certain circumstances, be out of phase giving rise to elliptical polarization. In this section, we will shortly discuss such conditions.

10.3.1 Elliptical Polarization from Bending Magnet Radiation

The direction of the electric component of the radiation field is parallel to the particle acceleration. Since radiation is the perturbation of electric field lines from the charge at the retarded time to the observer, we must take into account all apparent acceleration. To see this more clear, we assume an electron to travel counter clockwise on an orbit travelling from say a 12-o'clock position to 9-o'clock and then 6-o'clock. Watching the particle in the plane of deflection, the midplane, we notice only a horizontal acceleration which is maximum at 9-o'clock. Radiation observed in the midplane is therefore linearly polarized in the plane of deflection.

Now we observe the same electron at a small angle above the midplane. Apart from the horizontal motion, we notice now also a vertical motion. Since the electron follows pieces of a circle this vertical motion is not uniform but exhibits acceleration. Specifically, at 12-o'clock the particle seems to be accelerated only in the vertical direction (downward), horizontally it is in uniform motion; at 9-o'clock the acceleration is only horizontal (towards 3-o'clock) and the vertical motion is uniform; finally, at 6-o'clock the electron is accelerated only in the vertical plane again (upward). Because light travels faster than the electron, we observe radiation first coming from the 12-o'clock position, then from 9-o'clock and finally from 6-o'clock. The polarization

of this radiation pulse changes from downward to horizontal (left-right) to upward which is what we call elliptical polarization where the polarization vector rotates with time. Of course, in reality we do not observe radiation from half the orbit, but only from a very short arc segment of angle $\pm 1/\gamma$. Yet, even this short piece of the orbit has all the features just used to explain elliptical polarization in a bending magnet.

If we observe the radiation at a small angle from below the midplane, the sequence of accelerations is opposite, upward-horizontal (left-right)-downward. The helicity of the polarization is therefore opposite for an observer below or above the midplane. This qualitative discussion of elliptical polarization must become obvious also in the formal derivation of the radiation field. Closer inspection of the radiation field (9.105) from a bending magnet

$$\boldsymbol{E}_{\mathrm{r}}(\omega) = \frac{-1}{[4\pi\epsilon_0]}\frac{\sqrt{3}e}{cR}\frac{\omega}{\omega_{\mathrm{c}}}\gamma(1+\gamma^2\vartheta^2)\left[\mathrm{sign}(1/\rho)\,K_{2/3}(\xi)\,\boldsymbol{u}_\sigma - \mathrm{i}\,\frac{\gamma\vartheta\,K_{1/3}(\xi)}{\sqrt{1+\gamma^2\vartheta^2}}\,\boldsymbol{u}_\pi\right] \tag{10.94}$$

shows that both polarization terms are 90° out of phase. As a consequence, the combination of both terms does not just introduce a rotation of the polarization direction but generates a time dependent rotation of the polarization vector which we identify with circular or elliptical polarization. In this particular case, the polarization is elliptical since the π-mode radiation is always weaker than the σ-mode radiation. The field rotates in time just as expected from the qualitative discussion above.

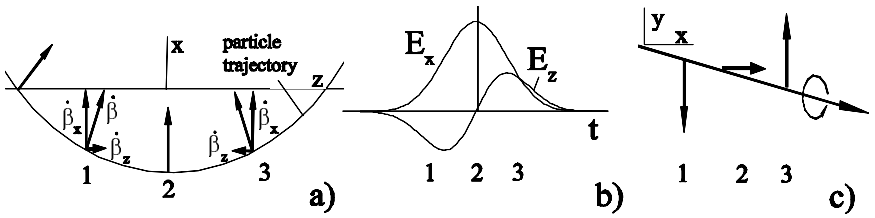

Fig. 10.13. Acceleration along an arc-segment of the particle trajectory in (**a**) a bending magnet, (**b**) polarization as a function of time, and (**c**) radiation field components as a function of time

We may quantify the polarization property considering that the electrical field is proportional to the acceleration vector $\dot{\boldsymbol{\beta}}$. Observing radiation at an angle with the horizontal plane, we note that the acceleration being normal to the trajectory and in the midplane can be decomposed into two components $\dot{\beta}_x$ and $\dot{\beta}_z$ as shown in Fig. 10.13a.

The longitudinal acceleration component together with a finite observation angle ϑ gives rise to an apparent vertical acceleration with respect to

the observation direction and the associated vertical electric field component is

$$\boldsymbol{E}_y \propto \dot{\beta}_y = n_y \dot{\beta}_z + n_x n_y \dot{\beta}_x .$$

An additional component appears, if we observe the radiation also at an angle with respect to the (x,y)-plane which we, however, ignore here for this discussion. The components n_x, n_y are components of the observation unit vector from the observer to the source with $n_y = -\sin\vartheta$. We observe radiation first from an angle $\vartheta > 0$. The horizontal and vertical radiation field components as a function of time are shown in Fig. 10.13b. Both being proportional to the acceleration (Fig. 10.13a), we observe a symmetric horizontal field E_x and an antisymmetric vertical field E_y. The polarization vector (Fig. 10.13c) therefore rotates with time in a counter clockwise direction giving rise to elliptical polarization with lefthanded helicity. Observing the radiation from below with $\vartheta < 0$, the antisymmetric field switches sign and and the helicity becomes righthanded. The visual discussion of the origin of elliptical polarization of bending magnet radiation is in agreement with the mathematical result (10.94) displaying the sign dependence of the π-mode component with ϑ.

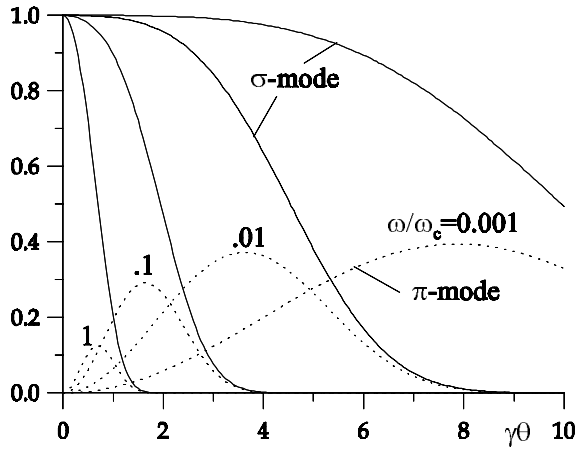

Fig. 10.14. Relative intensities of $\sigma-$mode and π-mode radiation as a function of vertical observation angle θ for different photon energies

The intensities for both polarization modes are shown in Fig. 10.14 as a function of the vertical observation angle ϑ for different photon energies. Both intensities are normalized to the forward intensity of the σ-mode radiation. From Fig. 10.14 it becomes obvious that circular polarization is approached for large observation angles. At high photon energies both radiation lobes

are confined to very small angles but expand to larger angle distributions for photon energies much lower than the critical photon energy.

The elliptical polarization is left or right handed depending on whether we observe the radiation from above or below the horizontal mid plane. Furthermore, the helicity depends on the direction of deflection in the bending magnet or the sign of the curvature, $\mathrm{sign}(1/\rho)$. By changing the sign of the bending magnet field the helicity of the elliptical polarization can be reversed. This is of no importance for radiation from a bending magnet since we cannot change the field without loss of the particle beam but is of specific importance for elliptical polarization state of radiation from wiggler and undulator magnets.

10.3.2 Elliptical Polarization from Periodic Insertion Devices

We apply the visual picture for the formation of elliptically polarized radiation in a bending magnet to the periodic magnetic field of wiggler and undulator magnets. The acceleration vectors and associated field vectors are shown in Fig. 10.15**a** and **b** for one period, and, similar to the situation in bending magnets, we do not expect any elliptical polarization in the mid plane where $\vartheta = 0$. Off the mid-plane, we observe now the radiation from a positive and a negative pole. From each pole we get elliptical polarization but the combination of lefthanded polarization from one pole with righthanded polarization from the next pole leads to a cancellation of elliptical polarization from periodic magnets (Fig. 10.15**c**). In bending magnets, this cancellation did not occur for lack of alternating deflection. Since there are generally an equal number of positive and negative poles in a wiggler or undulator magnet the elliptical polarization is completely suppressed. Ordinary wiggler and undulator magnets do not produce elliptically polarized radiation.

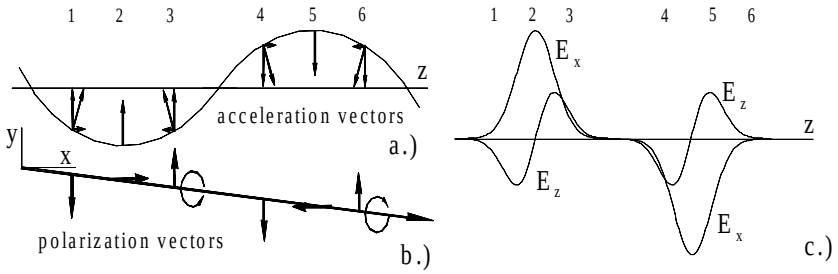

Fig. 10.15. Acceleration vectors along one period of (**a**) a wiggler magnet, (**b**) associated polarization vectors, and (**c**) corresponding radiation fields

Asymmetric wiggler magnet. The elimination of elliptical polarization in periodic magnets results from a compensation of left and righthanded helicity

and we may therefore look for an insertion device in which this symmetry is broken. Such an insertion device is the asymmetric wiggler magnet which is designed similar to a wavelength shifter with one strong central pole and two weaker poles on either side such that the total integrated field vanishes or $\int B_y \, \mathrm{d}s = 0$. A series of such magnets may be aligned to produce an insertion device with many poles to enhance the intensity. The compensation of both helicities does not work anymore since the radiation depends on the magnetic field and not on the total deflection angle. A permanent magnet rendition of an asymmetric wiggler magnet is shown in Fig. 10.16

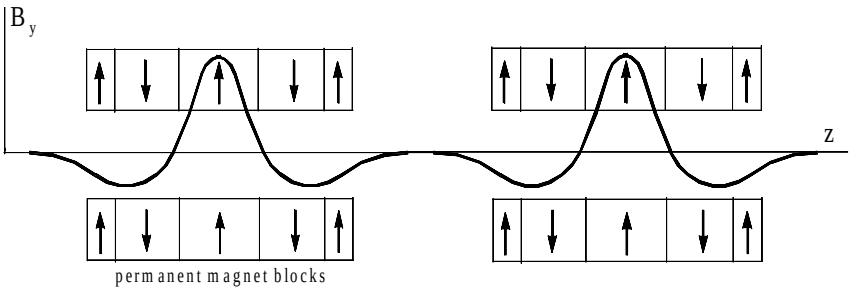

Fig. 10.16. Asymmetric wiggler magnet

The degree of polarization from an asymmetric wiggler depends on the desired photon energy. The critical photon energy is high for radiation from the high field pole, ϵ_c^+, and lower for radiation from the low field pole, ϵ_c^-. For high photon energies $\epsilon_{\mathrm{ph}} \approx \epsilon_c^+$ the radiation from the low field poles is negligible and the radiation is essentially the same as from a series of bending magnets with its particular polarization characteristics. For lower photon energies $\epsilon_c^- < \epsilon_{\mathrm{ph}} < \epsilon_c^+$ the radiation intensity from high and low field pole become similar and cancellation of the elliptical polarization occurs. At low photon energies $\epsilon_{\mathrm{ph}} < \epsilon_c^-$ the intensity from the low field poles exceeds that from the high field poles and we observe again elliptical polarization although with reversed helicity.

Elliptically polarizing undulator. The creation of elliptically and circularly polarized radiation is important for a large class of experiments using synchrotron radiation and special insertion devices have therefore been developed to meet such needs in an optimal way. Different approaches have been suggested and realized as sources for elliptically polarized radiation, among them for example, those described in refs. [62][63]. All methods are based on permanent magnet technology, sometimes combined with electromagnets, to produce vertical and horizontal fields shifted in phase such that elliptically polarized radiation can be produced. Utilizing four rows of permanent magnets which are movable with respect to each other and magnetized as shown in Fig. 10.17, elliptically polarized radiation can be obtained.

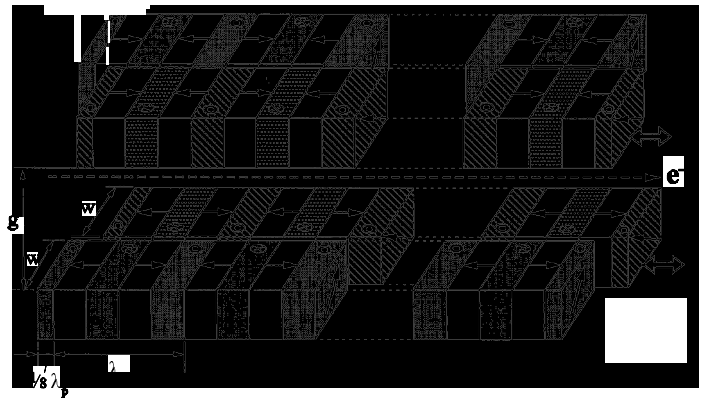

Fig. 10.17. Permanent magnet arrangement to produce elliptically polarized undulator radiation [64]

Figure 10.18 shows the arrangement in a three dimensional rendition to visualize the relative movement of the magnet rows [62][64].

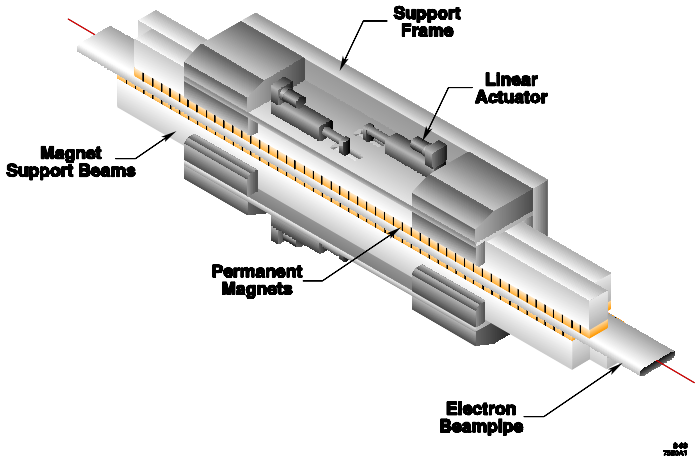

Fig. 10.18. 3-D view of an elliptically polarizing undulator, EPU [64]

The top as well as the bottom row of magnet poles are split into two rows, each of which can be shifted with respect to each other. This way, a continuous variation of elliptical polarization from left to linear to right handed helicity can be obtained. By shifting the top magnet arrays with respect to the bottom magnets the fundamental frequency of the undulator

radiation can be varied as well. Figure 10.19 shows a photo of such a magnet [63].

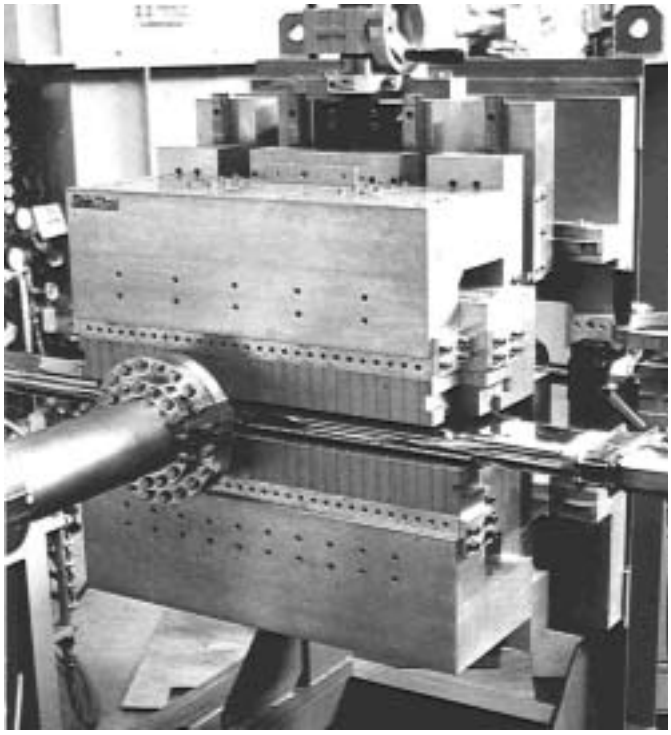

Fig. 10.19. Undulator for elliptically polarized radiation [63].

Exercises *

Exercise 10.1 (S). Consider an undulator magnet with a period length of $\lambda_p = 5$ cm in a 7 GeV storage ring. The strength parameter be $K = 1$. What is the maximum oscillation amplitude of an electron passing through this undulator? What is the maximum longitudinal oscillation amplitude with respect to the reference system moving with velocity $\bar{\beta}$?

Exercise 10.2 (S). An undulator with 50 poles, a period length of $\lambda_p = 5$ cm and a strength parameter of $K = 1$ is to be installed into a 1 GeV storage ring. Calculate the focal length of the undulator magnet. Does the installation

* The argument (S) indicates an exercise for which a solution is given in Appendix A.

of this undulator require compensation of its focusing properties? How about a wiggler magnet with $K = 5$?

Exercise 10.3 (S). Consider the expression (10.89) for the photon flux into the forward cone. We also know that the band width of undulator radiation scales like $\Delta\omega/\omega_k \propto 1/N_\mathrm{p}$. With this, the photon flux (10.89) becomes independent of the number of undulator periods!? Explain in words, why this expression for the photon flux is indeed a correct scaling law.

Exercise 10.4 (S). A hybrid undulator is to be installed into a 7 GeV storage ring to produce undulator radiation in a photon energy range of 4 keV to 15 keV. The maximum undulator field shall not exceed a value of $B_0 \leq 2$ T at a gap aperture of 10 mm. The available photon flux in the forward cone shall be at least 10% of the maximum flux within the whole spectral range. Specify the undulator parameters and show that the required photon energy range can be covered by changing the magnet gap only.

Exercise 10.5 (S). Consider an electron colliding head-on with a laser beam. What is the wavelength of the laser as seen from the electron system. Derive from this the wavelength of the "undulator" radiation in the laboratory system.

Exercise 10.6 (S). An electron of energy 2 GeV performs transverse oscillations in a wiggler magnet of strength $K = 1.5$ and period length $\lambda_\mathrm{p} = 7.5$ cm. Calculate the maximum transverse oscillation amplitude. What is the maximum transverse velocity in units of c during those oscillations. Define and calculate a transverse relativistic factor $\gamma_\perp$. Note, that for $K \gtrsim 1$ the transverse relativistic effect becomes significant in the generation of harmonic radiation..

Exercise 10.7 (S). Calculate for a 3 GeV electron beam the fundamental photon energy ($\vartheta = 0$) for a 100 period-undulator with $K = 1.0$ and a period length of $\lambda_\mathrm{p} = 5$ cm. What is the maximum angular acceptance angle ϑ of the beam line, if the radiation spectrum is to be restricted to a bandwidth of 10%?

Exercise 10.8. Add to the purely sinusoidal field of an ideal undulator additional terms (say 3-5), which would become necessary for a symmetric perturbation of the fundamental field, for example due to relativistic effects in strong undulators or due to long poles. Solve the equations of motion in the moving reference system (10.16a, 10.16b) . Which harmonics are involved in the perturbation of the purely sinusoidal motion? Can you relate them to the radiation spectrum in the laboratory system?

Exercise 10.9. The undulator radiation intensity is a function of the strength parameter K. Find the strength parameter K for which the fundamental radiation intensity is a maximum. Determine the range of K-values where the intensity of the fundamental radiation is at least 10% of the maximum.

Exercise 10.10. Verify the relative intensities of σ-mode and π-mode radiation in Fig. 10.15 for two quantitatively different pairs of observation angles ϑ and photon energies ϵ/ϵ_c.

Exercise 10.11. Design an asymmetric wiggler magnet assuming hard edge fields and optimized for the production of elliptical polarized radiation at a photon energy of your choice. Calculate and plot the photon flux of polarized radiation in the vicinity of the optimum photon energy.

Exercise 10.12. Show from (10.76) that along the axis, $\vartheta = 0$, radiation is emitted only in odd harmonics.

Exercise 10.13. Show from (10.73) that undulator radiation does not produce elliptically polarized radiation.

Exercise 10.14. Design a hybrid undulator for a 3 GeV storage ring to produce 4 keV to 15 keV photon radiation. Optimize the undulator parameters such that this photon energy range can be covered with the highest flux possible and utilizing lower order harmonics (order 7 or less). Plot the radiation spectrum that can be covered by changing the gap height of the undulator.

Exercise 10.15. Calculate the total undulator ($N_p = 50$, $\lambda_p = 4.5$ cm, $K = 1.0$) radiation power from a 200 mA, 6 GeV electron beam. Pessimistically, assume all radiation to come from a point source and be contained within the central cone. Determine the power density at a distance of 15 m from the source. Compare this power density with the maximum acceptable of 10 W/mm^2. How can you reduce the power density, on say a mask, to the acceptable value or below?

Exercise 10.16. Use the beam and undulator from Exercise 10.15 and estimate the total radiation power into the forward cone alone. What percentage of all radiation falls within the forward cone?